UNIVERSITAT POLITÈCNICA DE CATALUNYA
BARCELONATECH

Escola Tècnica Superior d'Enginyeria
de Telecomunicació de Barcelona

# DEVELOPMENT AND IMPLEMENTATION OF A UNIFIED HIERARCHICAL DC DROOP DC CONTROL SCHEME FOR DC MICROGRIDS

**A Master's Thesis**

**Submitted to the Faculty of the**

**Escola Tècnica d'Enginyeria de Telecomunicació de Barcelona**

**Universitat Politècnica de Catalunya**

**by**

**Lucas Bouzón Pousa**

**In partial fulfilment**

**of the requirements for the degree of**

**MASTER IN ELECTRONIC ENGINEERING**

**Advisor: Cristian Chillón Antón and Francesc Guinjoan Gispert**

**Barcelona, January 2020**

**Title of the thesis:** Development and implementation of a unified hierarchical DC droop control scheme for DC microgrids.

**Author:** Lucas Bouzón Pousa.

**Advisor:** Cristian Chillón Antón and Francesc Guinjoan Gispert.

## Abstract

This work focuses on the control design of a DC microgrid formed by two DC sources, two Dual Active Bridge (DAB) converters connecting theses sources to a DC bus which, in turn, constitutes the input of a DC/AC grid-connected inverter. The control strategy is based on a three-level Droop DC technique which is in charge of ensuring fast response, stable voltage and steady-state controlled power sharing. The work also suggests a variant of the Droop-based control to improve the system's performance. The proposed design is validated at simulation and experimental levels on a laboratory prototype of 40 kW performing tests at 12 kW.

## Acknowledgements

First of all, I would like to thanks CITCEA-UPC for several reasons. Firstly, I feel very grateful for the help they give to e-Tech Racing Formula Student Team now and before when I was there. Secondly, I especially want to thank them for allowing me to do my internships and for making me learn so much. Finally, I am extremely happy to have done my Master Thesis here with their support and be able to contribute to one of their projects.

I would like to make a special mention to different CITCEA-UPC people who had given me a special help. Thank you Cristian Chillón for being my tutor since my beginning in CITCEA-UPC, for teaching me and guiding me and for all the supervision of my Master Thesis and my work. Thank you Macià Capó for teaching me so well about power electronics, and specially about the Dual Active Bridge and its modulation techniques and for all the support in the implementation and the testing. Thank you Marc Llonch for your help in the implementation of the DC microgrid control, especially for your awesome proposed idea for the control and for your help in solving problems.

I also thank all the professors who had given me lessons during all the Master degree, but I would like to give the special thanks to my Master Thesis tutor, Francesc Guinjoan who have been the teacher of two of the most interesting subjects for me and who have helped me, teaching me and guiding me during all the Master Thesis.

The last but not the least, I would like to say that I am massively thankful for the given support of my family, my friends and my girlfriend, Espe. They have always been there for all the achievements and failures and they have always been pushing me to be a better person, a better student, a better professional…. To be the best version of myself.

# Revision history and approval record

| Revision | Date | Purpose |
|---|---|---|
| 0 | 12/09/2019 | Document creation |
| 1 | 15/01/2020 | Document revision |
| 2 | 20/01/2020 | Document reviewed |
| 3 | 24/01/2020 | Document approved |

| Written by: | | Reviewed and approved by: | |
|---|---|---|---|
| Date | 10/01/2020 | Date | 24/01/2020 |
| Name | Lucas Bouzón Pousa | Name | Cristian Chillón Antón |
| Position | Project Author | Position | Project Supervisor |

# Table of contents

# List of Figures

# List of Tables

# 1. Introduction: motivation and objectives

Nowadays, most of the electric energy generation is concentrated in huge power plants and then, transported to the consumers. Therefore, a large grid is needed all around the countries with long transportation lines. The grid has the mentioned big generation plants, such as nuclear, hydro-electric or coal plants which produces most of the power and normally are far away from the consumers. This energy is transported through very high voltage cables in order to reduce the current and consequently reducing the power losses in the transmission. Afterwards, this voltage is reduced to a high voltage. Smaller generation power plants, such as, little coal plants, big solar farms or big wind farms and big factories are connected to this high voltage line. Until this point, the grid is called transmission grid.

Then, the voltage is reduced and the grid is considered as distribution grid. At this point, high power consumers, such as industrial ones or farms; small power generation plants, such as solar farms, wind farms or small coal plants; and concentration of small consumers are connected to the grid. Figure 1 shows a scheme of the nowadays grid architecture described in this paragraph.

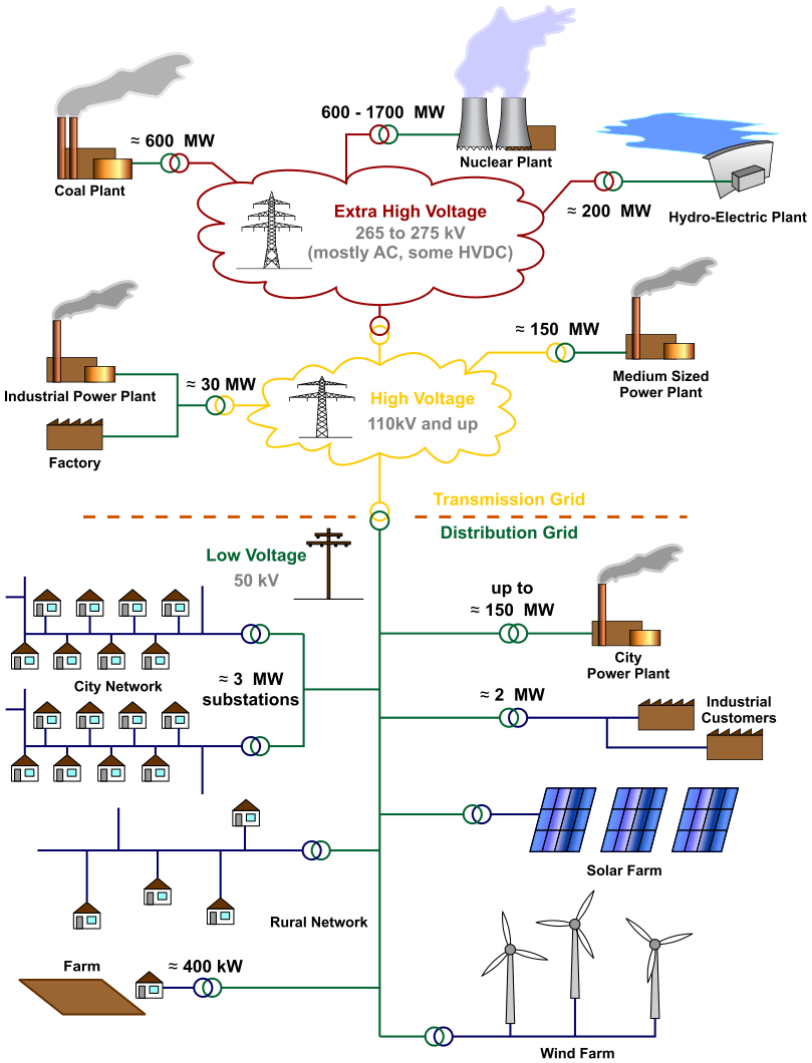


*Figure 1. Nowadays grid architecture [23]*

Great amount of the energy generation is based on non-renewable energies, such as fossil fuels or nuclear energy. Since 2013, although Spain produces more than the 40% of the total electrical energy with renewable sources [1], [2], the $CO_2$ emissions related to the energy generations are considerable, more than 50 million of $tCO_2$ every year. Table 1 shows the electrical energy generation in Spain in 2018 (without taking into account the islands).

*Table 1. 2018 electrical energy generation in the peninsular Spain*

| **Non-renewable energies** | | **Renewable energies** | |
|---|---|---|---|
| Nuclear | 20,6 % | Eolic | 19 % |
| Carbon | 13,5 % | Hydraulic | 13,2 % |
| Combined cycle | 10,2 % | Photovoltaic | 2,9 % |
| Cogeneration | 11,2 % | Solar thermic | 1,7 % |
| Non-renewable wastes | 0.9 % | Renewable wastes | 0,3 % |
| Other | 3,5 % | Other | 1,6 % |
| **Total energy [GWh]** | **149536,7** | **Total energy [GWh]** | **103958,3** |

In contrast to the energy generation data, Table 2 shows the power installation in the peninsular Spain according to the type of energy.

*Table 2. 2018 power installation in peninsular Spain*

| **Non-renewable energies** | | **Renewable energies** | |
|---|---|---|---|
| Nuclear | 7,2 % | Eolic | 23,4 % |
| Carbon | 9,7 % | Hydraulic | 17,3 % |
| Combined cycle | 24,9 % | Photovoltaic | 4,5 % |
| Cogeneration | 5,8 % | Solar thermic | 2,3 % |
| Non-renewable wastes | 0,5 % | Renewable wastes | 0,1 % |
| Other | 3,4 % | Other | 0,9 % |
| **Total power [MW]** | **50775,4** | **Total power [MW]** | **478197,6** |

It can be seen in Table 1 and Table 2 a direct comparison between the non-renewable energies and the renewables ones. On the one hand, the frequently used non-renewable energies are the nuclear one which normally has a stable energy production; the carbon

which has also a stable energy production but it allows faster variability than the nuclear one; the combined cycle which has a fast variability and it is used to produce greats amounts of energy within a very short time; and finally the cogeneration which produces less instant power than the other but it has a constant production all over the year. On the other hand, as the renewable energies are very variant and dependent on the climate conditions, the relation between the installed power and the energy produced is direct. Therefore, it can be seen that in Spain the two predominant renewable energies are the eolic and the hydraulic ones, followed by the photovoltaic and the solar thermic.

Although Spain produces more than the 40 % of its used electric energy from renewable sources, the overall energy consumption of the country (taking into account transportation, industrial activities, aviation, and so on) has only a 17,5 % origin from renewable sources. Ideally, in order to have 0 pollutant emissions, all the used and, therefore, produced energy should be renewable. Therefore, this is the objective to have a sustainable world. For this reason, the use of renewable energies should be growing. According to the European Council, the targets for Europe in 2030 which were set in October 2014 and revised in 2018 are [24]:

- At least 40 % cuts in greenhouse gas emissions (from 1990 levels).
- At least 32 % share for renewable energy.
- At least 32.5 % improvement in energy efficiency.

These objectives are more ambitious than the previous ones with the aim of accelerating the change to a sustainable world. Although, these objectives are for Europe in general, there are also objectives for each country. Concretely, the European Council wrote the objectives for Spain [25] and can be summarize in:

- 26 % reduction of the greenhouse gas emissions compared to 2005.
- 42 % of energy from renewable sources (not only electricity consumption but also transportation, industrial activities…).

Nowadays, Spain has reduced the greenhouse gas emission a 15 % compared to 2005 and its share of energy from renewable sources in gross final consumption of energy is 17,5 % (Figure 2 and Figure 3 show the evolution of these two parameters in the last years). The previous targets set for 2020 have not been fulfilled yet. Therefore, there is a necessity to make a big effort in the next years to introduce more renewables energies and to reduce the greenhouse gas emissions. One way to accomplish the objectives for 2030 is the introduction use of microgrids which favour the addition of distributed energy sources introducing renewable energies in a local level and have the needed intelligence to manage all the sources, and to take profit of all available energy in the most efficient way.

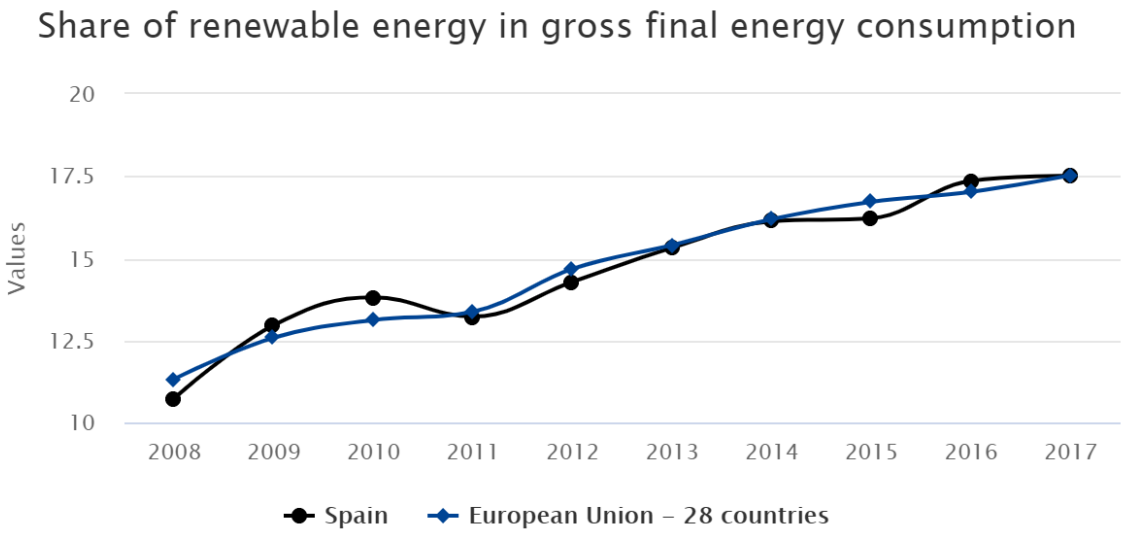


*Figure 2. Share of renewable energy in gross final energy consumption over the last years in Spain and Europe [26]*

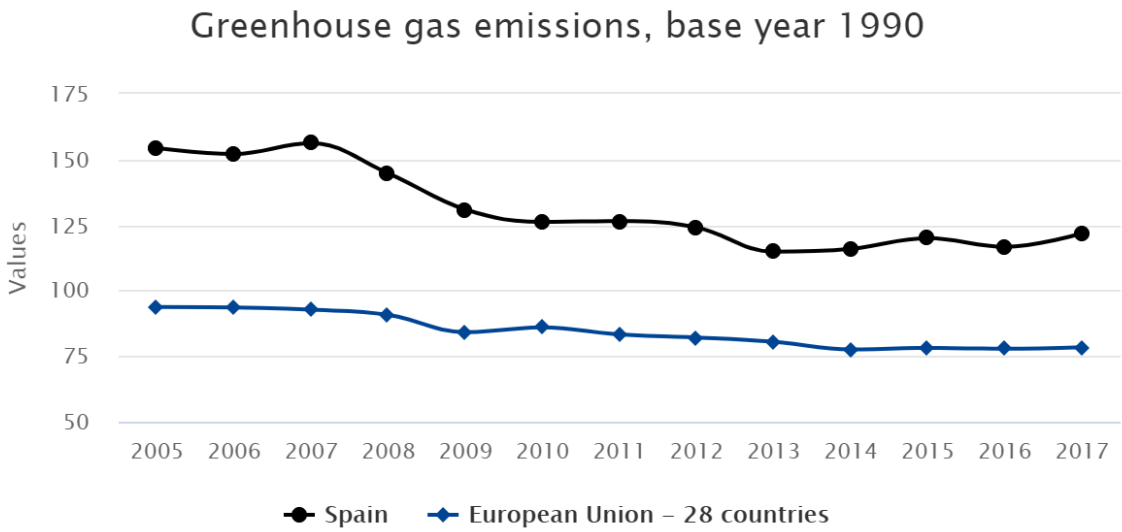


*Figure 3. Greenhouse gas emissions over the last years in Spain and Europe [26]*

The necessity to evolve to a more sustainable society where the $CO_2$ emissions and the greenhouse gas emissions are reduced to the minimum makes the current energy generation and distribution system unsuitable. Therefore, everything is changing and evolving and the tendency is to have more distributed power generators based on renewable energies and consequently, to have microgrids smart enough to extract the maximum energy from these renewable sources. In order to be able to take profit of all available energy of these renewable sources and to have more flexibility, the use of batteries is increasing to support these sources and even, the grid. For this reason, the use of DC microgrids formed by batteries and other renewable sources is a topic of interest.

This master thesis is part of the H2020 European project RESOLVD, which consists in the addition of two batteries of different chemistry to the grid to improve its flexibility. The two batteries can give extra power to the grid when the power consumption is higher than the

predicted one avoiding this way the extra generation of a pollutant power plant. The system also allows to equilibrate the consumptions of the phases and to compensate the harmonics of the grid. Moreover, these two batteries can be recharged when there is an extra production in the grid, when there is more renewable energy production or when the price of the energy is the lowest. The interconnection between the two batteries to the grid is made by two Dual Active Bridge (DAB) converters and one inverter, Figure 4.

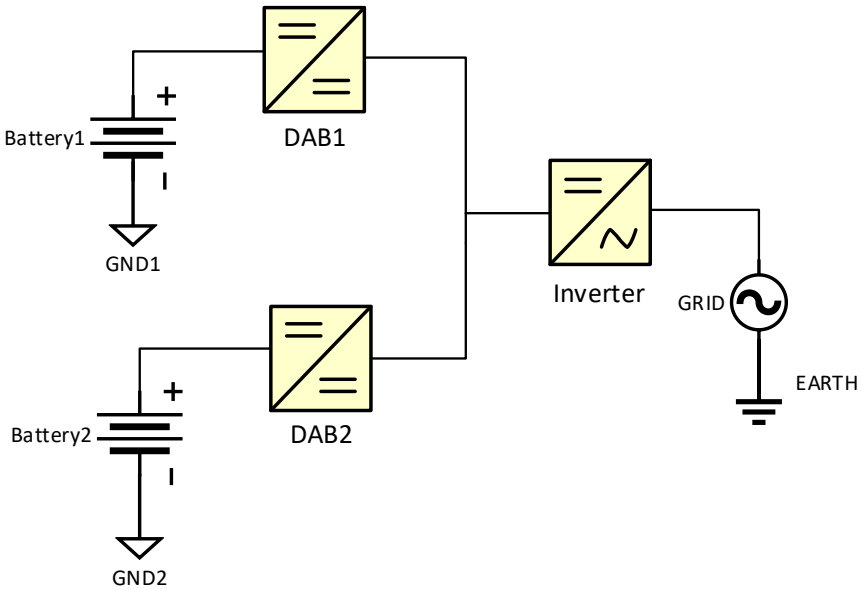


*Figure 4. System diagram*

This system hardware was designed and manufactured by CITCEA-UPC for the RESOLVD project. The master thesis is focused on the control of the small DC microgrid formed by the two DAB converters and the inverter. The responsibility of the correct behaviour of the DC microgrid belongs to both DAB converters and the inverter acts as a perturbation to the microgrid.

## 1.1. Objectives

The main objective of this thesis is to design, implement and test a working control for the aforementioned DC microgrid. Therefore, the design methodology has been divided in the following tasks.

1. Make a state of the art in order to have enough background to understand DC microgrids and to be able to design a control for it.
2. Study the system: the batteries and the converters.
3. Design the control of the DC microgrid making all the necessary calculations.
4. Generalize the calculations for more than two converters.
5. Simulate the designed control.
6. Implement the design into the hardware, programming the microcontroller.
7. Make the experimental test preparing the needed setup.
8. Compare the experimental results with the simulations.

## 1.2. Organization of this master thesis

This master thesis embraces all the mentioned objectives and it is accordingly organized in the following chapters:

1. **Introduction**. This is the current chapter where the theme, the objectives of the master thesis, the organization and the planning are introduced.
2. **State of the art**. In the State of the art chapter, the current bibliography of the microgrids, their different control schemes and the used converters is discussed.
3. **DC microgrid control**. The DC microgrid chapter presents in detail the used hardware, the theory of the selected control scheme and all the calculations to design the selected control scheme and to generalize it. Moreover, a variant of the selected control is presented and developed.
4. **Results**. In the Results chapter, the simulation setup and the experimental test setup is explained. Afterwards, the simulations and experimental tests are presented, compared and validated.
5. **Budget**. The Budget chapter shows the needed economic dispenses for the master thesis.
6. **Conclusions and future development**. Finally, the Conclusions and future development chapter summarizes all the work and extract the key points of the project and, suggest the basis to continue and improve the project.

## 1.3. Planning

The planning for this master thesis was done by a classical Gantt diagram (Figure 5) following the presented objectives. The official starting date for this master thesis was the 15th of September 2019 but, all the hardware was designed and manufactured before by CITCEA-UPC. The ending date for the master thesis was the 14th of January 2020. During this period the different tasks had been distributed and the amount of time of each one was estimated and fixed in order to have enough time to accomplish all the objectives and not to be blocked in one task.

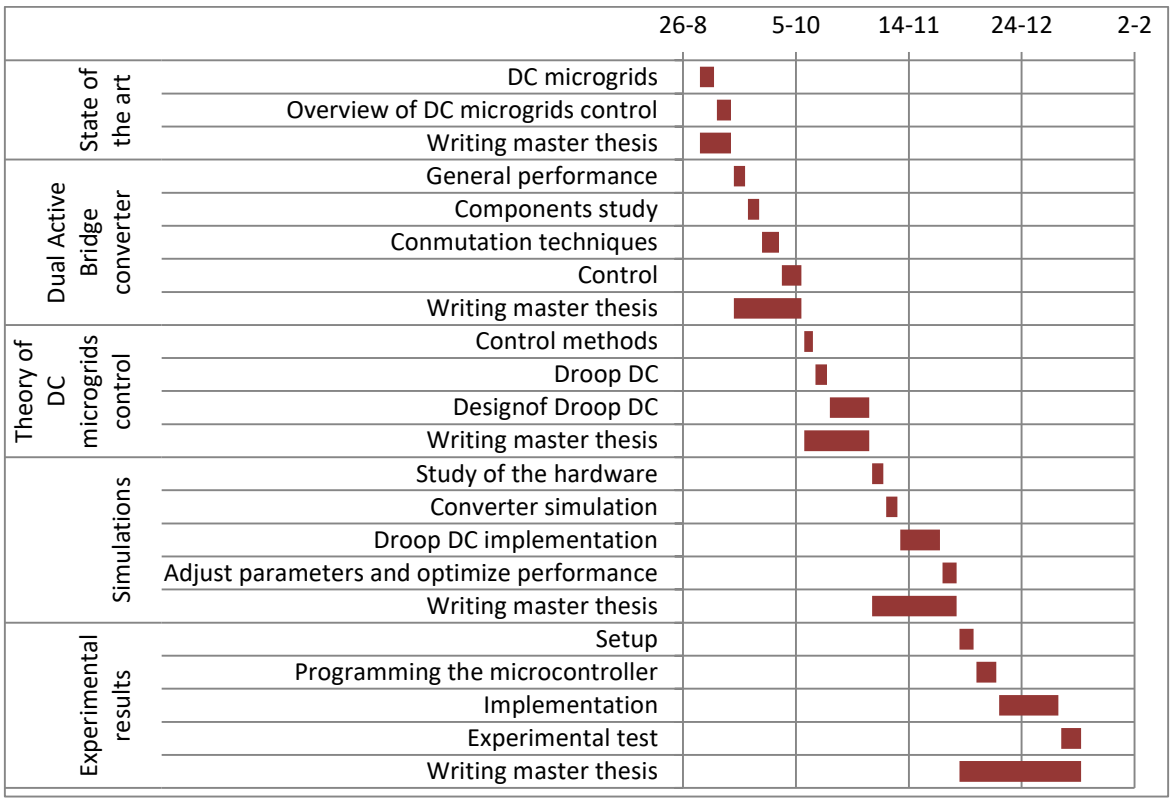


*Figure 5. Planning for the master thesis*

# 2. State of the art

Nowadays, the distribution scheme can be divided in three topologies [39]: a radial distribution system, a mesh distribution system and a network system. Figure 6 shows a simplified diagram of these topologies. Although these three well defined topologies, most of the distribution systems are formed by a combination of them.


*Figure 6. Distribution grid topologies*

The radial distribution systems are the most common ones and the most used ones because of its low price but, the main drawback of this topology is that, as it is based in a unique generator, any failure in the distribution grid or in the generator plant affects to all clients. The mesh distribution system has more than one generation plant, normally placed at the ends of the mesh. Therefore, if one plant or the distribution system has a failure, it does not affect to all consumers. This system is more expensive but it is more robust. Network systems are the most sophisticated interlocking mesh systems. Any consumer can be supplied from different power supplies and it surely adds a huge advantage in terms of reliability. This system is typically used only in crowded, high power requiring municipal or downtown areas because of excessive expenses.

All these distribution topologies are based in a unidirectional energy flow, from the generation plants to the consumers. The aim of a more sustainable society with zero emissions; the growing demand of electric energy; and the advances in distributed renewable sources, in power electronics and in control makes the power distribution scheme unsuitable because its inherent concept of using fossil fuels to generate electricity and the unidirectional power flow. One of the problems of the renewable sources is their dependence on weather, climate variations, season and hour of the day. For this reason, the renewable sources can be considered intermittent and they need a smart control to extract always the maximum energy possible. Therefore, the grid must evolve to a smarter and cleaner one, allowing more distributed renewable sources and consequently, allowing microgrids to be flexible enough to manage these renewable sources [3].

This section is divided in different parts. Firstly, an overview of microgrids is made describing the microgrids, its advantages and drawbacks, their classification and then, explaining in more detail the DC microgrids. Afterwards, the different DC microgrid control techniques found in literature are presented and explained. Finally, an overview of different converters used in DC microgrid is made according to the bibliography.

## 2.1. Microgrids

The microgrid definition varies slightly from one author to another, some definitions are

- A microgrid is a group of interconnected loads and distributed energy resources with clearly defined electrical boundaries that acts as a single controllable entity

with respect to the grid and can be connected and disconnected from the grid to enable it to operate in both grid-connected or island modes [4].

- Microgrid is a limited power supply network that is planned to deliver power for a small municipal area. It allows indigenous power generation for local loads. It contains many low capacity power generating resources that makes it highly flexible and efficient. Microgrid can be connected either islanded generating units, or the utility grid, or both of them to avoid undesired power outages. Additional power can be supplied to the utility grid. The size of the microgrid can be varied i.e. ranged from single house to community [5].
- A microgrid is a confined to a small area group of power generating units and loads that usually function interconnected, and acts as a single controllable unit that is analogous with the conventional unified grid (macro grid), but can be able to function autonomously in the absence of utility grid as physical and/or financial situations edict [6].

There are some key characteristics that appears in every definition [4], [5], [6]. The microgrid is a relatively small network compared to the utility grid. It interconnects loads and distributed energy resources. It can work connected to the grid extracting/delivering power or in island mode.

Moreover, microgrids have some benefits according to [3], [5], [7], [8]:

- **Reliability**: it is improved due to the intrinsic intelligence (control and automation systems) of microgrids and the utilization of distributed energy resources that allow islanded operation from the utility grid. Since the generation in community microgrids is located in close proximity to consumer loads, it is less prone to being affected by transport and distribution grid disturbances and infrastructure issues. Moreover, in case of black-out, the microgrids allow to move to a more meshed electric system that facilitates grid restoration by sections.
- **Power quality**: Microgrids provide a quick and efficient answer for addressing power quality needs by enabling local control of frequency, voltage and loads.
- **Carbon emissions**: they are reduced because although the distributed energy resources can be non-renewable, the aim is to only use renewable ones and therefore, being capable of making microgrids run using 100% renewable resources which make less emission of greenhouse gasses and eco-friendly.
- **Economics**: The microgrid, when it is operating in grid-connected operation mode can be used in order to enhance the quality of the consumed grid currents, balance the phases and dispatch reactive. This fact can derive in a retribution. Moreover, the proximity of generation to load in microgrids provides significant benefits in terms of reduced losses and transportation and distribution payments.
- **Efficiency**: As a microgrid can be considered by the utility as an active load, the direction of the power flow can be managed to the loads, to the storage systems and to the grid enhancing the performance of the network depending on the particular boundary conditions.
- **Modularity**: As a microgrid will use bus-links (AC or DC) to interconnect the different elements it is possible to scale the system if the microgrid requires more power. If various microgrids are interconnected, the concept of aggregated microgrid can be considered. An aggregated microgrid becomes a smart grid [23, 24] in order to take profit of all its resources and capabilities.

- **Island mode**: The islanding capability is the most salient feature of a microgrid, which is enabled by using switches at the PCC, and allows the microgrid to be disconnected from the utility grid in case of upstream disturbances or voltage fluctuations.

On the other hand, the microgrids also have some drawbacks: for backup power, microgrids might need energy storage units which may cause larger space requirement; when trying to reconnect with the utility grid, microgrids may face synchronization problems; design and implementation of protection schemes for microgrids are sometimes challenging and concerns such as standby charges and net metering may present difficulties. Although these few disadvantages, there is a growing interest in microgrid deployment which has made the research on the topic increase over the past few years [5].

## 2.2. Microgrids classification

Microgrids can be classified differently according to the type of management, architecture or the bus-link topology, Figure 7, [3].

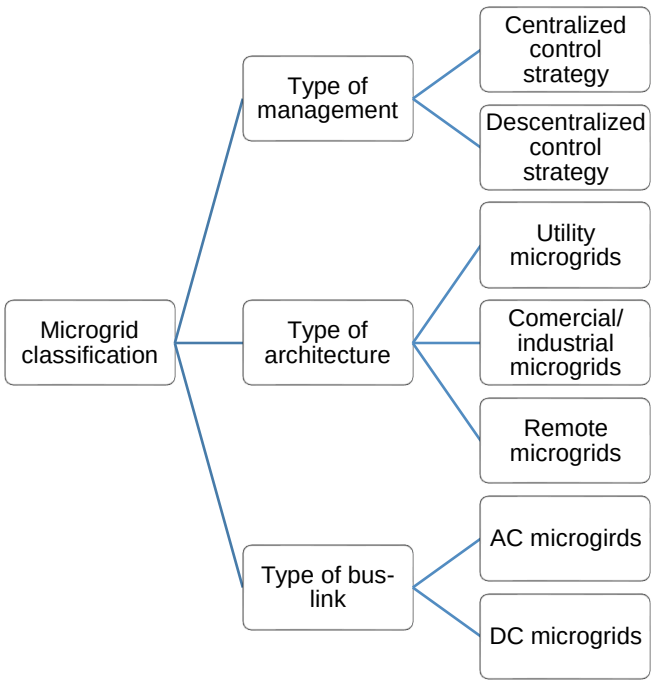


*Figure 7. Microgrid classification*

### 2.2.1. Type of management

A microgrid usually has some specification that permits an interaction with the utility. The control of a microgrid needs to be conceived from a manager that administrates the energy, storage the excess of renewable production and concentrates data from the electricity market and other parts of the system, as well as provides proper black-start and isolation procedures and decides how to operate other ancillary services. To achieve all these objectives, the management of a microgrid needs to be quite smart. This intelligence can be centralized or distributed. Therefore, two types can be differentiated:

- Centralized control strategy where there is a single element known as Microgrid Central Controller (MGCC) which is responsible of all these mentioned decisions and actions.

- Distributed control strategy where all the decisions and actions are distributed in different elements known as Local Controllers (LC).

Besides the distribution of the intelligence, there are also different network topologies to make all the communication between the MGCC and the LCs in the case of the centralized control strategy and only between LCs in the case of the distributed control strategy. These possible topologies are the following ones:

- Star. The MGCC connects to each LC, Figure 8. This topology is only valid for the centralized control strategy and has the advantage of having a fast communication error detection.

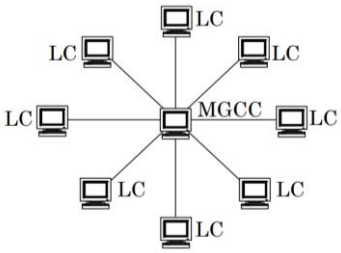


*Figure 8. Example of star network topology*

- Ring. The interconnection is made node by node (Figure 9), therefore, any information is transmitted by each node before reaching its destination. In central centralized control strategy, the MGCC can be any LC or it can be an external node if the computational requirements for it are higher than for a LC.

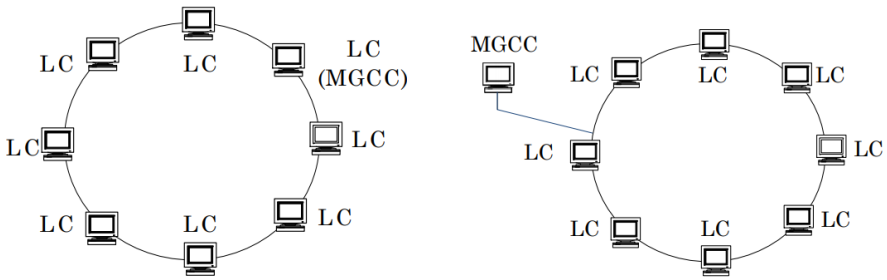


*Figure 9. Examples of ring network topology*

- Tree or bus. The interconnection is made through a common bus (bus topology). Moreover, if any local LC is branched to some other minor LC, the tree topology is accomplished, Figure 10. In centralized control strategy, the MGCC can be any LC, or it can be another node.

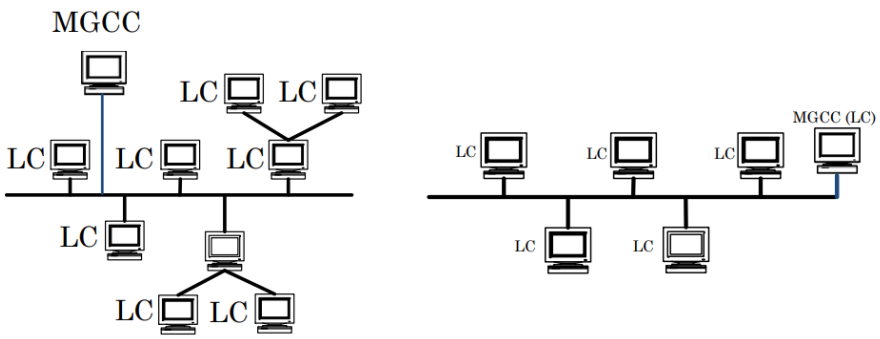

*Figure 10. Examples of tree and bus network topologies*

### 2.2.2. Type of architecture

Depending on the type of loads connected, the location of the microgrid, the available electrical infrastructure and the ownership of the land or the electrical system, three subtypes of architectures can be defined: utility microgrids, industrial/commercial microgrids and remote microgrids.

- Utility microgrids: the microgrid can be conceived as a way to integrate different distributed energy resources and obtain large-scale deployments. A utility microgrid allows to a distribution network operator to manage which portion of the required energy is supplied by the grid and which by the microgrid. The distribution network operator controls all the process and it is optimized as a function of the renewable availability.
- Industrial/commercial microgrids: this architecture priories power quality, reliability and resiliency. Therefore, the expected behaviour of an industrial or commercial microgrid is to disconnect if in grid-connected operation mode is not possible to meet the pre-specified quality requirements and start working in grid disconnected mode.
- Remote microgrids: A remote microgrid is the conventional concept of geographical areas or communities with absence of electrical infrastructure. Therefore, there is no possibility to be connected to the grid.

### 2.2.3. Type of bus-link

It is possible to classify microgrids according to the voltage link; DC microgrids, AC microgrids or the combination of both options.

- DC microgrids: this type of microgrid is the one where DC voltage is the link between distributed energy resources and loads. This type of microgrid will start to be an attractive way to distribute energy in next years due to the high penetration of distributed energy resources and considering DC loads or directly distributed energy resources production in DC.
- AC microgrid: in this type of microgrid the AC voltage is the link between distributed energy resources and loads. AC microgrids are intended to provide electricity for common residential or industrial consumptions.

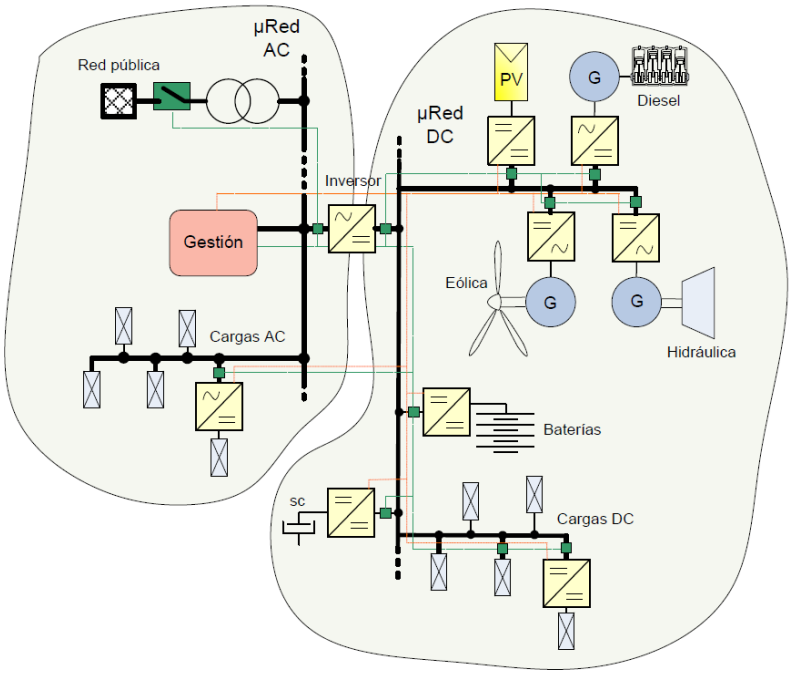


*Figure 11. Example of microgrids according to the type of bus-link*

## 2.3. DC Microgrids

Proliferation of renewable energy sources together with ever more electronic loads and electric vehicles in modern power networks has prompted an idea of considering the application of low-voltage dc distribution. Accompanied with technological advancements in power electronics and improvements in computational power of real-time controllers, dc systems of today are capable of achieving much broader functions than simple voltage regulation. Hence, they are becoming an increasingly popular solution for many types of residential and industrial applications, such as dc-powered homes, fast electric vehicle charging stations, hybrid energy storage systems, and renewable energy parks [9].

The advantages of DC microgrid when compared to its AC counterpart can be summarised in [3], [10], [11]:

- Higher efficiency and reduced losses due to the reduction of multiple converters stages.
- Easier integration of various DC distributed energy resources, such as energy storage or solar photovoltaic.
- Most efficient supply of DC loads (electrical vehicles, industrial DC loads).
- Easier management of electric parameters. The frequency has not to be controlled, so, there are not losses due to the reactive power.
- Allow to dispose of a robust system against seasonal phenomena when storage systems are considered.

On the other hand, DC protections are more expensive than AC equivalent ones and usually more voluminous. However, due to the penetration of electric vehicles more efforts on new protections based on static semiconductors are being developed. It should be also remarked that when a DC microgrid does not dispose of any storage system, the energy must be consumed when it is produced, as in AC systems.

### 2.3.1. Microgrid control

Microgrid control must ensure that: new distributed generation and storage systems can be added or removed from the microgrid seamlessly, equal and stable current sharing between parallel power converters is enabled, output voltage fluctuations can be corrected, and desired power flow from/to the microgrid together with technically and economically viable operation is enabled. Therefore, a microgrid control is often implemented in a hierarchical manner, with three control loops: tertiary loop manages the power flow from/to the microgrid, secondary loop corrects output voltage fluctuations, and primary loop performs current sharing control between power converters [12].

Normally, the primary loop is performed in the LCs while the secondary and the tertiary control are performed in the MGCC. This MGCC should be interchanging information with the Distribution System Operator (DSO) or the Transmission System Operator (TSO) in order to know what should be the given/extracted to/from the grid and what is the optimal voltage reference for the microgrid. Figure 12 shows a diagram of a microgrid with the LCs and the MGCC with the control levels.

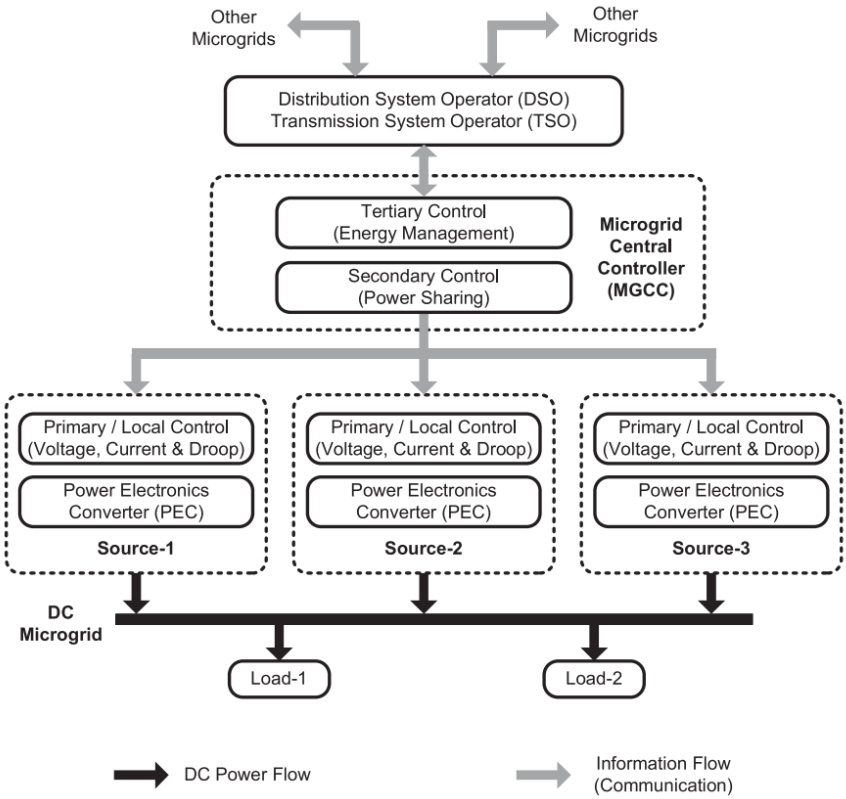


*Figure 12. Levels of a DC microgrid control [13]*

There is a fairly large number of methods for paralleling power converters. From the viewpoint of the operating mechanism to current sharing and output voltage level management, control methods are classified into two basic categories: active load sharing, and droop control methods.

#### 2.3.1.1. Active load sharing

The active load sharing control need intercommunication links. Although these links limit the flexibility of the microgrid and degrade its redundancy, both tight current sharing and

low-output-voltage fluctuations can be achieved. The active load sharing control methods can be classified into three different types: centralized control, master-slave control, and circular chain control:

- Centralized: The centralized control (Figure 13 shows a diagram of the control) consists of dividing the total load current by the number of modules (MODs) N, so that this value becomes the current reference of each module. The current reference value is subtracted by the current of each module, obtaining the current error, which is processed through a current control loop (CL). An outer control loop in the centralized control, i.e. voltage control loop (VL), adjusts the load voltage. Using this approach, it is necessary to measure the total load current, so it cannot be used in large distributed systems. Consequently, a central control board (CCB) is necessary.

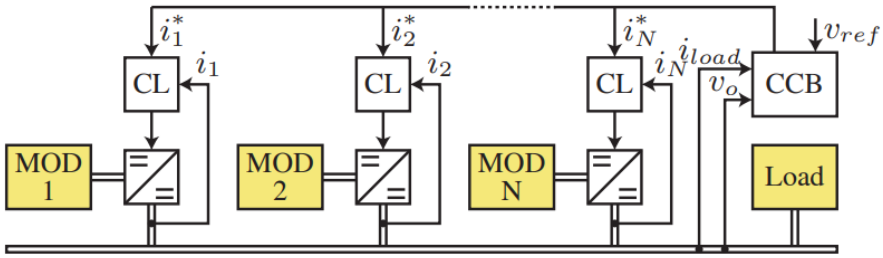


*Figure 13. Diagram of centralized active load sharing control method*

- Master-slave: In the master-slave control (Figure 14 shows a diagram of the control), the master module regulates the output voltage. Hence, the master fixes the current references of the rest of the modules (slaves). Consequently, the master acts as a voltage source converter, whereas the slave works as a current source converter. If the master unit fails, another module will take the role of master in order to avoid the overall failure of the system. There exist different variants of this control method, depending on the role of the master: dedicated, where the master is one fix module, rotary, where the master is arbitrarily chosen, and high-crest current, where the module that brings the maximum current automatically becomes the master.

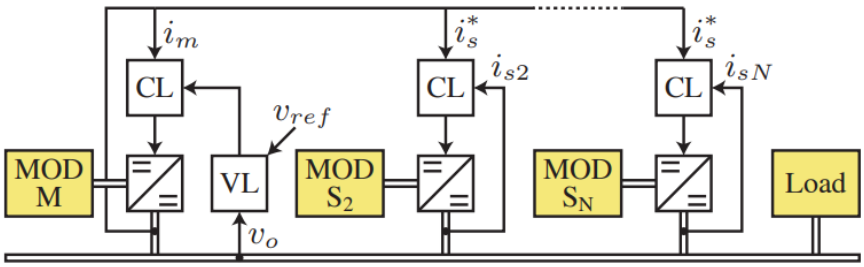


*Figure 14. Diagram of master-slave active load sharing control method*

- Circular chain: The circular chain control (Figure 15 shows a diagram of the control), consists of the current reference of each module taken from the other module, forming a control ring. Note that the current reference of the first unit is obtained from that of the last unit to form a circular chain information. The current limitation control is a variant of the circular chain control. In this case, the load voltage is controlled by the master module, whereas the slave modules are only for sharing the load current. Except for the master module, the current command of the slave is generated by its previous module and limited in amplitude. In this scheme, any module can be the master (dedicated, rotating, high-crest current).

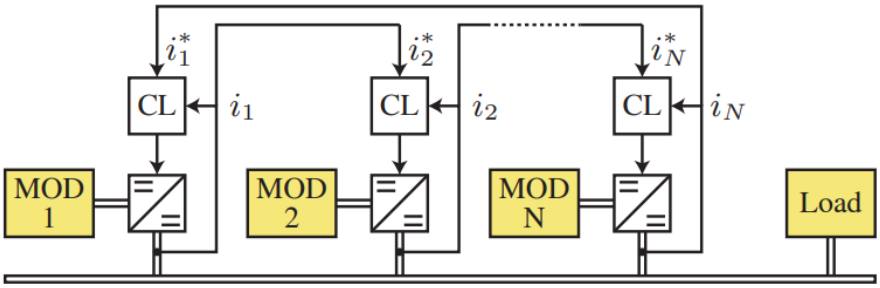


*Figure 15. Diagram of circular chain active load sharing control method*

### 2.3.1.2. Droop control method

Droop control methods are able to avoid critical communication links. The absence of critical communications between the modules improves the reliability without restricting the physical location of the modules.

In the Droop control method, shown in Figure 16, the current at the module output is sensed and sent back to the module input via virtual impedance $R_D$, where it is compared with the output voltage reference at no-load state. This control loop has the inherent load-dependent voltage deviation. To solve the problem of the voltage deviation, the voltage level in the microgrid $V_{MG}$ is sensed and compared with the voltage reference $V^*_{MG}$, and the error processed through a compensator is sent to all the modules to restore the output voltage.

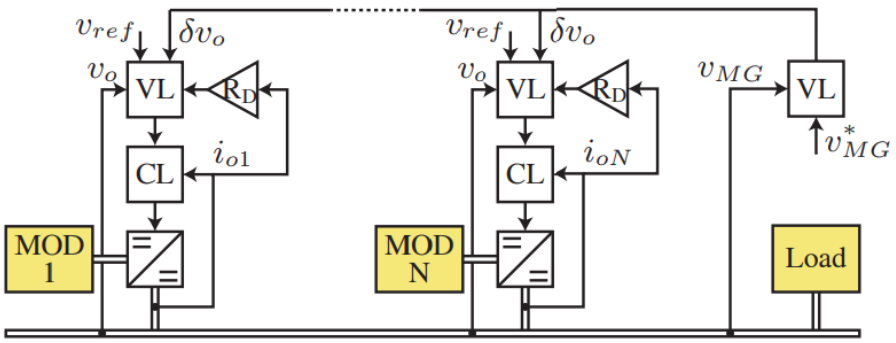


*Figure 16. Diagram of Droop control method*

In [13], this control scheme is used with two converters and its performance is analysed concluding with a well performance of a simple droop control but emphasizing in the addition of communications in order to make the secondary control to stabilize the voltage and improve the overall performance of the system.

The addition of a third control loop making this way the tertiary control is presented in [32]. Therefore, the traditional three-level droop DC control is designed, implemented and tested. The proposed control is a hierarchical control which consists of three levels. The primary control is based on the droop method, including an output-impedance virtual loop. The secondary control allows the restoration of the deviations produced by the primary control. Finally, the tertiary control manages the power flow between the microgrid and the external electrical distribution system. This is the control scheme adopted for this master thesis.

There are plenty of modifications and variations of the droop control method. These variations always search for performance improvements or adding functions depending on the application.

In [14], the droop control use power deviations instead of current and the secondary control is applied in parallel with the primary (Figure 17). This control achieves a decentralized primary control according to the slopes of the droop and a stable bus voltage by the addition of the centralized secondary control through a PID controller.

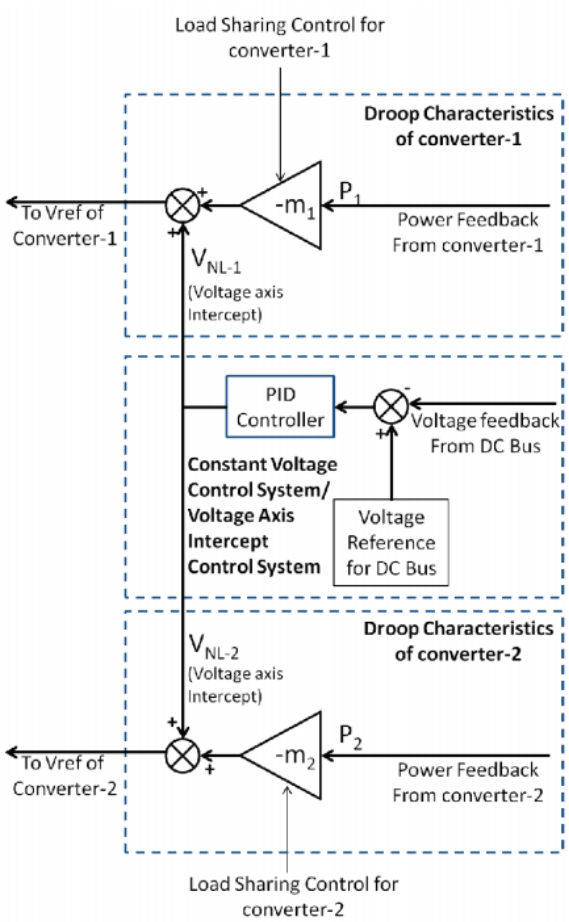


*Figure 17. Diagram of a Droop control method variant*

One of the inconvenient for the Droop Control Method in large microgrids is the influence of the cables resistance if they have a significant high value in comparison with the virtual resistances. In [27] [28], this cables resistance effect is reduced by making a variable virtual resistance Droop Control. Therefore, in order to achieve a lower deviation in the bus voltage and an improvement in the accuracy of the current sharing, this paper proposes an on-line adaptation algorithm to update the droop control resistance depending on the current difference and voltage deviation.

An improvement from the previous proposals is presented in [29]. It proposes an improved voltage control method in which the virtual resistance is variable and calculated by a droop coefficient compensator to improve the current distribution accuracy reducing thereby, the effect of the cabled resistances. Moreover, a secondary voltage compensation controller is also used to restore the bus voltage to a desired voltage.

Focusing more in the economic side of the microgrids, unlike traditional proportional power sharing based droop scheme, the proposed scheme in [30] considers the generation costs of distributed generators and dynamically tunes their droop gradients to produce more power from less costly distributed generators and vice versa. The propose scheme reduces the total generation cost in the DC microgrid without centralized economic dispatch and communication links and hence will enhance the overall reliability.

In [31], the objective is optimizing the performance of the batteries. The droop control method is implemented with two levels. The virtual resistance is adjusted according to individual state of charge of the different batteries of the microgrid, aiming dynamic power sharing and state of charge balance among batteries. Moreover, in the secondary control level, voltage based and state of charge based droop shifting strategies are respectively employed by interfacing and interlinking converters to restore the DC bus voltage to the nominal value and state of charge to the reference value.

## 2.4. Converters

Converters in microgrids are a key element. They allow to interconnect all the elements keeping the microgrid bus and the connected elements controlled. Focusing on DC microgrids, all converters used must have a DC connection to the DC microgrid and another connection to the battery, energy source, load or grid. The converters can be bidirectional or unidirectional depending on the energy flow of the element connected, for example, the converter of a solar panel is only unidirectional because it only can give energy but a converter of a battery must be bidirectional. The converters can also be divided into isolated and non-isolated. According to “Boletín Oficial de Estado (BOE)” in the fifteenth article of the third capitol, all the generators must have a galvanic separation between the grid and the generator facility [22]. For that reason, when using non-isolated converters, the isolation to the grid is normally made by a 50 Hz transformer. Another classification for converters can be done according to the control strategy. In [33], an overview of the different bidirectional DC/DC topologies and the control is done. Figure 18 show the classification of bidirectional converters according to their topology and their control.

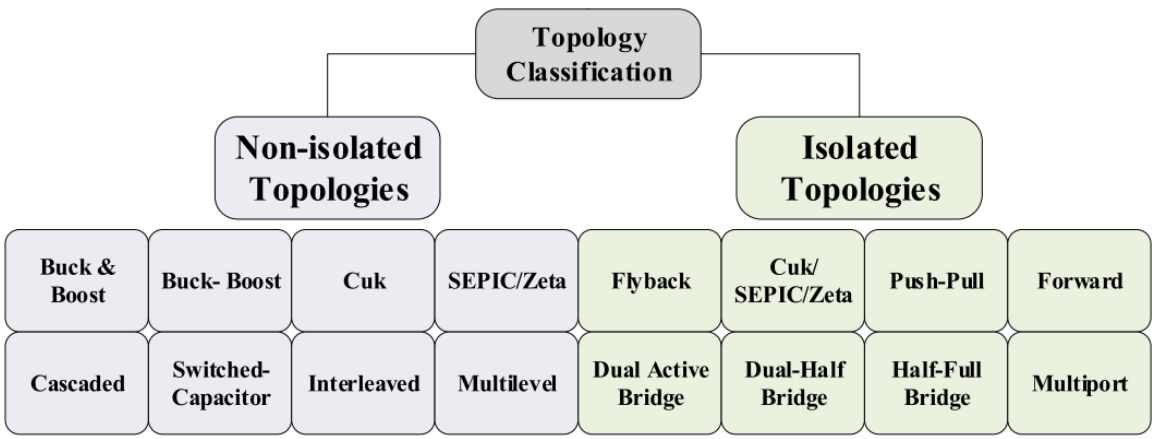


*Figure 18. Converters classification*

### 2.4.1. Non-isolated converters

Most basic and used topologies of non-isolated converters are the widely known buck, boost and buck-boost. These topologies, can be unidirectional or bidirectional if the used diode is replaced by a controllable switch. Besides these topologies, there are many others. In [33], some of the most common non-isolated topologies are presented, Figure 19.

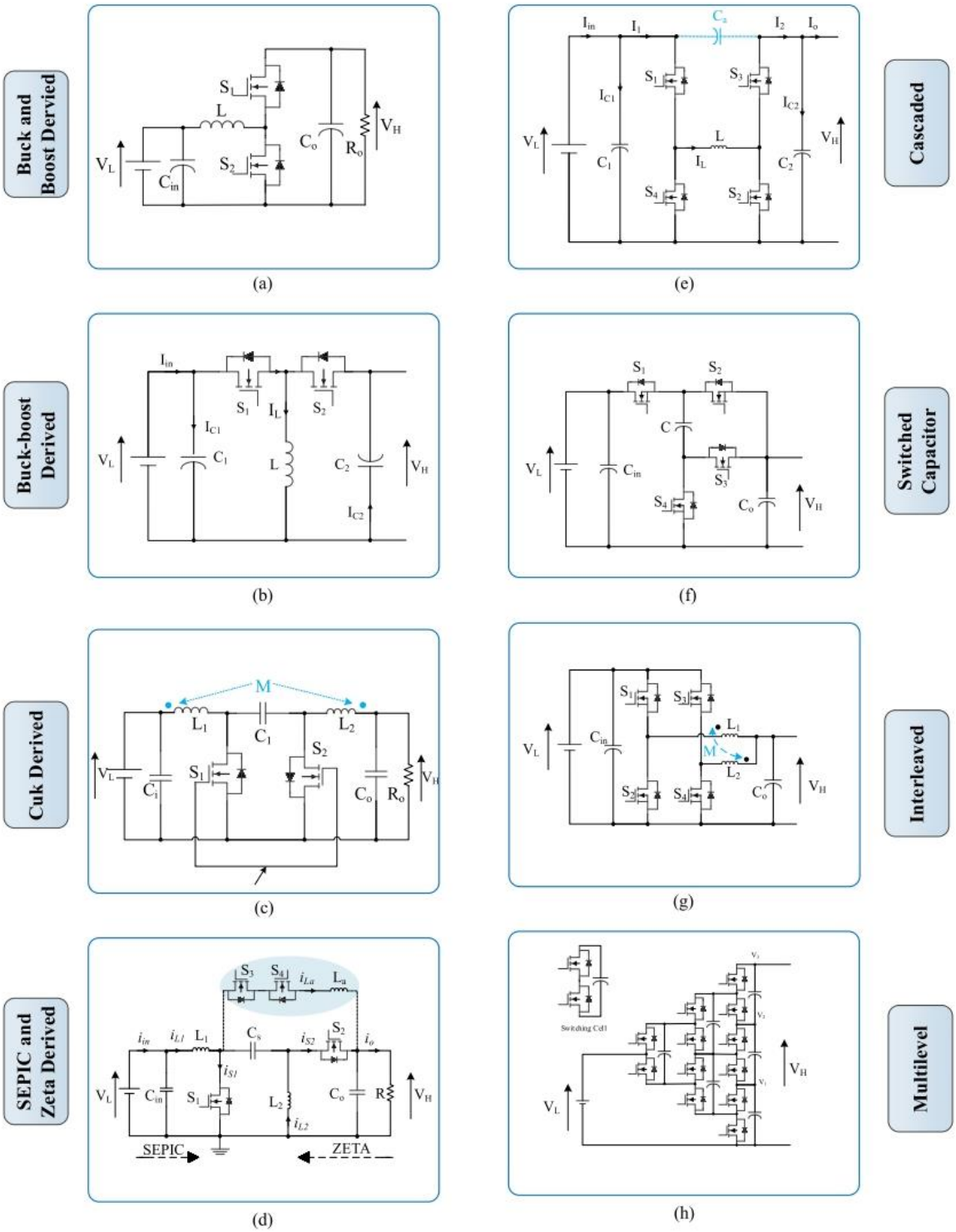


*Figure 19. Non-isolated bidirectional DC/DC converters topologies*

Figure 19 (a) shows the buck and boost topology, which is the most simple one with few number of switches and passive components. The buck topology steps-down the voltage and the boost topology steps-up the voltage. Their drawbacks are that they have a non-continuous input current and they have less voltage gain and more ripple than other topologies. The buck-boost topology shown in Figure 19 (b) shares the same advantages and disadvantages than the buck and the boost, but it can step-down and step-up the voltage having a negative output voltage. The bidirectional cuk topology shown in Figure 19 (c) uses more switches and passive components and, as the buck-boost, it can step-down and step-up the voltage having a negative voltage output but it accomplish a continuous input current and reducing the current ripple by coupling the inductors. Figure 19 (d) presents the SEPIC and Zeta derived topologies which accomplish a continuous input current having the possibility of stepping-down or stepping-up the voltage keeping the voltage output positive. Moreover, it can reduce current ripples using an auxiliary branch. The cascaded topology presented in Figure 19 (e) is an evolution of the buck converter and it is able to have a higher voltage gain and a low current stress by the addition of switches. The switched capacitor topology of Figure 19 (f) allows to duplicate the input voltage without the necessity of an inductor accomplishing this way, a reduced size and weight. The interleaved converter shown in Figure 19 (g) is another evolution of the boost and buck topology and it reduce the current ripples and therefore, smaller passive components can be used. Finally, the multilevel topology presented in Figure 19 (h) is an evolution of the switched capacitor that allows to multiply the input voltage without the necessity of an inductor.

In [15], different bidirectional topologies are presented. Firstly, a non-isolated bidirectional buck-boost topology is presented to connect a battery to a given microgrid. Afterwards, two non-isolated bidirectional buck/boost converters are connected in parallel to connect a hybrid storage system formed by a battery and a super capacitor to a microgrid. Then, in order to improve power density, reduce current stresses and reduce inductor and capacitor sizes, a three-phase interleaved non-isolated bidirectional buck/boost converter is presented to connect a battery to a microgrid. Finally, an improvement of this interleaved buck-boost converter is proposed as a floating interleaved converter (Figure 20 shows an example of this converter). This topology enables higher efficiency, higher voltage gains, and lower current ripples.

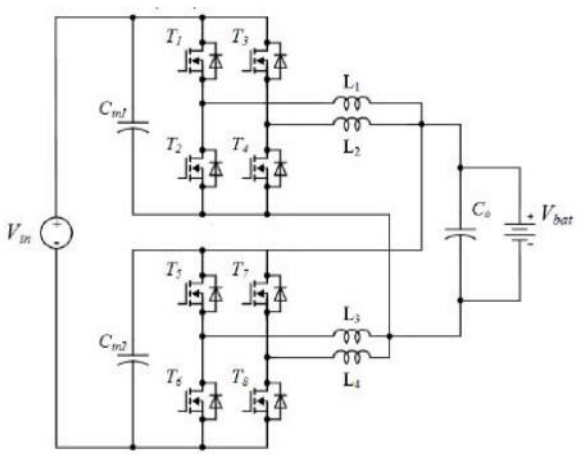


*Figure 20. Non-isolated bidirectional floating interleaved converter*

In [16], a non-isolated unidirectional LLC resonant converter (Figure 21) is proposed. The advantages of this converter are the extensive range of soft-switching operation, the high achievable efficiencies, the wide voltage gain range, and the simple control.

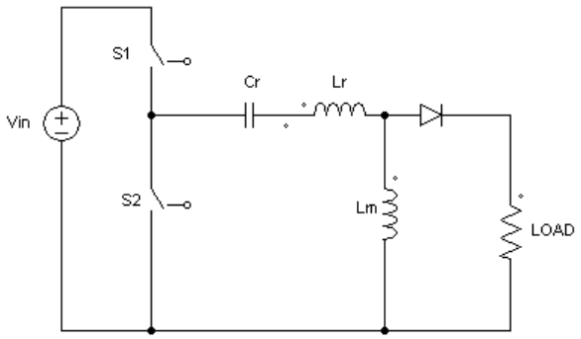


*Figure 21. Non-isolated unidirectional LLC resonant converter*

In [17], a non-isolated unidirectional dual-input DC/DC converter (Figure 22) is presented to hybridize voltage sources, such as, solar panels or fuel cells. This topology reduces the number of switches and passive components while keeping two different DC sources. It is a variant of the boost topology and therefore, it allows to step-up the input voltages.

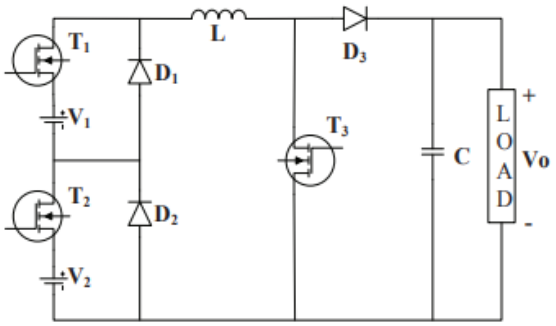


*Figure 22. Non-isolated unidirectional dual-input DC/DC converter*

A non-isolated unidirectional dual-input-dual-output DC-DC converter (Figure 23) is presented in [18]. This converter was designed to interface a solar PV and a fuel cell (FC) sources to a low-voltage dc microgrid. The proposed converter uses less number of switches and has only one inductor. Hence, this converter is efficient, compact and cheap. The proposed converter ensures MPPT operation of the PV source and also regulates one of the pole voltages of the dc link.

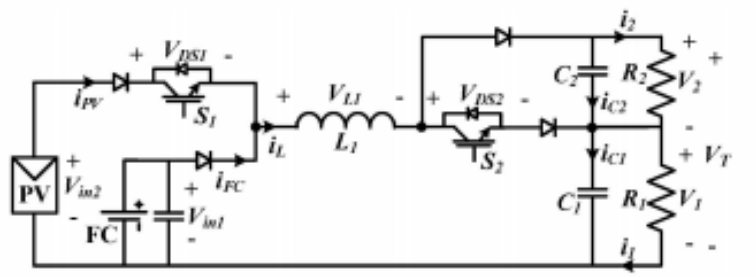


*Figure 23. Non-isolated unidirectional dual-input-dual-output DC-DC converter*

### 2.4.2. Isolated converters

There are many isolated topologies. These topologies have an important advantage of being isolated with a smaller high-frequency transformer and therefore, avoiding the use of a huge 50 Hz transformers when connecting the microgrid to the grid. In [33], some of the most common isolated topologies are presented, Figure 24.

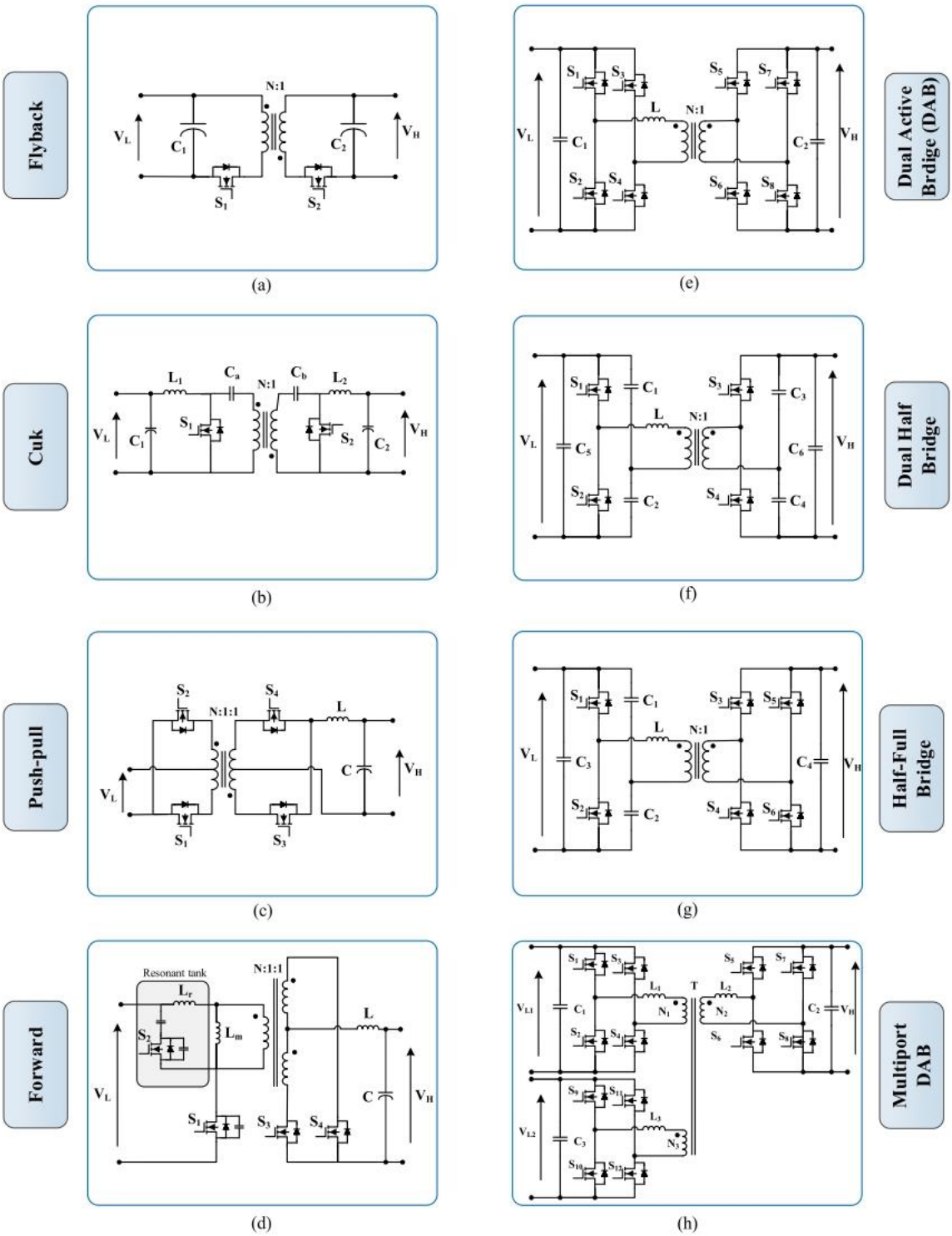


*Figure 24. Isolated bidirectional DC/DC converters topologies*

Figure 24 (a) shows the flyback topology which is the most basic one. It has no inductor, it allows to step-down and step-up the input voltage but it has not a continuous input current. The isolated cuk topology shown in Figure 24 (b) also allows to step-down and step-up the input voltage but it have a continuous input and output currents and it can reduce the current ripples by coupling the input and output inductors. Figure 24 (c) shows the push-pull topology which achieve a continuous output current with less passive component and uses a multi-winding transformer. The forward topology presented in Figure 24 (d) accomplishes a continuous output current with the less switches and passive components but it has a limited duty cycle which limits it to a low power applications. The dual active bridge (DAB) shown in Figure 24 (e) is the most popular isolated topology and it can be used for high power applications. Figure 24 (f) shows the dual half bridge topology which, in contrast to the DAB topology, uses less switches but more passive components. This topology is used for lower power application than the dual active bridge. The half-full bridge topology shown in Figure 24 (g) is a variant of the dual half bridge converter with less switches and more passive components which allows a simpler control making it suitable for uninterruptable low power supplies. Finally, the multiport dual active bridge presented in Figure 24 (h) is another variant of the DAB which allows multiple inputs.

#### 2.4.2.1. Dual Active Bridge (DAB) converter

As the classical Dual Active Bridge converter is the one used in this master thesis, the isolated converters subsection of the state of the art is focused on this topology. This Dual Active Bridge (DAB) converter consists of two full-bridge circuits linked by an isolated transformer and a leakage inductor (Figure 25). This converter provides isolation by topology, and its transformer is much smaller because of the high rate operational frequency. Moreover, the DAB converter can work in buck or boost mode and allow different control techniques which allow soft-switching improving consequently the efficiency. This converter is commonly used in microgrid applications to interconnect batteries or solar panels into the DC microgrid [19][35][36].

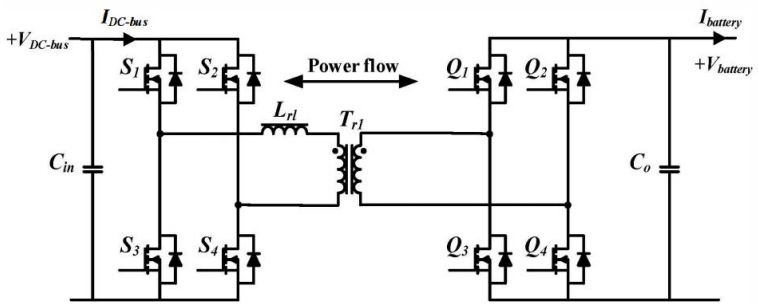


*Figure 25. Dual Active Bridge converter [19]*

There are topology variations of this Dual Active Bridge converter to improve soft switching range, efficiency, voltage gains or voltage operation ranges. For example, a 5-level Dual Active bridge is proposed in [34] for very high voltage applications (Figure 26). While using the simplest commutation technique, this topology allows to improves its ability to regulate power flow and to improve also the overall efficiency of the converter.

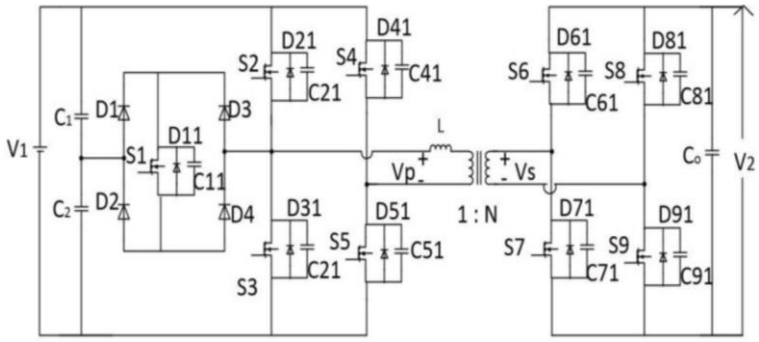


*Figure 26. 5 level Dual Active bridge topology*

Another variant of the Dual Active Bridge converter is proposed in [37] where a series resonant tank is added to improve soft switching range (Figure 27). With this resonant tank and a proposed modulation scheme, a zero switching current for all range of voltages and powers of the converter is accomplished. Therefore, this topology improves efficiency of the classical dual active bridge converter by the addition of an inductor and a capacitor placed in series with the transformer with a specific modulation scheme.

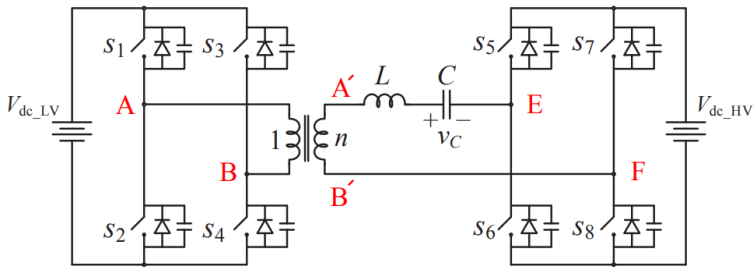


*Figure 27. Dual Active bridge topology with series resonant coupling network*

An improvement of this series resonant Dual Active Bridge converter is presented in [38]. This converter is called a Dual-Bridge series resonant DC–DC converter with dual tank. Figure 28 shows the scheme of this converter. This topology allows higher voltage gains, a wider soft-switching region, and a larger output power than the series resonant Dual Active Bridge using the widely simplest modulation scheme.

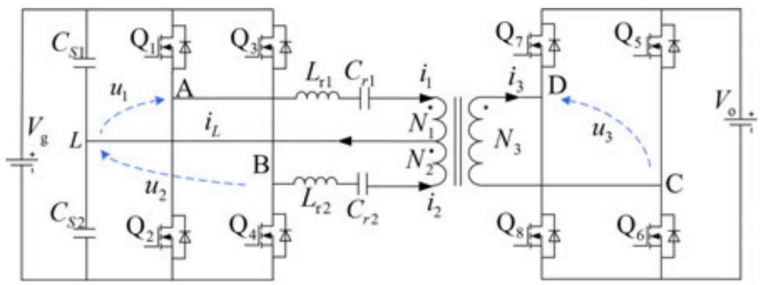


*Figure 28. Dual-Bridge series resonant DC–DC converter with dual tank*

# 3. DC microgrid control

This section describes the main development of the thesis, the design of the DC microgrid control. First of all, the system is described to make sure everything is in context. In this section an overview and the requirements of the system is presented and then, the decision of which type of control is explained. Afterwards, the theory of this control is explained to continuing with the final design of the control. Finally, all the development of the control is shown diving it in three sections: the primary control, the secondary control and the tertiary control.

## 3.1. System description

The system is composed by two batteries connected through two Dual Active Bridge (DAB) converters to the DC microgrid and this microgrid is connected to the grid through an inverter, Figure 29. The system is used as a support to the grid in the case there is an unexpected extra consume. The two batteries give this extra power when the grid is congested. This way, the commercial companies can save some money avoiding intraday buys when the power consumptions are underestimated and the distribution companies also can save money avoiding the disconnection of flexible loads or topology readjustments.

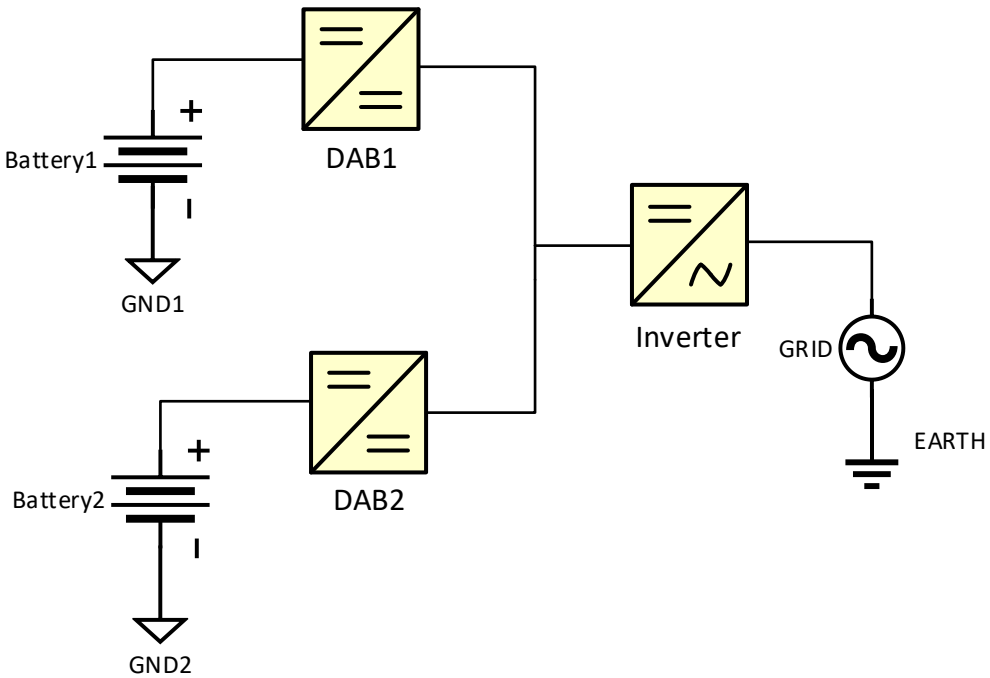


*Figure 29. System simplified diagram*

Moreover, the batteries are made of second life cells which has two different chemistries in order to have different characteristic in each battery and make the whole system affordable. One battery is made of Lithium cells which can provide a faster response without being degraded and the other one is made of Lead which gives support to the Lithium battery in steady-state conditions. Although, Lead batteries have worse characteristics, they are used because of their reduced price, they are significantly cheaper than the Lithium ones. According to [20] Lithium-ion batteries are 5 times more expensive than Lead-Acid batteries. Besides, as the volume is not a problem in this case, the

power/energy densities of the batteries are not the main concern. The characteristics of both batteries are shown in Table 3 and Table 4.

*Table 3. Lithium battery characteristics*

| | |
|---|---|
| Capacity | 90 Ah |
| Energy | 30 kWh |
| Nominal Voltage | 348 V |
| Minimum Voltage | 302 V |
| Maximum voltage | 387 V |
| Maximum charge current | 90 A |
| Maximum discharge current | 90 A |

*Table 4. Lead battery characteristics*

| | |
|---|---|
| Capacity | 58 Ah |
| Energy | 18 kWh |
| Nominal Voltage | 240 V |
| Minimum Voltage | 192 V |
| Maximum voltage | 280 V |
| Maximum charge current | 15 A |
| Maximum discharge current | 100 A |

The DAB converters (characteristics in Table 5) are isolated by topology and they are controlled in an innovative soft-switching technique. As they are connected in parallel, they form a small DC microgrid and some controls are needed to make sure the correct behaviour of this microgrid.

*Table 5. DAB characteristics*

| | |
|---|---|
| Maximum power | 20 kVA |
| Maximum bus voltage | 1200 V |
| Maximum battery voltage | 600 V |
| Current control time constant | 1 ms |

| | |
|---|---|
| Capacitor of the output filter | 120 µF |
| Inductor of the output filter | 4,4 µH |
| Switching frequency | 40 kHz |

Finally, the inverter is the connection between the grid and the DC microgrid. It is in charge of the power exchange between the DC microgrid and the utility grid. The characteristics of the inverter and the bus voltage are shown in Table 6.

*Table 6. Inverter and bus characteristics*

| | |
|---|---|
| Maximum power of the inverter | 75 kVA |
| Minimum input DC voltage | 700 V |
| Maximum bus voltage | 820 V |
| Bus voltage ripple | 40 V |
| Bus capacitor | 7,2 mF |
| Switching frequency | 30 kHz |

### 3.1.1. Requirements

The control of the DC microgrid has to be designed and the requirements of this control are the following ones:

1. The DC microgrid should be able of working in acceptable limits (fulfilling the minimum and maximum input voltage for the inverter, Table 6) without the necessity of digital communications.
2. The voltage of the DC microgrid should not be fixed by a single device and should be regulated to a stable value.
3. The control should be able to distributed the power given by each converter while ensuring the previous points.
4. The control should be stable in all the working region and should be as fast as possible.

### 3.1.2. Decisions

According to the requirements, the control of the DC microgrid should be selected. As the first requirement force not to use digital communications to ensure the working limits of the microgrid, all the controls based on the explained active load sharing are not valid. Therefore, the selected control is the Droop DC. In order to fulfil the second requirement, a secondary control must be added as some of the presented literature already had done. Moreover, a tertiary control must be also needed to fulfil the third requirement and be able to control the power sharing in steady-state conditions. Finally, the last requirement will be fulfilled by a stability analysis of all the implemented controllers.

### 3.2. Dual Active Bridge (DAB) converter

As both batteries must be isolated and they need a converter to be connected together, and taking into account the power range of the microgrid, the Dual Active Bridge (DAB) converter topology had been selected for its advantages. The DAB is a converter based in a high frequency transformer, an additional inductor, four branches of switches and an input and output filters as shown in Figure 30.

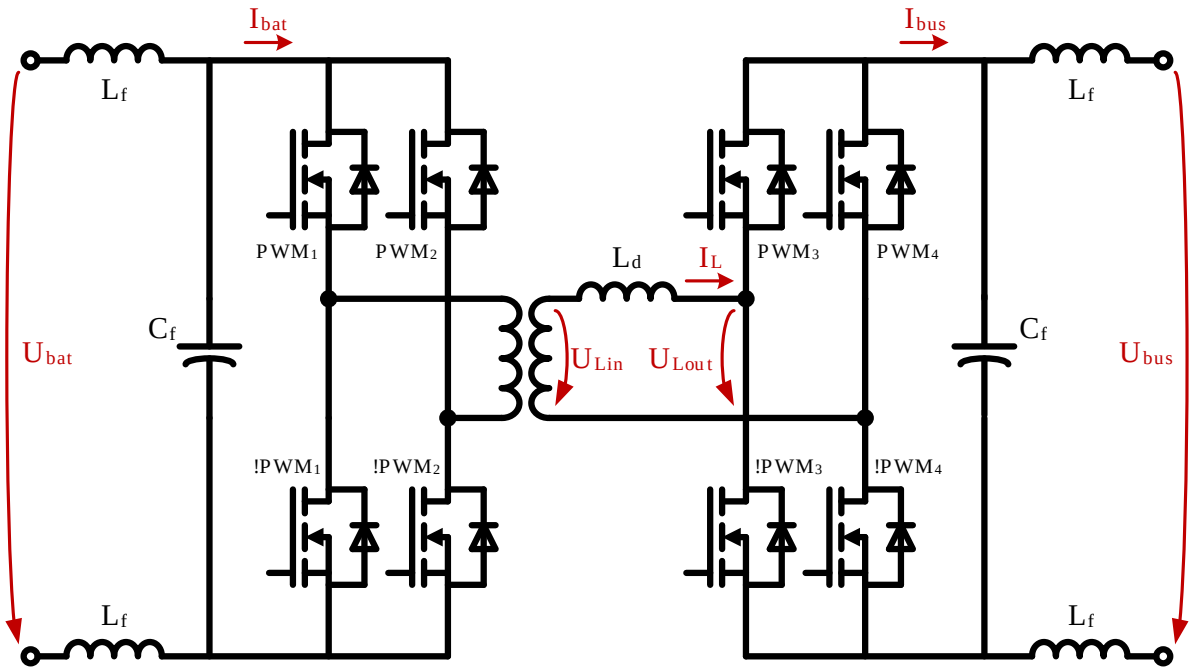


*Figure 30. Dual Active Bridge converter topology*

$U_{bat}$ is the battery voltage, $U_{bus}$ is the bus voltage, $C_f$ and $L_f$ are the input/output filters, the first two branches of switches are made of IGBTs and they are used to synthetize through the high frequency transformer the input voltage ($U_{Lin}$) of the inductor $L_d$ and the two other branches of switches are made of Silicon Carbide (SiC) MOSFETs and they are used to generate the $U_{Lout}$ of the inductor. Controlling the voltage of the inductor, its currents is controlled and consequently the power transfer between the bus and the battery.

There are many control techniques for this topology. In [21] an overview of the DAB converters and its control technique is done. The most common technique is the single phase shift (SPS) where all the PWMs have a 50% and the only controlled parameter is the phase shift between the two first branches and the two other ones. This way, the phase-shift ratio between $U_{Lin}$ and $U_{Lout}$ is adjusted controlling consequently the current through the inductor, the power flow direction and its magnitude. With this technique a zero voltage switch (ZVS) can be accomplish but not on the whole operation range. An improvement of this SPS is the extended phase shift (EPS) which allows to improve the efficiency by expanding the ZVS range and reduce the current stress. This is accomplished by having a phase shift between the PWMs of the two first branches in addition to the phase shift between the two pair of branches.

Other widely control technique used is the dual phase shift (DPS) which is based in having an inner phase shift between the PWMs of the first two branches and the PWMs of the two others in addition to the phase shift between the two pairs of branches. Compared with the SPS control, DPS control can decrease current stress and steady-state current, improve

efficiency, expand the ZVS operation range, and minimize the output capacitance. Moreover, DPS control is easier to implement, and its dynamic performance may be more excellent than the EPS.

Finally, there is another technique called three phase shift (TPS) which functional principle is the same as the DPS but the inner phase shift between the two PWMs of the first two branches and the other two may be unequal. The TPS control is the most difficult to implement, and there is also not a unified implement standard at present.

The control technique used in this system is an innovative one which was developed by CITCA-UPC and ensures zero current switching (ZCS) in all branches expect in one in the whole range of operation. For this reason, there is a one branch made of SiC MOSFETs. The control is also base in phase shifts between the PWMs but in a different way. The PWMs of the first and third branches are fixed as a reference and controlling the phase shift between them and the PWMs of the second and four branches the current between the inductor is controlled and therefore, the power direction and magnitude (Figure 31 and Figure 32 show a qualitative behaviour of this control technique).

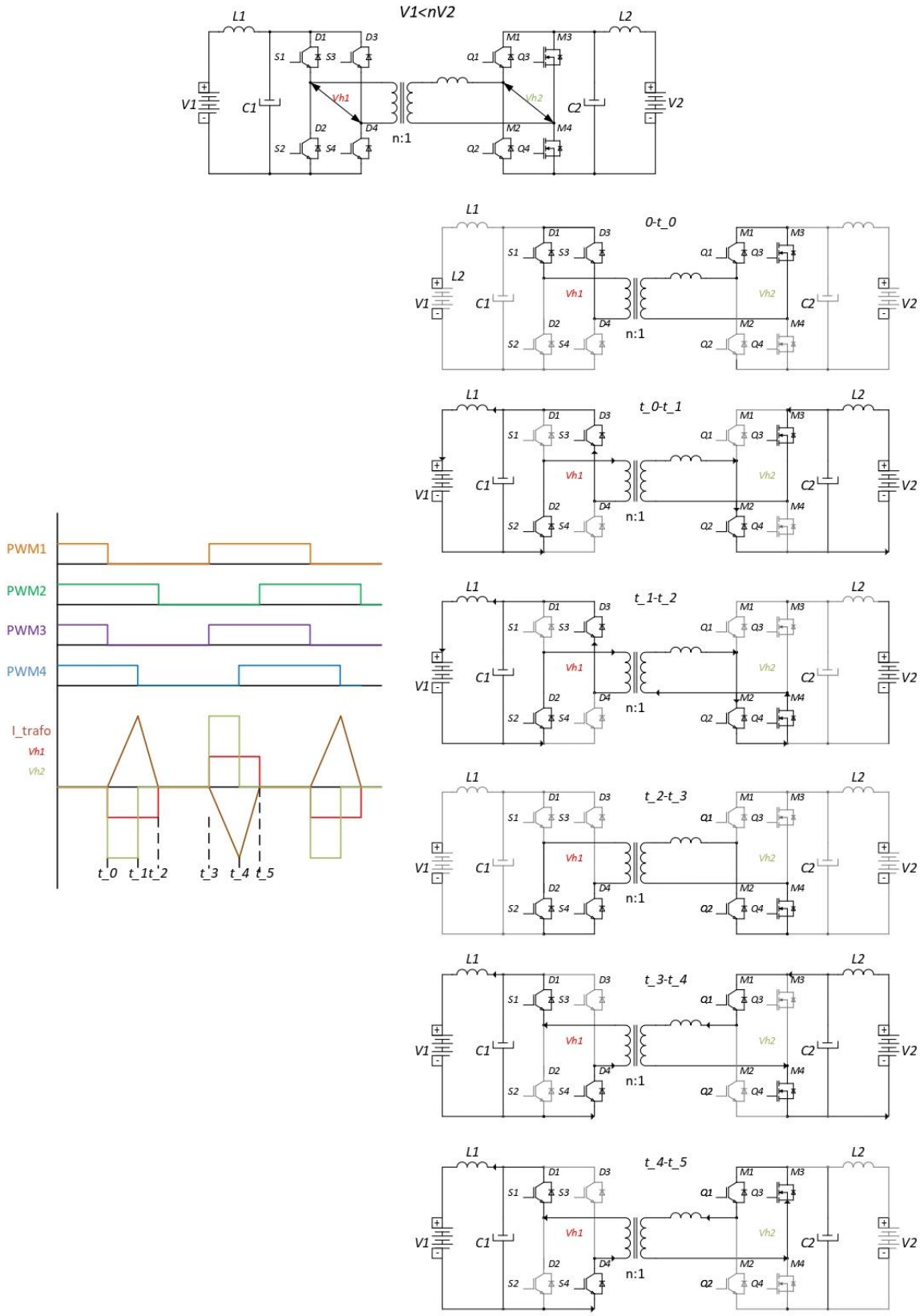


*Figure 31. Qualitative behaviour of the Dual Active Bridge with the innovative commutation technique when the power flow is negative (charging the battery, from V2 to V1)*

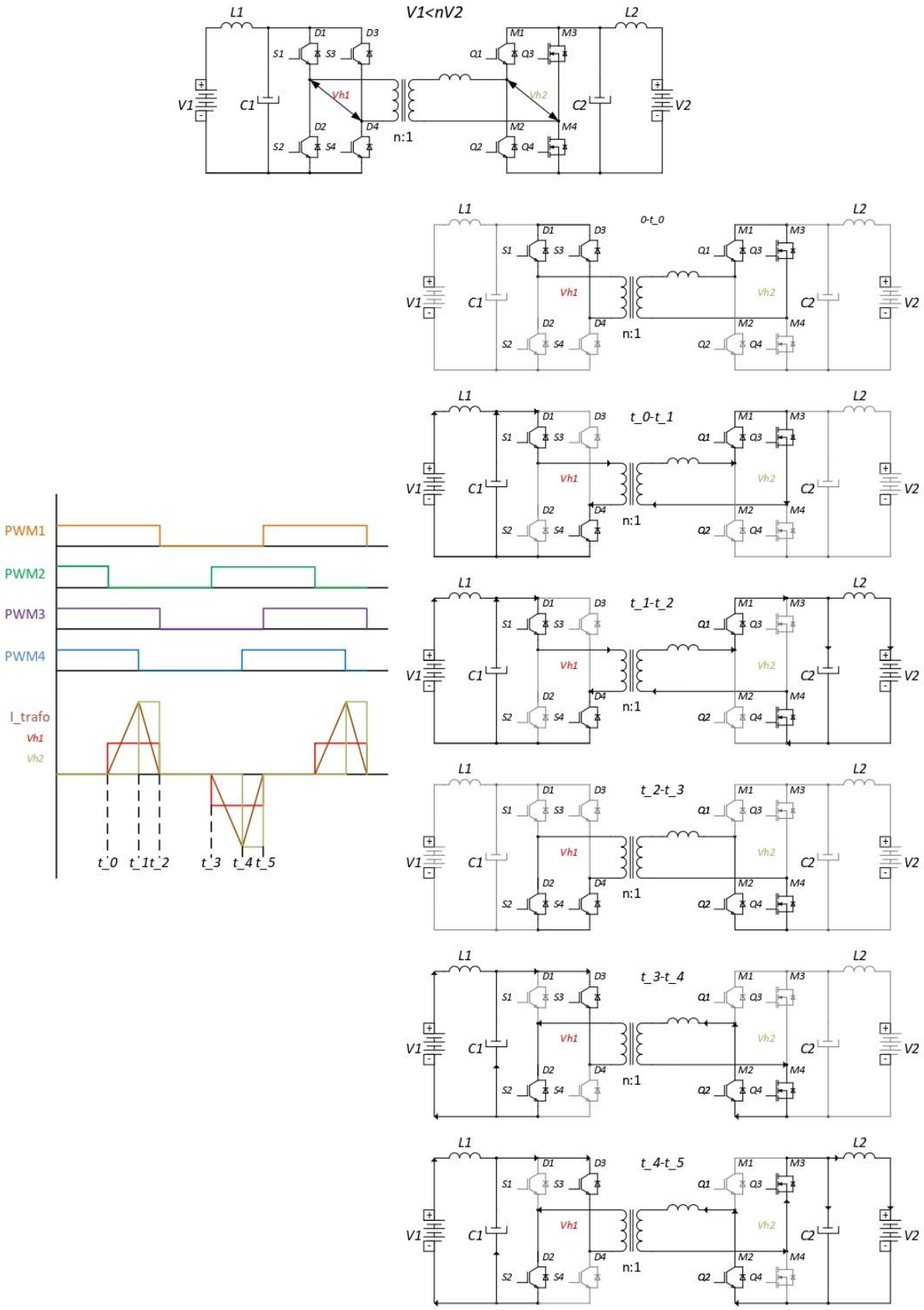


*Figure 32. Qualitative behaviour of the Dual Active Bridge with the innovative commutation technique when the power flow is positive (discharging the battery, from V1 to V2)*

The phase shift of the second and fourth PWMs are calculated by taking into account the output current set point, the frequency of the PWMs, the inductor, the battery voltage and the bus voltage. Therefore, this control technique is an open loop control. These calculations are a little bit different when the current reference is positive or negative. For positive current the expressions to calculate the phase shift are expressed in ( 1 ) and ( 2 ).

$$PWM2_{phaseshift} = \frac{(1 - D_{pos} - D'_{pos})t_s}{2} \quad (1)$$

$$PWM4_{phaseshift} = \frac{(1 - D'_{pos})t_s}{2} \quad (2)$$

Where $t_s$ is the PWMs period, and $D_{pos}$ and $D'_{pos}$ are expressed in ( 3 ) and ( 4 ).

$$D_{pos} = \sqrt{\frac{4\, I_{REF}\, L\, (V_2 - rt\, V_1)}{V_1^2 rt^2\, t_s}} \quad (3)$$

$$D'_{pos} = \frac{V_1 rt}{V_2 - rt\, V_1}\, D_{pos} \quad (4)$$

Where $I_{REF}$ is the current reference, $L$ is the inductance value and $rt$ is the transformation relation of the transformer.

For negative current references, the phase shift between the PWMs are expressed in ( 5 ) and ( 6 ).

$$PWM2_{phaseshift} = \frac{(D_{neg} + D'_{neg})t_s}{2} + \frac{t_s}{2} \quad (5)$$

$$PWM4_{phaseshift} = \frac{D_{neg}\, t_s}{2} + \frac{t_s}{2} \quad (6)$$

Where $t_s$ is the PWMs period, and $D_{neg}$ and $D'_{neg}$ are expressed in ( 7 ) and ( 8 ).

$$D_{neg} = \sqrt{\frac{-4\, I_{REF}\, L}{(V_2 - rt\, V_1)\, t_s}} \quad (7)$$

$$D'_{neg} = \left(\frac{V_2}{rt\, V_1} - 1\right) D_{neg} \quad (8)$$

Where $I_{REF}$ is the current reference, $L$ is the inductance value and $rt$ is the transformation relation of the transformer.

### 3.3. Theory of the Droop DC

The Droop DC is a control strategy to drive parallel converters. It usually is based in a primary control to achieve the current sharing between converts. If only the primary control is taken into account, the control method is very easy to implement and moreover, has the characteristic of being independent because each converter has its own control and does not depend on the others. It is also very common to add a secondary control to improve

the output voltage regulation. There is also the possibility to add a tertiary control to distribute the power between converters.

### 3.3.1. Primary control

The primary control of the Droop DC is based on characteristic I-V curves for each converter. Although the most common and easy are the linear curves, they could follow any function (Figure 33 shows some examples of possible curve). The basic idea behind these curves is to define a relation between the current a converter must inject in function of the bus voltage. Therefore, a V* is set as the nominal voltage where there is no current flowing and as the voltage of the bus increases or decreases the current does the same, however, they normally are limited because of power limitations.

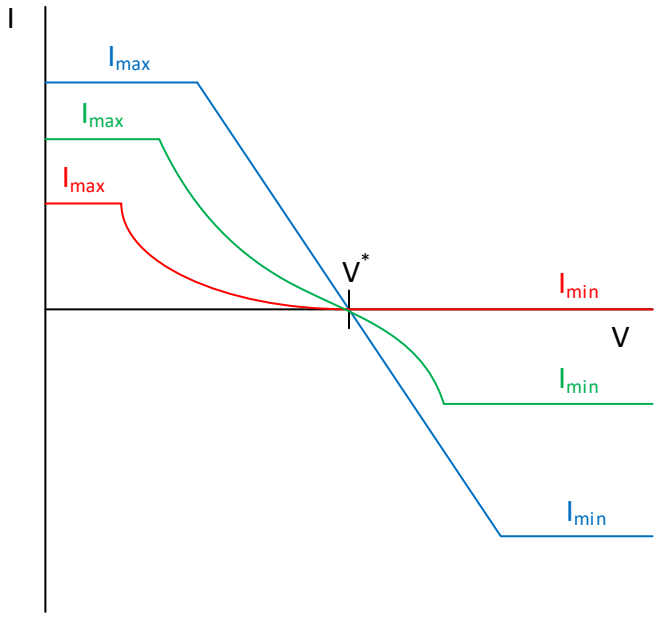


*Figure 33. Examples of I-V curves of the Droop DC primary control*

When considering linear curves, the concept of virtual resistance appears. The virtual resistance is the inverse of the slope of the curve, and therefore, is the relation between the voltage droop and the current. Figure 34 shows an example of a qualitative linear I-V curves that can be implemented in two converters in parallel as the system described above.

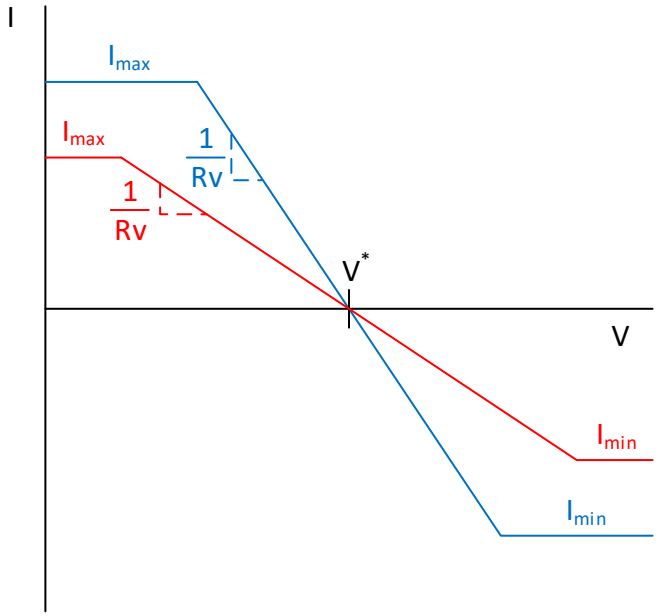


*Figure 34. Examples of two linear I-V curves of the Droop DC primary control*

Therefore, the block diagram that represent this primary control of the Droop DC, with two converters and taking into account a capacitor at the output plant to regulate, is the one shown in Figure 35.

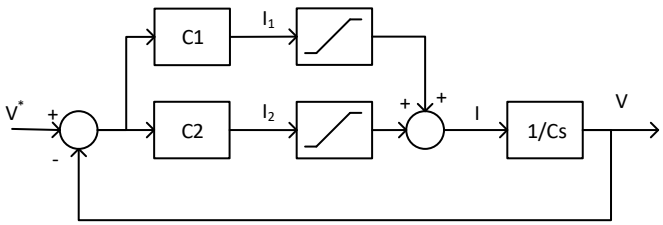


*Figure 35. Example block diagram of the primary control for two converters*

Where C1 and C2 are the slopes of each curve, $V^*$ set the 0 A output, V is the bus voltage and C is the capacitance of the bus capacitor.

### 3.3.2. Secondary control

The secondary control has the objective to regulate the output voltage. This may be needed to have a stable voltage output. The normal behaviour of the primary control is to response to a current perturbation because it gives a current set point according to the voltage. Therefore, depending on this current perturbation the output voltage will stabilize at one value which can be different to the desire one. The secondary control has to drive this value and take it to the desired voltage value independently of the current perturbation. It is often accomplished by adding or subtracting a variable horizontal offset to the curves of the primary control. For that reason, this control is not independent for each converter. This offset is generally computed by a proportional-integral (PI) controller and it is added to the primary control loop, as shown in Figure 36. The resulting offset adjustment is schematized in Figure 37.

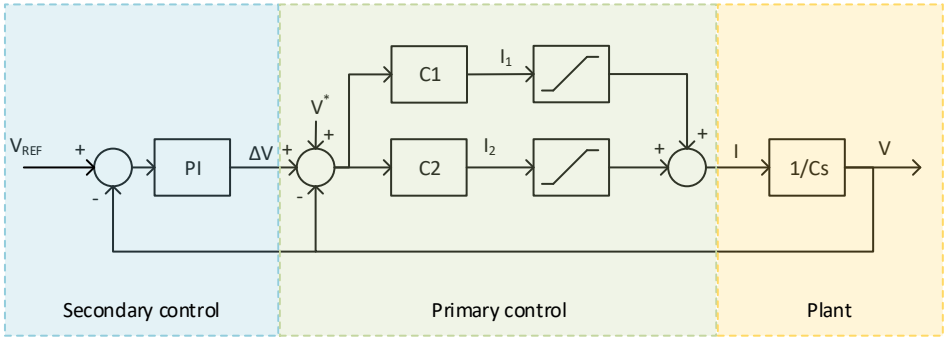


*Figure 36. Block diagram of the primary and secondary control for two converters*

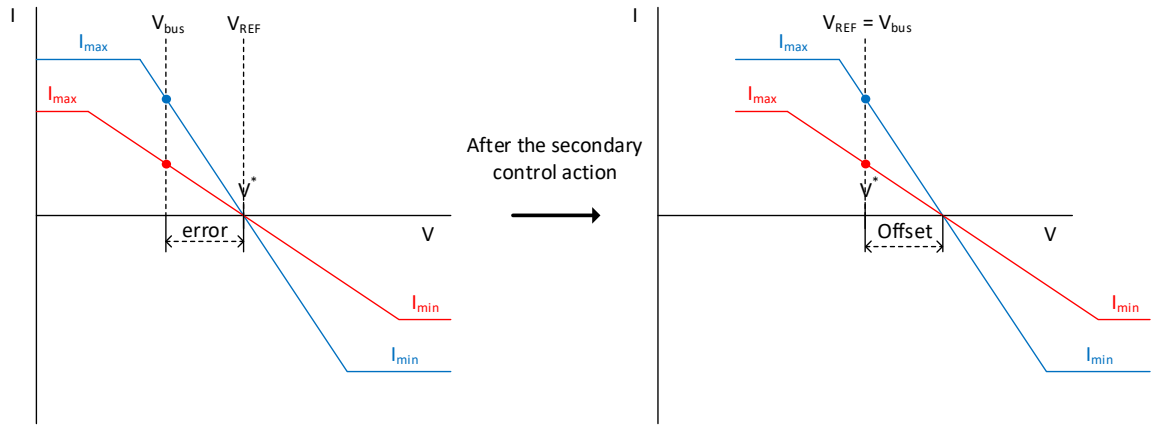


*Figure 37. Qualitative behaviour of the secondary control for two converters*

### 3.3.3. Tertiary control

In contrast to the secondary control, the goal of the tertiary control is to fix the power at a desired power reference. It does so by adding or subtracting a horizontal offset to each individual converter of the microgrid. It must be said that the total power of the system is fixed by the load and, for that the reason, the tertiary control only acts in all the converters except one to not over determinate the system. The converter without tertiary control is called usually as *slack* converter, giving or absorbing the remaining power flow.

Figure 38 shows an example of the Droop control with all three levels and only two converters. Each converter has its own primary control, the secondary control is made by a common proportional-integrator controller which generates and horizontal offset to both converters to stabilize the voltage of the bus and the tertiary control is made by another proportional-integrator controller which generate an offset to one converter to fix the power given by it.

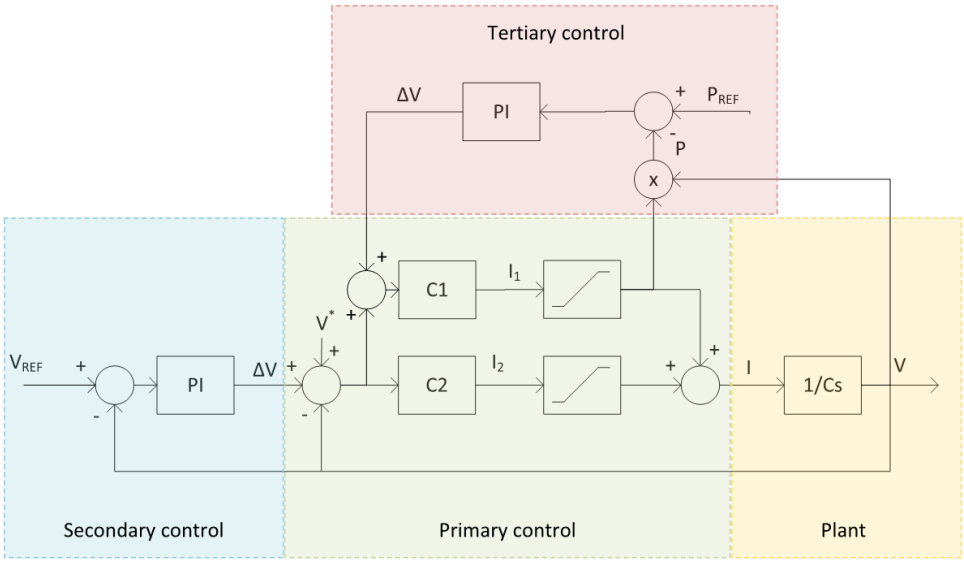


*Figure 38. Block diagram of the primary, secondary and tertiary control*

Figure 39 shows a qualitative behaviour of the secondary and the tertiary control for to converters to a perturbation. In this case, the blue converter where the tertiary control is applied is set to deliver a slightly lower current than the red one.

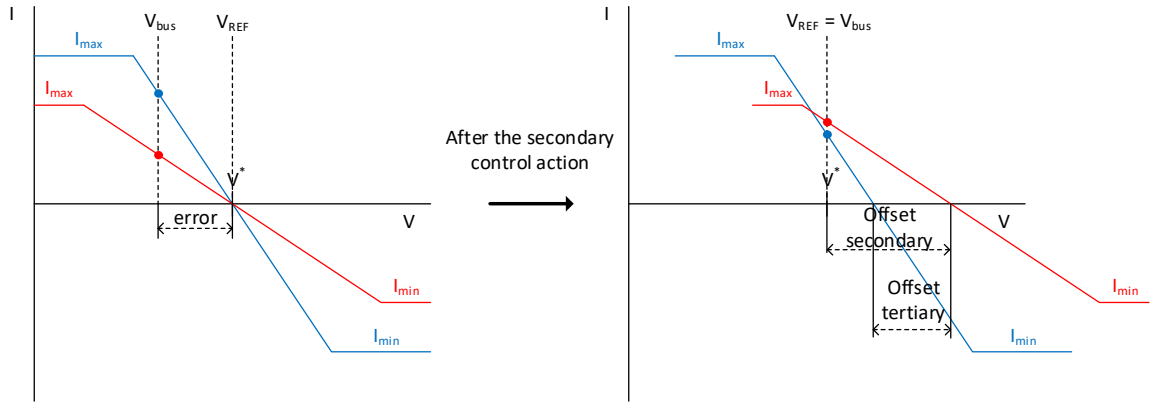


*Figure 39. Qualitative behaviour of the secondary and tertiary control for two converters*

## 3.4. Primary control

As it is explained in the previous section, the primary control is made implementing characteristic I-V curves for both converters. These curves are limited by the power of the converter and the battery capacity. The objective of this section is two define these curves for both converters.

To start the design, the converter is initially supposed to be ideal and its response is supposed to be instantaneous. For that reason, the plant is modelled as current sources, which replace the two converters with their batteries, the bus capacitor and finally a controlled current source which simulate the perturbation generated by the inverter when exchanging power with the grid.

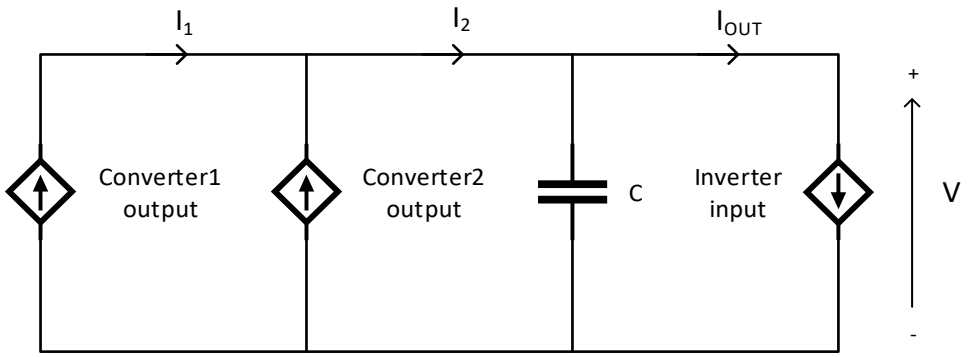


*Figure 40. Simplified system*

The easiest curves are the linear ones where the maximum power of the converter, the current limit and voltage limit of some components and the battery capacity should be taken into account. Accordingly, there will have saturations in the current output. Therefore, taking into account the simplified system and these saturations, the block diagram of the system is the same that was shown in Figure 35.

When doing the calculations, the saturations add discontinuities and consequently make the analysis much more complicated. For this reason, the saturations are not taken into account when defining the curves but afterwards, this effect is analysed and the system is simulated to make sure that the result is as expected. The resulting block diagram is shown in Figure 41.

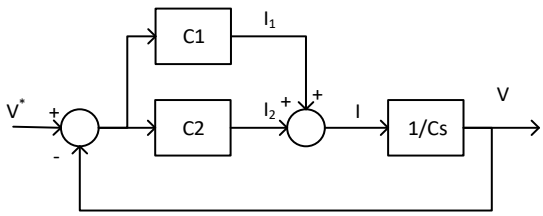


*Figure 41. Block diagram of the primary control without saturation*

Besides the primary control, there is also the converter which have to be taken into account. As it is explained before, the control of the converter is made by an open loop calculation and change instantly the phase between the PWMs when the reference change is applied. Therefore, ideally, the transformer current also change instantly, making the output/input (depending on the power flow) CL filter responsible of the overall dynamic behaviour of the converter. For this reason, a digital filter is applied to the reference. This digital filter has as objectives the softening of the response, to avoid possible unwanted ripples produced by the output/input if a current step is applied and to fix the overall behaviour of the converter. Therefore, the converters of the system can be modelled as a digital filter and a CL filter. The resulting block diagram is represented in Figure 42.

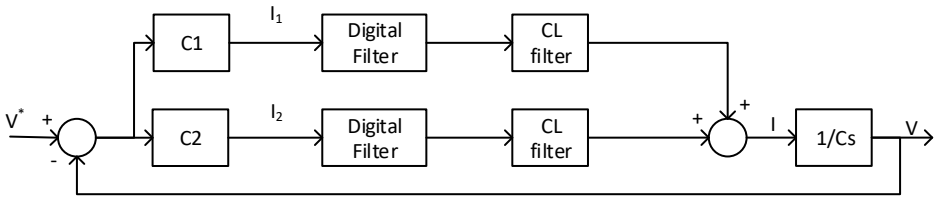


*Figure 42. Block diagram of the primary control with the converter*

The digital filter is a first order one with a time constant of 1 ms and the CL filter is composed by a 120 µF capacitor and a 4,4 µH inductor. In order to estimate the overall behaviour of the converter, a simulation is done. This simulation consists in applying a current step to the CL filter (Figure 43a), to the first order delay (Figure 43b) and to the sum of both ((Figure 43c). The results of the simulations are shown in the Figure 44.

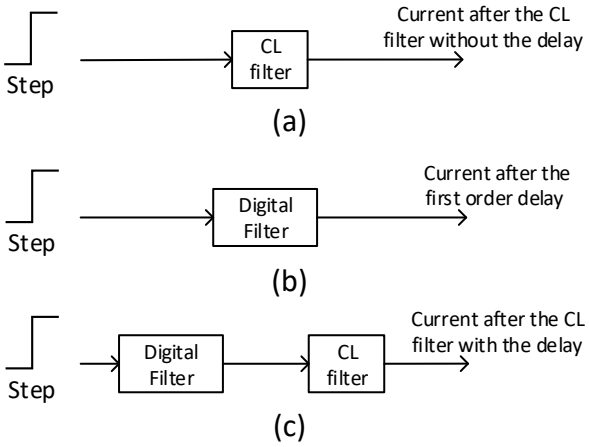


*Figure 43. Simulation diagrams to estimate the converter behaviour*

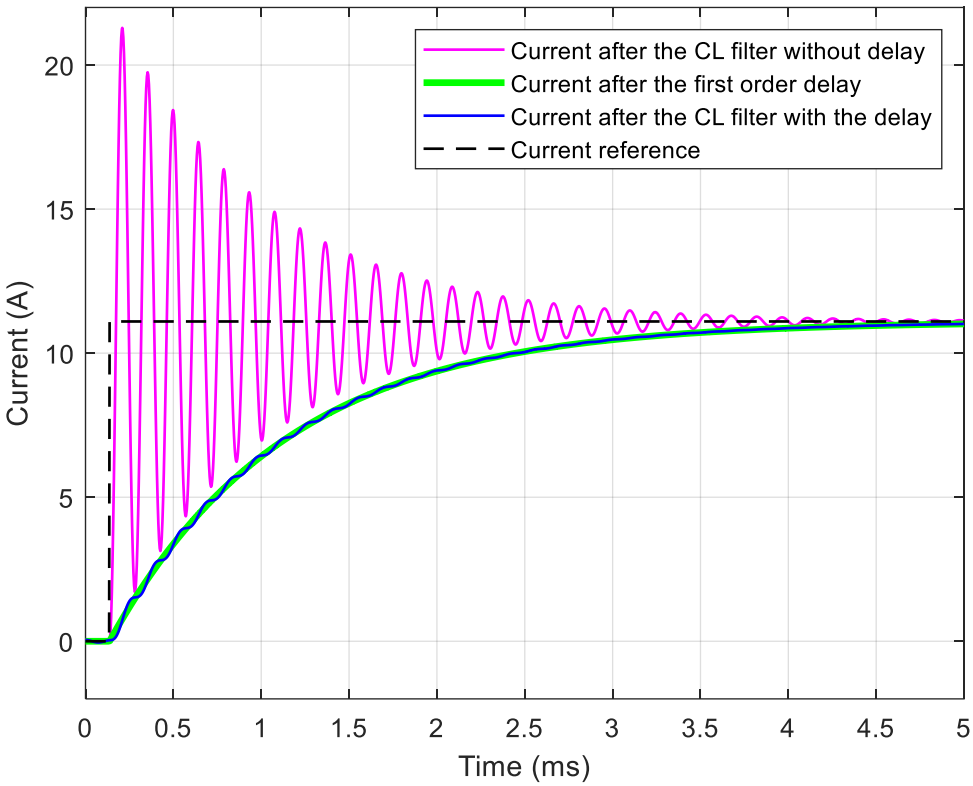


*Figure 44. Response of the current to a step input in different situations*

As it can be seen in Figure 44, the response of the CL filter is a second order one with heavy oscillations. Therefore, the digital filter was designed initially to have the same stabilization time than the CL filter but avoiding the oscillations and being a first order one. As the response of the filter is much faster than the digital filter, the overall behaviour can be supposed to be only the first order delay as it was wanted and therefore, all the converter can be simplified as this first order delay. The final block diagram with these first order delays are represented in Figure 45.

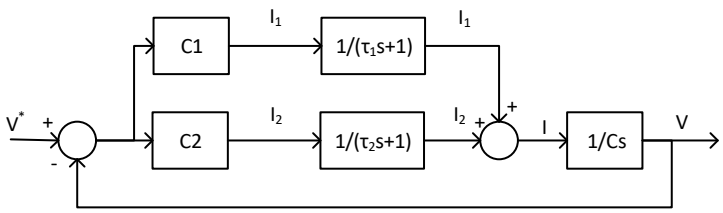


*Figure 45. Block diagram of the primary control with first order delays*

Where $\tau_1$ and $\tau_2$ are the time constants of the first order delays of each converter, C1 and C2 are the slopes of each curve, $V^*$ set the 0 A output, V is the bus voltage and C is the capacitance of the bus capacitor. C1 and C2 are positive because the negative factor of the slope is accomplished by the subtraction of $V^*$ and V.

### 3.4.1. Stability analysis

According to Figure 45 the transfer function is shown in ( 9 ).

$$\frac{V(s)}{V^*(s)} = \frac{s(C_1\tau_2 + C_2\tau_1) + (C_1 + C_2)}{s^3(C\tau_1\tau_2) + s^2(C\tau_1 + C\tau_2) + s(C + C_1\tau_2 + C_2\tau_1) + (C_1 + C_2)} \quad (9)$$

If both converters are equal, and consequently they have the same time constant, the resulting transfer function is the expressed in ( 10 ).

$$\frac{V(s)}{V^*(s)} = \frac{C_1 + C_2}{s^2C\tau + sC + (C_1 + C_2)} \quad (10)$$

Where $\tau = \tau_1 = \tau_2$ are the time constants of the first order delays of each converter, $C_1$ and $C_2$ are the slopes of each curve, $V^*$ set the 0 A output, $V$ is the bus voltage and $C$ is the capacitance of the bus capacitor.

In order to ensure the stability of the system all the poles of ( 10 ) must have negative real part. Therefore, the poles are determined by the equation in ( 11 ).

$$p_{1,2} = \frac{-C \pm \sqrt{C^2 - 4\,C\,\tau\,(C_1 + C_2)}}{2\,C\,\tau} \quad (11)$$

Analysing ( 11 ), there are different possibilities in function of the result of the square root. The first one is having a 0 result of the square root and ( 12 ) is obtained as the expression for the poles.

$$C^2 - 4\,C\,\tau\,(C_1 + C_2) = 0$$

$$p_{1,2} = -\frac{1}{2\,\tau}\ (\text{double}) \quad (12)$$

As $\tau$ is always positive, the poles will have a negative real part and consequently, the system will be stable.

The next possibility is to have a complex result of the square root, equation ( 13 ) shows the expression for the poles.

$$C^2 - 4\,C\,\tau\,(C_1 + C_2) < 0$$

$$p_{1,2} = \frac{-C \pm \sqrt{C^2 - 4\,C\,\tau\,(C_1 + C_2)}}{2\,C\,\tau} \rightarrow \mathrm{Re}(p_{1,2}) = -\frac{1}{2\,\tau} \quad (13)$$

Then, with the same reasoning than before, the system will be stable because $\tau$ is always positive. The last possibility is to have a real result of the square root and the equations obtained are ( 14 ) and ( 15 ).

$$C^2 - 4\,C\,\tau\,(C_1 + C_2) > 0$$

$$p_1 = \frac{-C - \sqrt{C^2 - 4\,C\,\tau\,(C_1 + C_2)}}{2\,C\,\tau} \quad (14)$$

$$p_2 = \frac{-C + \sqrt{C^2 - 4\,C\,\tau\,(C_1 + C_2)}}{2\,C\,\tau} \quad (15)$$

In ( 14 ), as $C$ is always positive, $\tau$ is also always positive and $C^2 - 4\,C\,\tau\,(C_1 + C_2)$ is also positive, the real part of this pole will be negative. Now, considering the pole obtained in ( 15 ), the following expressions can be deduced.

$$\frac{-C + \sqrt{C^2 - 4\,C\,\tau\,(C_1 + C_2)}}{2\,C\,\tau} < 0 \qquad (16)$$

$$\frac{1}{2\,\tau} > \frac{\sqrt{C^2 - 4\,C\,\tau\,(C_1 + C_2)}}{2\,C\,\tau} \qquad (17)$$

$$C^2 > C^2 - 4\,C\,\tau\,(C_1 + C_2) \qquad (18)$$

$$-4\,C\,\tau\,(C_1 + C_2) < 0 \qquad (19)$$

As ( 19 ) will be fulfilled for any value positive value of $C, \tau, C_1$ and $C_2$, the real part of the pole will be negative and the system will be stable.

Finally, as a conclusion of the stability analysis, as $\tau$ is a positive time constant, $C$ is a positive value for the capacitor and $C_1$ and $C_2$ are the selected slopes which will be positive, the poles of the system will always have negative real part and therefore, the system will be stable.

### 3.4.2. Considerations of the system

According to the system characteristics, operation voltage limits must be set. Taking into account the voltage ripple caused by the single-phase consumptions that can be after the inverter and the bus voltage limits for the inverter operation, the maximum voltage of the primary control curve ies defined as, ( 20 ).

$$V_{droop_{max}} = V_{bus_{max}} - \frac{\Delta V}{2} = 820 - \frac{40}{2} = 800\,V \qquad (20)$$

The same reasoning can be applied for the lower limit, ( 21 ).

$$V_{droop_{min}} = V_{bus_{min}} + \frac{\Delta V}{2} = 700 + \frac{40}{2} = 720\,V \qquad (21)$$

The easiest reasoning is centring the 0 A in the middle, ( 22 ).

$$V^* = \frac{V_{bus_{max}} + V_{bus_{min}}}{2} = 760\,V \qquad (22)$$

Now, the limitations of each pair of battery and converter are searched. This is done by taking into account the maximum charge/discharge current and the voltage limits of the batteries and the maximum power of the converter, ( 23 ).

$$P_{max} = MIN(P_{converter}, P_{bat}) \qquad (23)$$

The maximum power of the battery is calculated in the worst case scenario for the primary control, ( 24 ). This is when the battery can give the maximum power, because as the primary control acts in the output current of the converter, when the power of the battery

decreases, the output current does the same and therefore, the bus voltage stays in-between the limits.

$$P_{battery} = V_{max}\, I_{max} \quad (24)$$

From now on the Lithium battery and its converter are referred as “1” or first converter and the Lead battery and its converter as “2” or second converter.

$$P_{bat1} = V_{1_{max}}\, I_{1_{max}} = 387 * 90 = 34{,}83\ kW \quad (25)$$

$$P_{bat2} = V_{2_{max}}\, I_{2_{max}} = 280 * 100 = 28\ kW \quad (26)$$

Therefore, the maximum power of each pair is:

$$P_{1_{max}} = MIN(P_{converter}, P_{bat1}) = MAX(20\ kW, 34{,}83\ kW) = 20\ kW \quad (27)$$

$$P_{2_{max}} = MIN(P_{converter}, P_{bat2}) = MAX(20\ kW, 28\ kW) = 20\ kW \quad (28)$$

Finally, the maximum power of each pair is set by the maximum power of both converters and, consequently, the limits for the Droop DC curves will be also set by these maximums.

### 3.4.3. Virtual resistance

Once known the voltage and power limits, the virtual resistance limits can be set. Assuming that the converter is considered to be ideal and lossless, the equation to define the maximum slope allowed to fulfil the voltage limits can be extracted from ( 29 ) which expresses the relation between the slope and two points, in this case the current at $V^*$ and the current at the minimum voltage. Finally, the maximum allowed slope can be expressed as known values in ( 30 )

$$C_{i_{max}} = \frac{I_{V^*} - I_{max}}{V^* - V_{min}} \quad (29)$$

$$C_{i_{max}} = \frac{0 - \frac{P_{i_{max}}}{V^*}}{V^* - (V^* - \Delta V_{max})} = \frac{P_{i_{max}}}{V^*\, \Delta V_{max}} \quad (30)$$

Where $V^*$ is the voltage defined in ( 22 ), $P_{i_{max}}$ is the maximum power defined in ( 27 ) or ( 28 ) as they are the same and $\Delta V_{max}$ is the maximum excursion of the bus voltage and is defined in ( 31 ).

$$\Delta V_{max} = V^* - V_{droop_{min}} = 760 - 720 = 40\ V \quad (31)$$

Therefore, the virtual resistance is the inverse of the slope and as both pairs of converter and battery have the same power, the virtual resistances will be the same, ( 32 ).

$$R_{vi_{max}} = \frac{1}{C_{i_{max}}} = \frac{V^*\, \Delta V_{max}}{P_{i_{max}}} = \frac{760 * 40}{20000} = 1{,}52\ \Omega \quad (32)$$

As both batteries are different and, consequently, it is desired that the two batteries have different behaviours by selecting different virtual resistances. A criterion to select the

relation between virtual resistance or slopes is determined by the battery characteristics. As the Lithium battery suffer less with rapid changes in its current, it should have a bigger slope or lower virtual resistance. Moreover, the stored energy of the Lithium battery is bigger than the energy of the Lead one. In order to take profit of all energy and make the two batteries discharge at the same time (equation ( 33 ) must be fulfilled), the relation between slopes, $k_{R_v}$ should be the relation between energies (expressed in ( 34 )) which also fulfil the condition that the Lithium battery should have a bigger slope.

$$E_2\, k_{R_v} = E_1 \rightarrow P_1\, dt\, k_{Rv} = P_2\, dt \rightarrow \frac{V^{*2}\, dt}{R_{v2}} k_{Rv} = \frac{V^{*2}\, dt}{R_{v1}} \quad (33)$$

$$k_{Rv} = \frac{R_{v2}}{R_{v1}} = \frac{E_1}{E_2} = \frac{30}{18} = 1{,}6 \quad (34)$$

Applying the obtained relation obtained in ( 34 ) and the maximum resistance value obtained in ( 32 ), the maximum values of the virtual can be expressed as ( 35 ) and ( 36 ).

$$R_{v2} < 1{,}52\ \Omega \quad (35)$$

$$R_{v1} < \frac{R_{v2}}{k_{Rv}} \rightarrow R_{v1} < 0{,}91\ \Omega \quad (36)$$

Therefore, plotting the acceptable area for the I-V curves of the primary control, the Figure 46 is obtained.

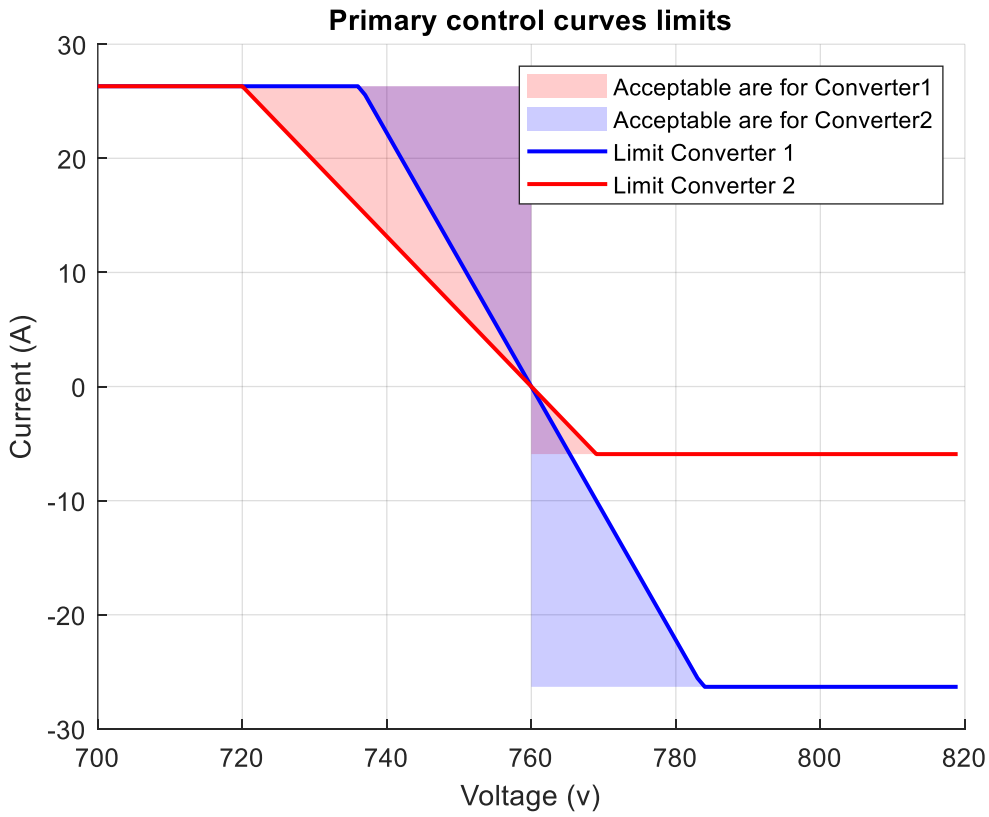


*Figure 46. Primary control curve limits and acceptable area*

As the current limits of the Lead battery for charging and discharging have not the same value, the resulting profitable area of the primary control is reduced if the $V^*$ parameter is centred in the middle of the maximum and minimum bus voltage allowed. As it can be seen in Figure 46, the acceptable area can be expanded by recalculating the $V^*$ parameter. This way, the maximum allowed virtual resistances also can be increased.

Knowing that the limit corresponding to the minimum voltage (equation ( 21 )) will be set by the converter 2, the limit corresponding to the maximum voltage (equation ( 20 )) will be set by the converter 1 and the relation between the two virtual resistances (equation ( 34 )), the $V^*$and the maximum values of $R_{v1}$ and $R_{v2}$ can be recalculated.

$$R_{v1}\, k_{Rv} = R_{v2} \rightarrow \frac{1}{C_1}\, k_{Rv} = \frac{1}{C_2} \qquad (37)$$

$$V^* \frac{V_{droop_{max}} - V^*}{P_{1_{max}}} k_{Rv} = V^* \frac{V^* - V_{droop_{min}}}{P_{2_{max}}} \rightarrow V^* = 770\ V \qquad (38)$$

$$R_{v1} < 1{,}15\ \Omega \qquad (39)$$

$$R_{v2} < 1{,}92\ \Omega \qquad (40)$$

With these new values (equations ( 38 ), ( 39 ) and ( 40 )) the acceptable area for the I-V curves of the primary control is different as shown in Figure 47.

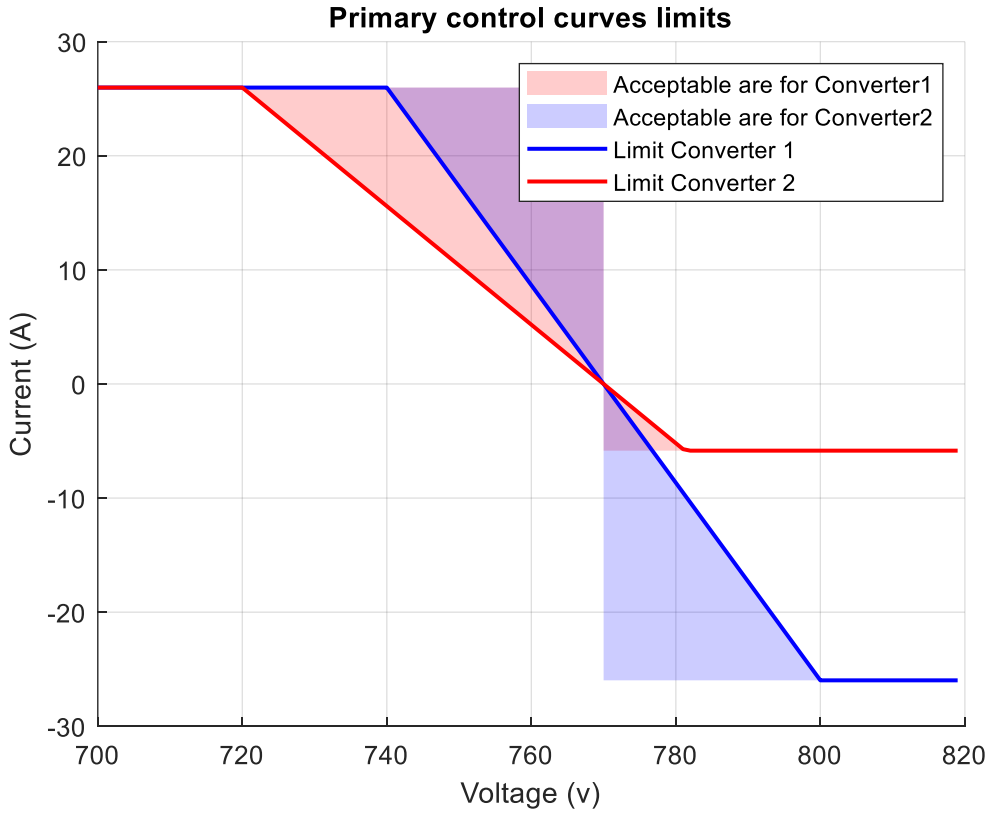


*Figure 47. Recalculated primary control curve limits and acceptable area*

Now the acceptable limits go from $V_{droop_{min}}$ to $V_{droop_{max}}$ and the limits of the virtual resistances are slightly greater. The equations ( 41 ) and ( 42 ) show the final acceptable limits for the two virtual resistances.

$$0 < R_{v1} < 1{,}15\ \Omega \quad (41)$$

$$0 < R_{v2} < 1{,}92\ \Omega \quad (42)$$

Now, the exact values of the virtual resistances are calculated according to the dynamic behaviour of the system and taking into account the previous limits. Therefore, starting from the system equation ( 10 ) and supposing it has two real poles $-A$ and $-B$, the characteristic equation of the system can be expressed as the equation of the poles, ( 43 ).

$$s^2 C\tau + sC + (C_1 + C_2) = (s + A)(s + B) \quad (43)$$

Using the expression ( 43 ) which relates the characteristic equation of the system with the poles equation, the expression ( 34 ) and supposing a proportional relation between $A$ and $B$ such as $A = k_{poles}\, B$, the values of the virtual resistances can be expressed as ( 44 ) and ( 45 ).

$$R_{v1} = \frac{\tau \left(k_{poles} + 1\right)^2 (k_{Rv} + 1)}{k_{Rv}\, k_{poles}\, C} \quad (44)$$

$$R_{v2} = \frac{\tau \left(k_{poles} + 1\right)^2 (k_{Rv} + 1)}{k_{poles}\, C} \quad (45)$$

Where $\tau$ is the time constant of the converters, the $k_{R_v}$ is the relation between both virtual resistances, $C$ is the capacitance of the bus and $k_{poles}$ is the relation of the two real poles. The initial aim of this relation between poles is to be greater than 10, in order to have the response of one pole much faster than the other making it dominant and be able to simplify the system as a first order one. As trying values above ten of the $k_{poles}$ gives virtual resistances out of the limits expressed in ( 41 ) and ( 42 ), the expression ( 45 ) has been derived respect to $k_{poles}$ (expression ( 46 )) to find which value gives the minimum resistance.

$$\frac{\partial R_{v2}}{\partial k_{poles}} = \frac{2\,\tau \left(k_{poles} + 1\right)(k_{Rv} + 1)}{k_{poles}\, C} - \frac{\tau \left(k_{poles}^2 + 1\right)^2 (k_{Rv} + 1)}{k_{poles}^2\, C} = 0 \quad (46)$$

Therefore, solving to know the values of $k_{poles}$ which gives the minimum virtual resistance is obtained that $k_{poles} = \pm 1$ and consequently, supposing two real poles the virtual resistance should have the following limits.

$$1{,}48\ \Omega < R_{v2} < \infty \quad (47)$$

In order to have a visual idea of the function, Figure 48 shows the $R_{v2}$ in function of the $k_{poles}$.

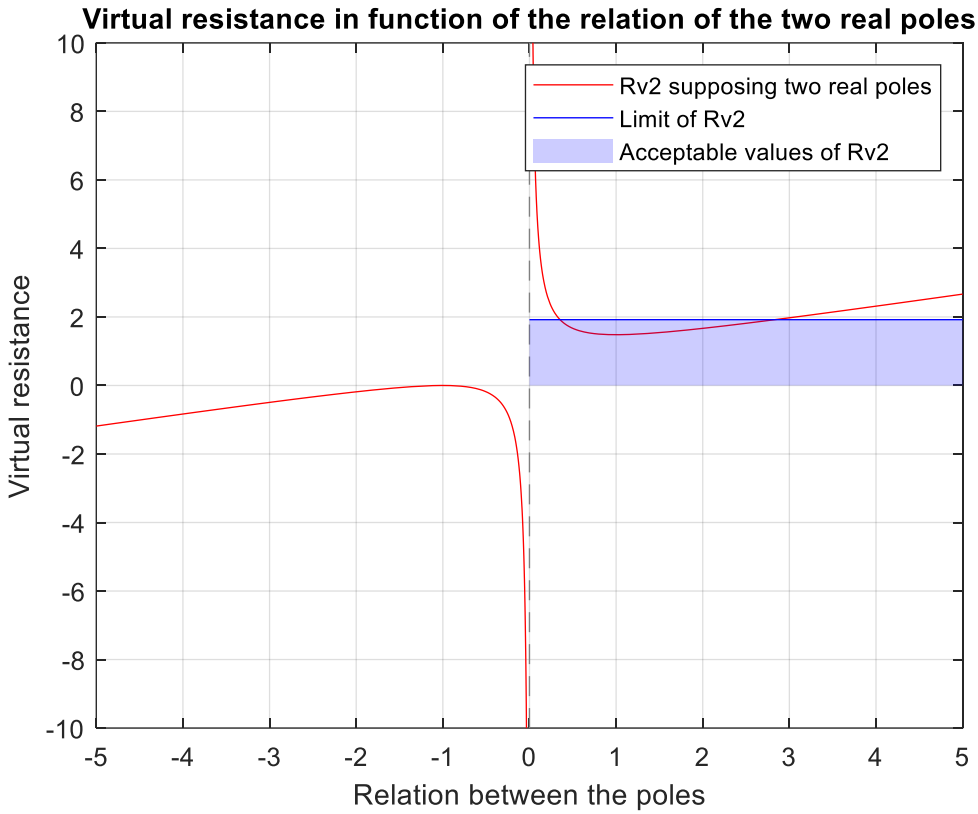


*Figure 48. Virtual resistance in function of the relation of the two real poles*

On the one hand, the assumption of having two real poles can be done without a dominance of one over the other, and, therefore, this assumption is discarded. On the other hand, it can be assumed to have two equal real poles. If this assumption is done, the values of the poles will be the ones expressed in ( 48 ), the virtual resistances will be the ones expressed in ( 49 ) and ( 50 ) and the overall time constant of the system will be 2 ms, ( 51 ).

$$p_1 = p_2 = 500 \quad (48)$$

$$Rv_1 = 0{,}89\ \Omega \quad (49)$$

$$Rv_2 = 1{,}48\ \Omega \quad (50)$$

$$\tau_{system} = 2\ ms \quad (51)$$

With these values, the expected behaviour of the system is shown in figures ( 43 ), ( 44 ) and ( 45 ).

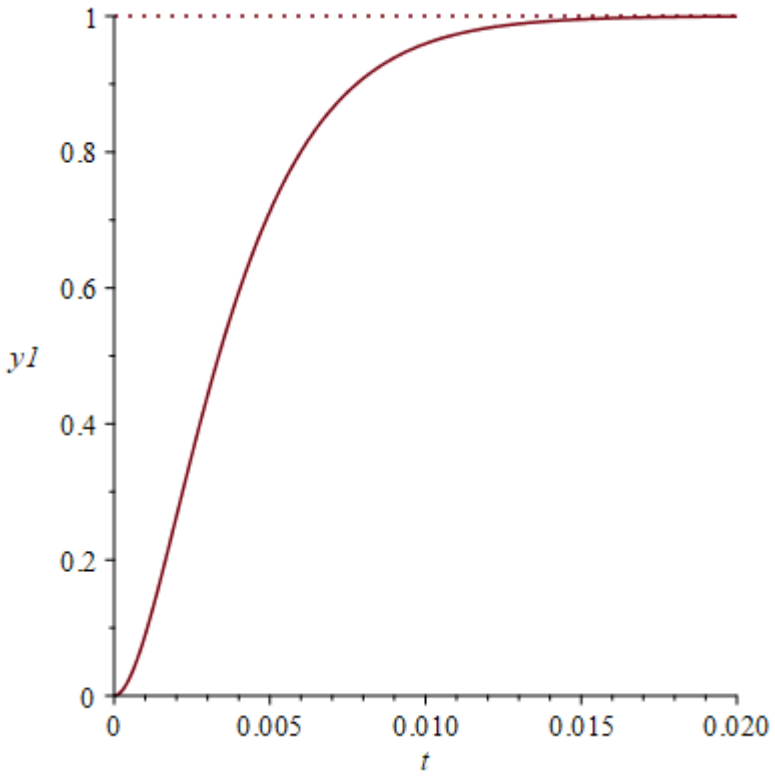


*Figure 49. Response of the voltage to a step input in $V^*$ assuming first order behaviour*

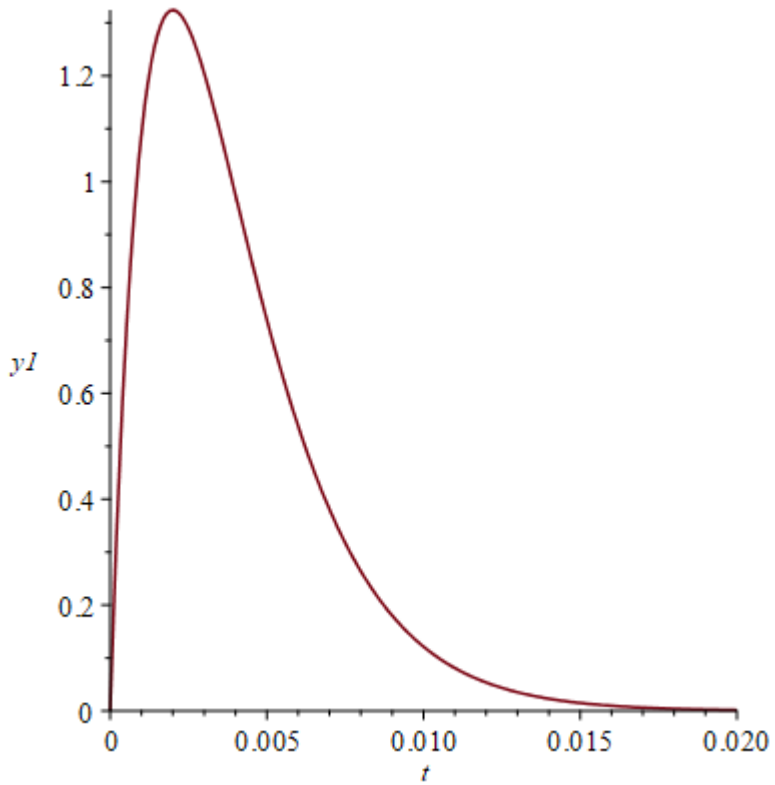


*Figure 50. Response of the current to a step input in $V^*$ assuming first order behaviour*

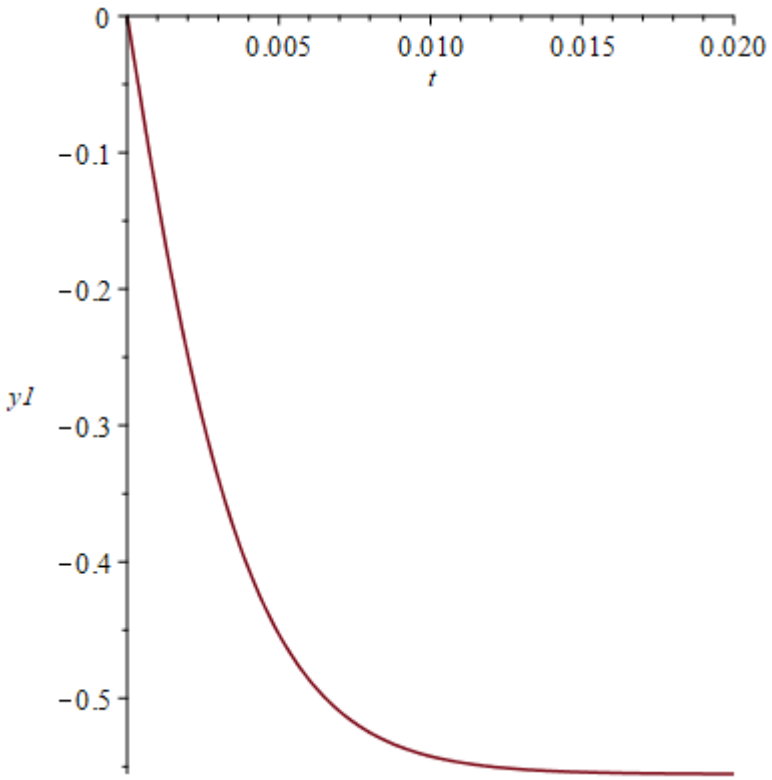


*Figure 51. Response of the voltage to a current perturbation assuming first order behaviour*

The other possibility is two have a pair of complex conjugate poles. Therefore, starting from the system equation ( 10 ) and supposing it a pair of complex conjugate poles, the characteristic equation of the system can be expressed as a second order equation, ( 52 ).

$$s^2 C\tau + sC + (C_1 + C_2) = s^2 + \chi\, w_n\, s + w_n^2 \qquad (52)$$

$$\chi = -ln(SP)\sqrt{\frac{1}{\pi^2 + ln(SP)^2}} \qquad (53)$$

Knowing also the expression to relate $\chi$ with the peak (expression ( 53 )) the virtual resistances can be expressed as ( 54 ) and ( 55 ).

$$R_{v1} = \frac{4\,\tau\, ln(SP)^2\,(k_{R_v} + 1)}{(\pi^2 + ln(SP)^2)\, k_{R_v}\, C} \qquad (54)$$

$$R_{v2} = \frac{4\,\tau\, ln(SP)^2\,(k_{R_v} + 1)}{(\pi^2 + ln(SP)^2)\; C} \qquad (55)$$

Where $\tau$ is the time constant of the converter, the $k_{R_v}$ is the relation between both virtual resistances, $C$ is the capacitance of the bus and $SP$ is the maximum peak in pu.

Having these equations (expression ( 54 ) and ( 55 )), the virtual resistances are selected according to the system response. Trying to minimize the peak, a swept of this peak from the minimum value is done to see the response of the system to different situations.

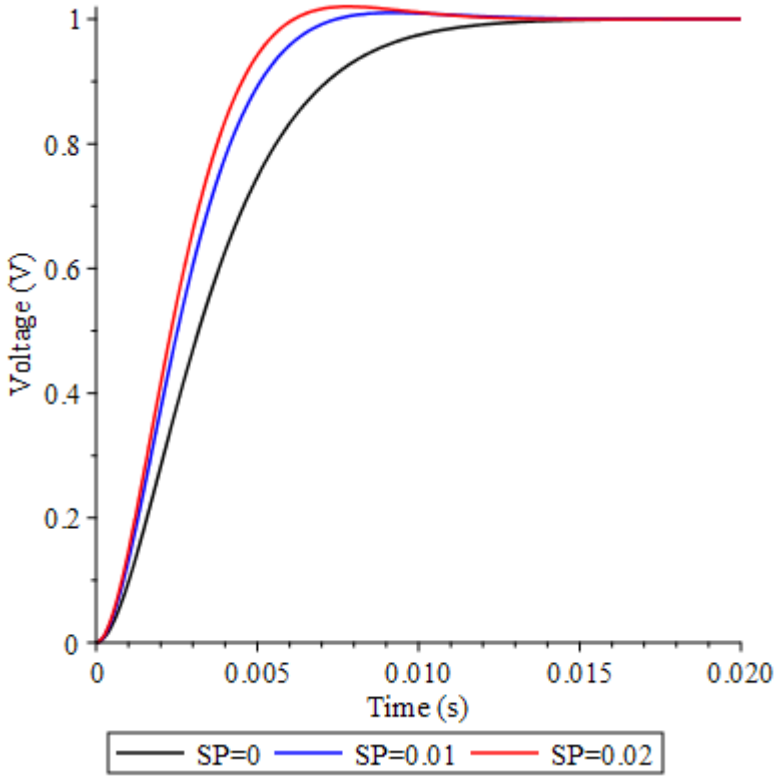


*Figure 52. Response of the voltage to a step input in $V^*$ with different SP*

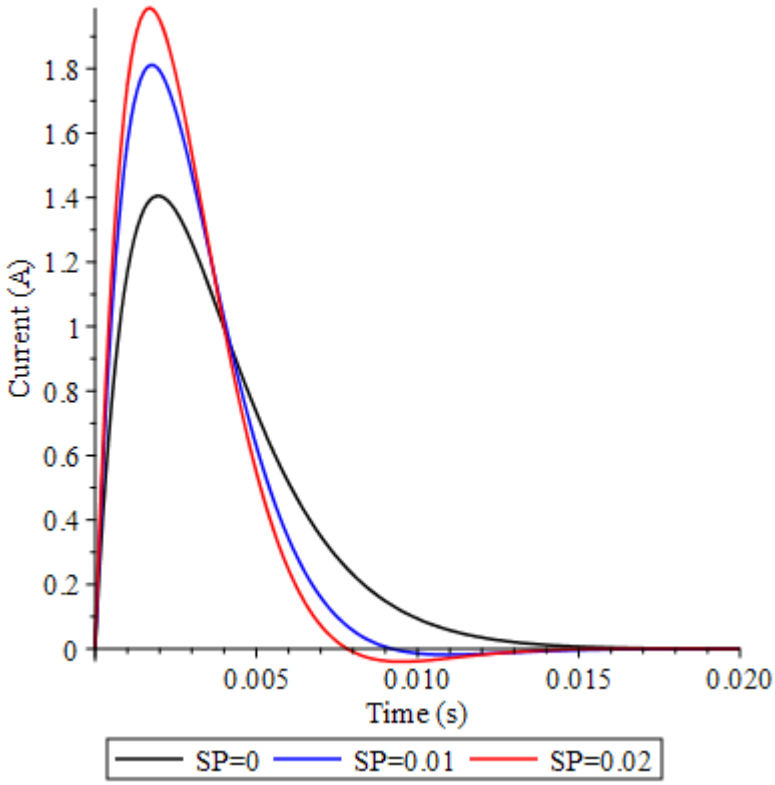


*Figure 53. Response of the current to a step input in $V^*$ with different SP*

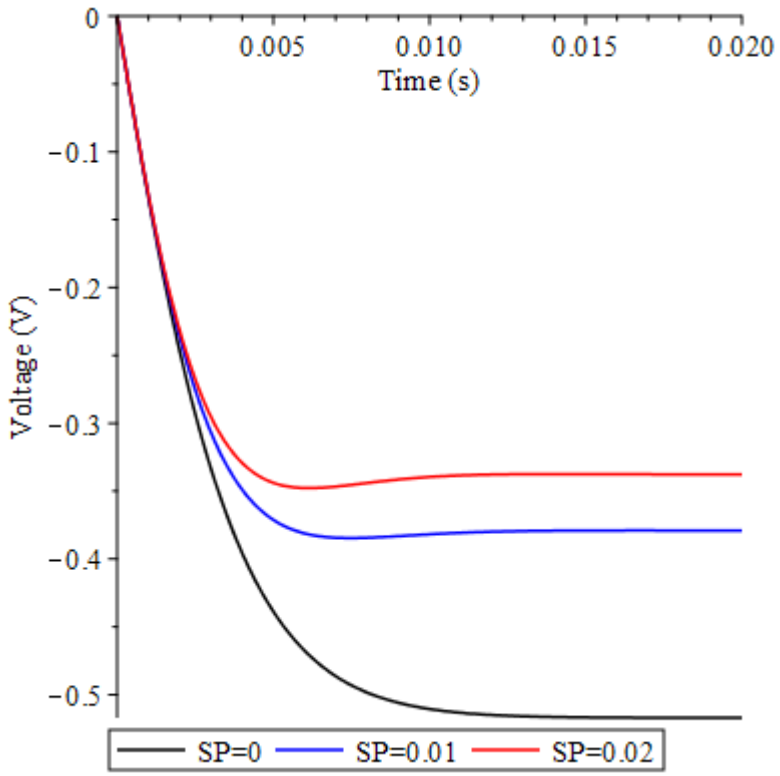


*Figure 54. Response of the voltage to a current perturbation step on the capacitor*

In Figure 52, Figure 53 and Figure 54 different responses of the system can be seen. The first one is the response to an input step and as expected, as the $SP$ increases the peak does it also. The response in current to the same input step has the same behaviour but, when a current perturbation is applied which will be the normal behaviour of the system, the voltage become stable in a higher value as the $SP$ is lower. Therefore, the best response to an input step is accomplish with lower $SP$ but, aversely, the best response to a current perturbation is accomplish with higher $SP$.

### 3.4.3.1. Final curves

The final selected behaviour is the second order one because its fast response, which is approximately two times faster than the first order one. Between the different behaviours according to $SP$, it is selected the $SP = 0.02$ because it gives the fastest response and the peak is considerably low and acceptable. Therefore, the final virtual resistances are calculated with expressions ( 54 ) and ( 55 ) and expressed in ( 56 ) and ( 57 ).

$$R_{v1} = 0{,}6\ \Omega \quad (56)$$

$$R_{v2} = 1{,}0\ \Omega \quad (57)$$

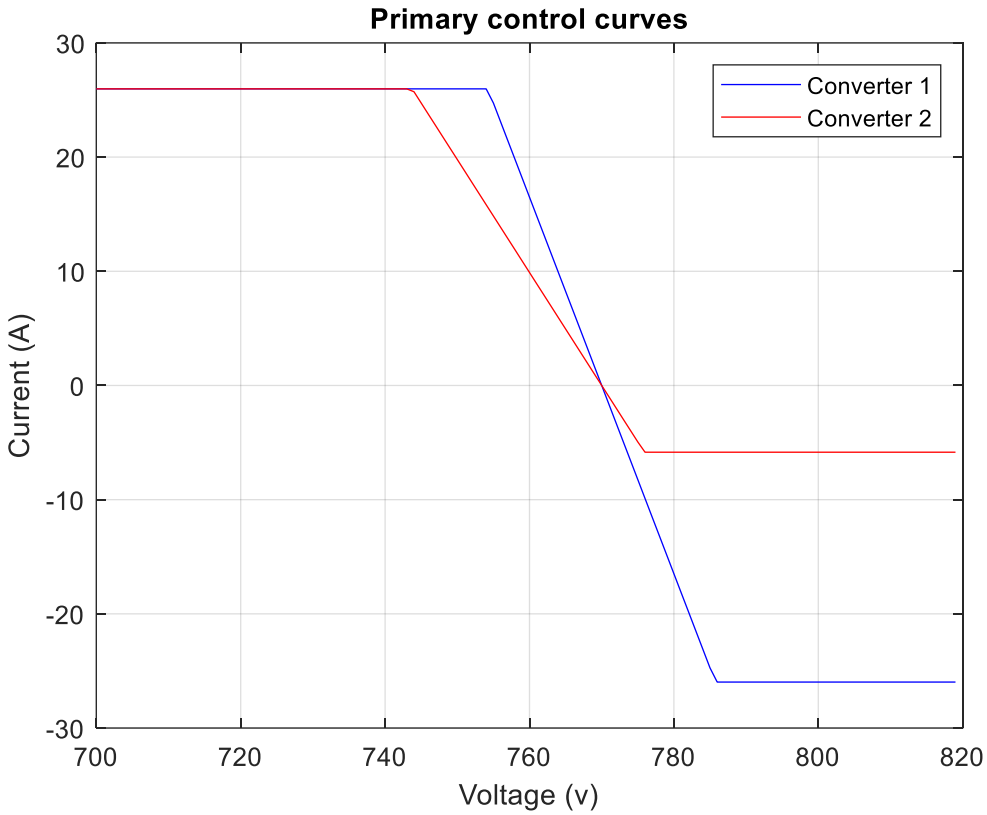


*Figure 55. Primary control curves*

### 3.4.4. Extension to more converters

When more than two converters are considered, the block diagram changes from the one presented before. If the microgrid is supposed to have N converters which behave as a first order delay, the resulting block diagram is shown in Figure 56.

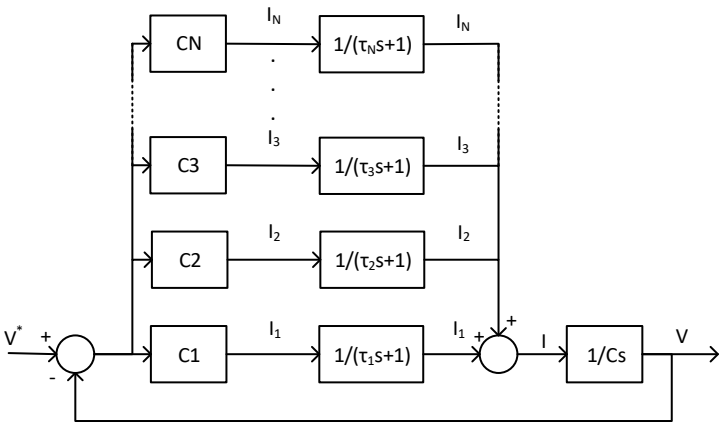


*Figure 56. Block diagram of the primary control with first order delays with N converters*

Therefore, the resulting transfer function when considering N converters has a variable order depending on the number of converters. For this reason and in order to make a criterion to extend the design to more converters, it is supposed that every converter act as a first order delay and that the time constant of all converters are the same. Although the converter can have different topologies, the overall behaviour of the converter can be

simplified to a much slower first order delay by adding this filter to the reference for example. The resulting transfer function of the system taking into account these assumptions is expressed in ( 58 ).

$$\frac{V(s)}{V^*(s)} = \frac{\sum_{i=1}^{N} C_i}{s^2 C\tau + sC + \sum_{i=1}^{N} C_i} \quad (58)$$

As, there can be N converters and each one with its slope, the analysis and the extension is made according to the sum of the N slopes of the converters, ( 59 ), and therefore, a criterion to select this sum is made to ensure an overall behaviour of the microgrid, but each individual slope will have to be selected afterwards according to other parameters.

$$CN = C_1 + C_2 + C_3 + \cdots + C_N \quad (59)$$

With these considerations, the resultant transfer function is ( 60 ).

$$\frac{V(s)}{V^*(s)} = \frac{CN}{s^2 C\tau + sC + CN} \quad (60)$$

According to Stability analysis, $CN$ must be greater than 0 to ensure stability, ( 61 ).

$$CN > 0 \quad (61)$$

Now, the behaviour of the primary control can be set as a first order behaviour supposing two real poles and making one of them dominant over the other or as a typical second order behaviour.

#### 3.4.4.1. First order behaviour

Starting with the first order behaviour, the characteristic equation can be expressed as a function of the two real poles $A$ and $B$, ( 62 ).

$$s^2 C\tau + sC + CN = (s + A)(s + B) \quad (62)$$

Using the expression ( 62 ) which relates the characteristic equation of the system with the poles equation and supposing a proportional relation between $A$ and $B$ such as $A = k_{poles}\, B$, the virtual resistances sum value, $CN$, can be expressed as ( 63 ).

$$CN = \frac{C\ k_{poles}}{\tau \left(k_{poles} + 1\right)^2} \quad (63)$$

In this assumption $B$ dominates over $A$ (taking into account $k_{poles} \gg 1$), so the stabilization time will only depend on $B$ following expression ( 64 ).

$$ts = \frac{4}{B} \quad (64)$$

Using ( 62 ) and ( 64 ), the stabilization time can be expressed in function of $k_{poles}$ and $\tau$, ( 65 ).

$$ts = 4\,\tau\,(k_{poles} + 1) \quad (65)$$

#### 3.4.4.2. Second order behaviour

Supposing a second order behaviour, it is supposed to have a pair of complex conjugate poles and consequently, the characteristic equation can be expressed as the second order equation, ( 66 ).

$$s^2 C\tau + sC + CN = s^2 + \chi\, w_n\, s + w_n^2 \quad (66)$$

With this expression ( 66 ), the sum of the virtual resistances can be expressed as ( 67 ).

$$CN = \frac{C}{4\,\chi^2\,\tau} \quad (67)$$

If it is a damped system, the sum of virtual resistances can also be expressed in function of the overshoot, $SP$. Using expression ( 53 ) to relate $\chi$ and $SP$, the expression ( 68 ) is obtained.

$$CN = \frac{(\pi^2 + ln(SP)^2)\,C}{4\,ln(SP)^2\,\tau} \quad (68)$$

### 3.5. Secondary control

As it is explained previously, the secondary control is often done by a PI controller with the aim of calculating an offset for the primary control in order to regulate the voltage to a desired value. This section objective is to select the values of this PI controller according to a desired dynamic behaviour while keeping the system stable.

Although the expected behaviour of this control is often needed to be relatively slow (with stabilization times above the second) because it is normally executed with a much lower frequency than the primary control by an external microcontroller. It is not the case of this system because there is a centralized powerful microcontroller, with two cores and two control law accelerators, which control both converters and execute the controls. Therefore, the controller is local and as there is no delay due to digital communications, so the control can be executed at the same frequency than the primary.

Taking into account the block diagram of the system with the secondary control (Figure 36) and the considerations of the primary control and the simplification of the converter to a first order delay, the resulting block diagram is shown in Figure 57.

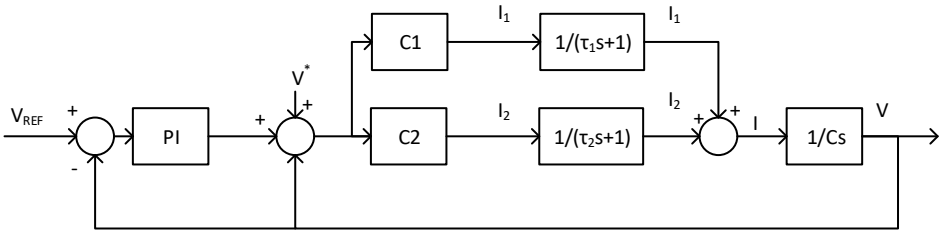


*Figure 57. Block diagram of the system with the primary and secondary control and the simplified converter*

From Figure 57, the transfer function of the whole system with the secondary control is obtained in ( 69 ) (the $V^*$ is considered as a perturbation).

$$\frac{V(s)}{V_{REF}(s)} = \frac{(k_p\, s + k_i)\left((C_1\,\tau_2 + C_2\,\tau_1)\, s + C_1 + C_2\right)}{X\, s^3 + Y\, s^2 + Z\, s + k_i\,(C_1 + C_2)} \qquad (69)$$

where,

$$X = C\,\tau_1\,\tau_2$$
$$Y = \left(\tau_2\left(k_p + 1\right) C_1 + \tau_1\left(k_p + 1\right) C_2 + C\right)$$
$$Z = \left(\left(k_i\,\tau_2 + k_p + 1\right) C_1 + C_2\left(k_i\,\tau_1 + k_p + 1\right)\right)$$

Considering both time constants equal such that $\tau = \tau_1 = \tau_2$, the equation ( 69 ) can be simplified to ( 70 ).

$$\frac{V(s)}{V_{REF}(s)} = \frac{\left(k_p\, s + k_i\right)(C_1 + C_2)}{C\,\tau\, s^3 + C\, s^2 + \left(k_p + 1\right)(C_1 + C_2)\, s + k_i\,(C_1 + C_2)} \qquad (70)$$

### 3.5.1. Stability analysis

To evaluate the stability of the system, as the characteristic equation is a third order one, the Routh–Hurwitz theorem has been applied. Expression ( 71 ) shows the result of this theorem.

$$\begin{array}{ccc} s^3 & C\,\tau & C_1\,k_p + C_2\,k_p + C_1 + C_2 \\ s^2 & C & C_1\,k_i + C_2\,k_i \\ s & C_1\,k_p + C_2\,k_p + C_1 + C_2 - \tau\,(C_1\,k_i + C_2\,k_i) & 0 \\ 1 & C_1\,k_i + C_2\,k_i & 0 \end{array} \qquad (71)$$

In order to ensure stability, the theorem affirms that must be no sign change in the first column, expression ( 72 ).

$$The\ system\ is\ stable\ if \begin{cases} C\,\tau > 0 \\ C > 0 \\ C_1\,k_p + C_2\,k_p + C_1 + C_2 - \tau\,(C_1\,k_i + C_2\,k_i) > 0 \\ C_1\,k_i + C_2\,k_i > 0 \end{cases} \qquad (72)$$

Taking the theorem into account, knowing that $C$, $\tau$, $C_1$ and $C_2$ are positive and imposing that $k_i$ and $k_p$ must be positive to avoid zeros in the right half-plane, the conditions that $k_i$ and $k_p$ must follow to accomplish system stability can be deduced, ( 73 ).

$$The\ system\ is\ stable\ if \begin{cases} k_p > 0\ and\ k_p > \tau\,k_i - 1 \\ k_i > 0 \end{cases} \qquad (73)$$

### 3.5.2. Controller tuning

As $k_p$ and $k_i$ should be selected according to the dynamic behaviour while keeping the stability of the system and the characteristic equation is a third order one, a dominance of

poles or zero cancelation should be done. To make these calculations, the characteristic equation of the system is expressed as the equation of the poles, ( 74 ).

$$C\,\tau\,s^3 + C\,s^2 + \left(k_p + 1\right)(C_1 + C_2)\,s + k_i\,(C_1 + C_2) = (s + A)(s + (B + E\,i))(s + (B - E\,i)) \quad (74)$$

It must be taking into account that, although the equation ( 74 ) is expressed as the combination of one real pole and a pair of complex conjugate poles, this equation ( 74 ) can be expressed as a combination of three real poles if $E$ is a complex number. Simplifying ( 74 ) and collecting the terms of s, the resulting expression is ( 75 ).

$$s^3 + \frac{s^2}{\tau} + \frac{\left(k_p + 1\right)(C_1 + C_2)}{C\,\tau}s + k_i\frac{C_1 + C_2}{C\,\tau} = s^3 + (A + 2\,B)\,s^2 + (2\,A\,B + B^2 + E^2)s + A\,(B^2 + E^2) \quad (75)$$

From now, the calculations must be done according to the assumption of having one dominant real pole, having a pair of dominant complex conjugate poles or simplifying the expression with a zero cancelation.

#### 3.5.2.1. One dominant real pole

As it is wanted to make one pole dominant, all the parameters should be calculated according to this pole. In this case, the dominant pole will be $A$.

Taking a look to the terms of $s^2$ a relation between $A$ and $B$ can be expressed as ( 76 ).

$$B = \frac{1}{2\,\tau} - \frac{A}{2} \quad (76)$$

Therefore, in order to ensure stability, all the poles should be negative which means that $B$ must be positive. According to this, a maximum value for $A$ can be found to ensure stability, ( 77 ).

$$A < \frac{1}{\tau} \quad (77)$$

With the expression ( 75 ), the constant terms and the term of $s$, the $k_p$ and $k_i$ can be expressed in functions of $A$, $E$, $C_1$, $C_2$ $C$ and $\tau$, resulting in expressions ( 78 ) and ( 79 ).

$$k_p = -\frac{3\,A^2\,C\,\tau^2 - 4\,C\,E^2\,\tau^2 - 2\,A\,C\,\tau + 4\,C_1\,\tau + 4\,C_2\,\tau - C}{4\,\tau\,(C_1 + C_2)} \quad (78)$$

$$k_i = A\,C\,\frac{A^2\,\tau^2 + 4\,E^2\,\tau^2 - 2\,A\,\tau + 1}{4\,\tau\,(C_1 + C_2)} \quad (79)$$

Having $k_p$ snd $k_i$ expressed as ( 78 ) and ( 79 ), respectively, the zero of the system can also be found in function of the same parameters, $A$, $E$, $C_1$, $C_2$ $C$ and $\tau$. Therefore, the zero of the system is expressed as ( 80 ).

$$z = -\frac{A\,C\,(A^2\,\tau^2 + 4\,E^2\,\tau^2 - 2A\,\tau + 1)}{3\,A^2\,C\,\tau^2 - 4\,C\,E^2\,\tau^2 - 2\,A\,C\,\tau + 4\,C_1\,\tau + 4\,C_2\,\tau - C} \quad (80)$$

In this assumption, the real pole should dominate over the other poles and over the zero of the system which means that $A$ must be much lower than the other poles and the zero, expressions ( 81 ) and ( 82 ), respectively.

$$A \ll B \quad (81)$$

$$A \ll z \quad (82)$$

With ( 76 ) and ( 81 ) and supposing a dominance is accomplished only if $A$ is lower than ten times $B$, the condition ( 83 ) should be fulfilled by $A$ (for both assumptions, having three real poles and having one real pole and a pair of complex conjugate poles).

$$A < \frac{1}{21\,\tau} \quad (83)$$

With the expression ( 80 ) and ( 82 ), the function of $E$ to dominate over the zero is given by ( 84 ).

$$E = \frac{\sqrt{C\,(31\,A^2\,C\,\tau^2 - 22\,A\,C\,\tau + 40\,C_1\,\tau + 40\,C_2\,\tau - 9\,C)}}{6\,C\,\tau} \quad (84)$$

Figure 58 plots equation (73) to give a graphical information about the poles dominance.

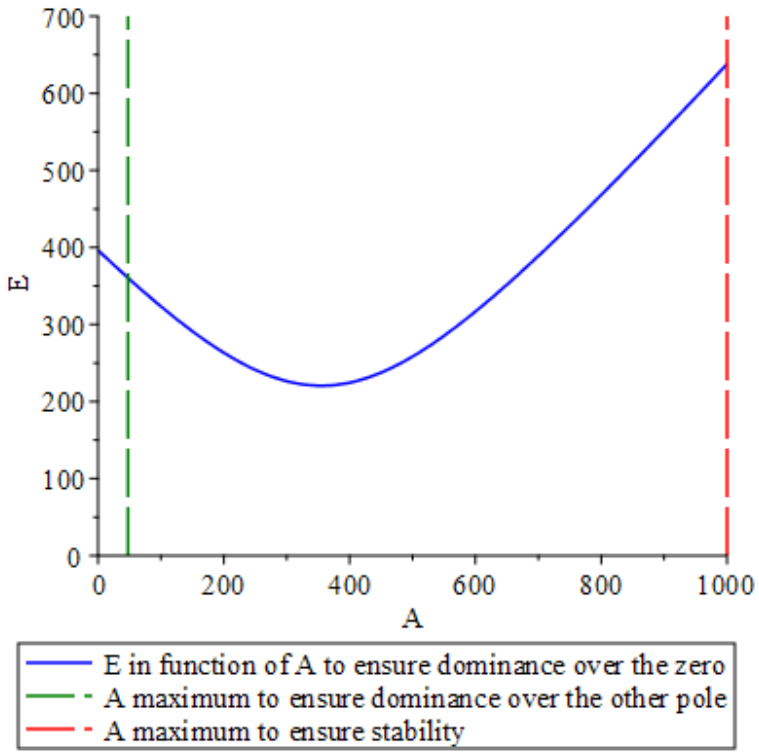


*Figure 58. A to ensure the dominance of the simple real pole over the zero*

Therefore, a dominance of the real pole over the other poles and the zero is possible if it expressions ( 83 ) and ( 84 ) are fulfilled. In order to have the fastest system possible, $A$ must be as big as possible. For this reason, $A$ is selected to be $\frac{1}{21\,\tau}$ and consequently, the overall time constant of the system will be $21\,\tau$. With these values, the resultant values for

$k_p$ and $k_i$ are expressed in ( 85 ) and ( 86 ), and the response of the system to a $V_{REF}$ step and a current perturbation are shown in Figure 59 and Figure 60.

$$k_p = 0{,}097 \quad (85)$$

$$k_i = 46{,}36 \quad (86)$$

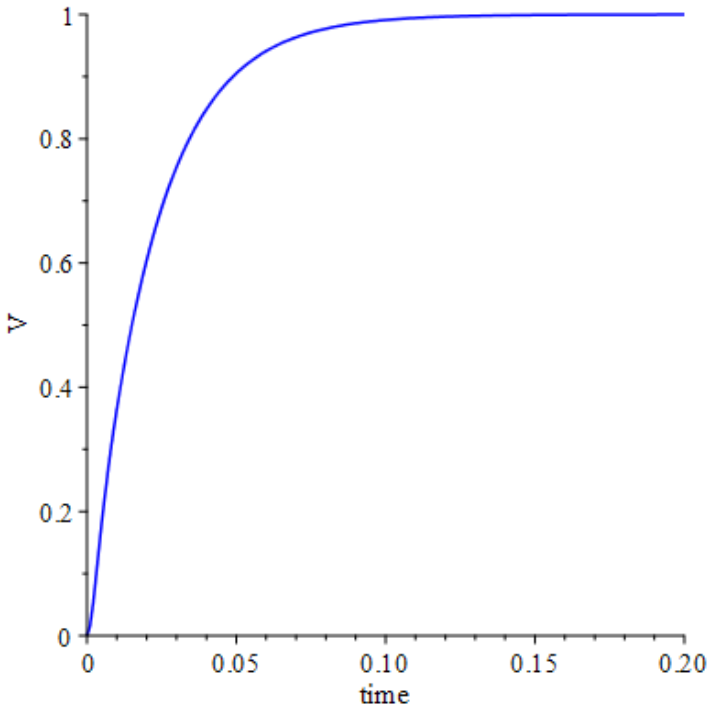


*Figure 59. Response of the system to an input step with the secondary control imposing the real pole dominant*

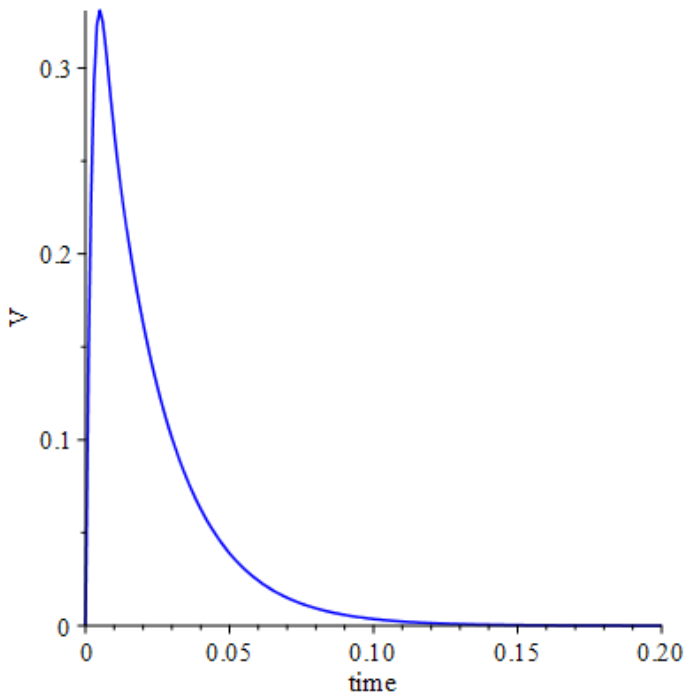


*Figure 60. Response of the system to a current perturbation step with the secondary control imposing the real pole dominant*

### 3.5.2.2. Pair of dominant complex conjugate poles

As it is wanted to make the pair of complex conjugate poles dominant, all the parameters should be calculated according to these poles. In this case, the dominant poles will be $B \pm Ei$.

Following the previous steps, taking a look to the terms of $s^2$ a relation between $A$ and $B$ can be expressed as ( 87 ).

$$A = -\frac{2\,B\,\tau - 1}{\tau} \tag{87}$$

Therefore, in order to ensure stability, all the poles should be negative which means that $A$ must be positive. According to this, a maximum value for $A$ can be found to ensure stability, ( 88 ).

$$B < \frac{1}{2\,\tau} \tag{88}$$

With the expression ( 87 ), the constant term and the term of $s$ of ( 75 ), the $k_p$ and $k_i$ can be expressed in functions of $A$, $E$, $C_1$, $C_2$ $C$ and $\tau$ (expressions ( 89 ) and ( 90 )).

$$k_p = \frac{-\big(2\,(2\,B\,\tau - 1)\big)\,B\,C + B^2\,C\,\tau + C\,E^2\,\tau - C_1 - C_2}{C_1 + C_2} \tag{89}$$

$$k_i = -(2\,B\,\tau - 1)\,C\,\frac{B^2 + E^2}{C_1 + C_2} \tag{90}$$

Having $k_p$ and $k_i$ expressed as ( 89 ) and ( 90 ), respectively, the zero of the system can also be found in function of the same parameters $B$, $E$, $C_1$, $C_2$ $C$ and $\tau$. Therefore, the zero of the system is expressed as ( 91 ).

$$z = -C\,\frac{2\,B^3\,\tau + 2\,B\,E^2\,\tau - B^2 - E^2}{3\,B^2\,C\,\tau - C\,E^2\,\tau - 2\,B\,C + C_1 + C_2} \tag{91}$$

In this assumption, the pair of complex conjugate poles should dominate over the other pole and over the zero of the system which means that $B$ must be much lower than the other pole and the zero, expressions ( 92 ) and ( 93 ), respectively.

$$B \ll A \tag{92}$$

$$B \ll z \tag{93}$$

With ( 87 ) and ( 92 ), and supposing a dominance is accomplish only if $B$ is lower than ten times $A$, the ( 94 ) condition should be fulfilled by $B$.

$$B < \frac{1}{12\,\tau} \tag{94}$$

With the expression ( 91 ) and ( 93 ) it is obtained the relation between the real part ($B$) and the imaginary part ($E$) of the pole over the zero, ( 95 ).

$$E = \frac{\sqrt{\left(C\ (3\ B\ \tau - 1)\ B\ (B^2\ C\ \tau - B\ C + C_1 + C_2)\right)}}{C\ (3\ B\ \tau - 1)} \quad (95)$$

The function obtained in ( 95 ) is plotted in Figure 61 with the previous limits of $B$ (expressions ( 88 ) and ( 94 )) to make the system stable and to have a dominance over the pole.

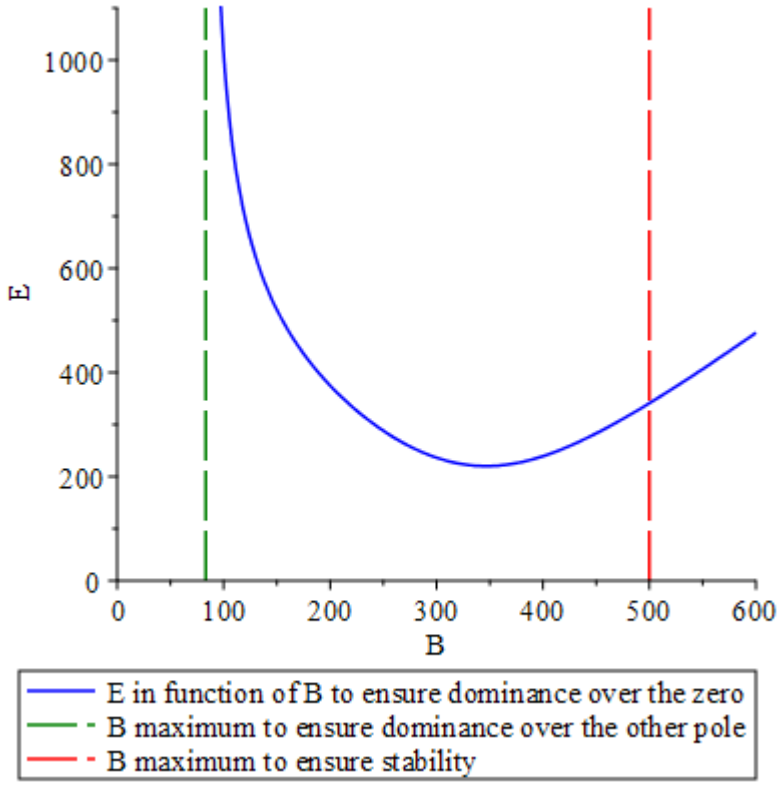


*Figure 61. Relation between B and E to ensure dominance over the zero when trying to have a pair of complex conjugate poles dominant*

As can be seen in Figure 61, there is no value of $B$ that ensures both dominance over the zero and dominance over the other pole because the maximum value of $B$ is one assimptote of the function that relates $B$ and $E$. Therefore, a swept of parameters is done to see the dynamic behaviour of the system. There are two options to make at least the pair of complex conjugate poles dominant over the other pole or over the zero.

#### 3.5.2.2.1. Dynamic response ensuring dominance over the zero

In this subsection $B$ is swept from the maximum one to ensure dominance over the pole to the maximum that ensures stability and $E$ is calculated with ( 95 ). The resulting responses to a step input and to a current perturbation step are shown in Figure 62 and Figure 63.

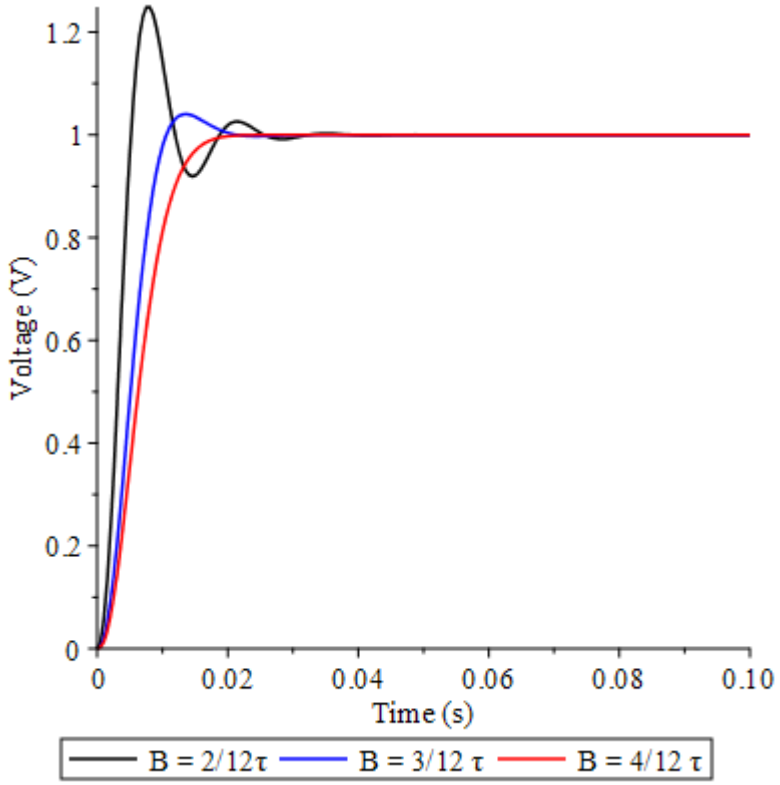


*Figure 62. Response in voltage of the secondary control to a voltage input step sweeping the real part of the pair of complex conjugate poles with a pair of complex conjugate poles dominant only over the zero*

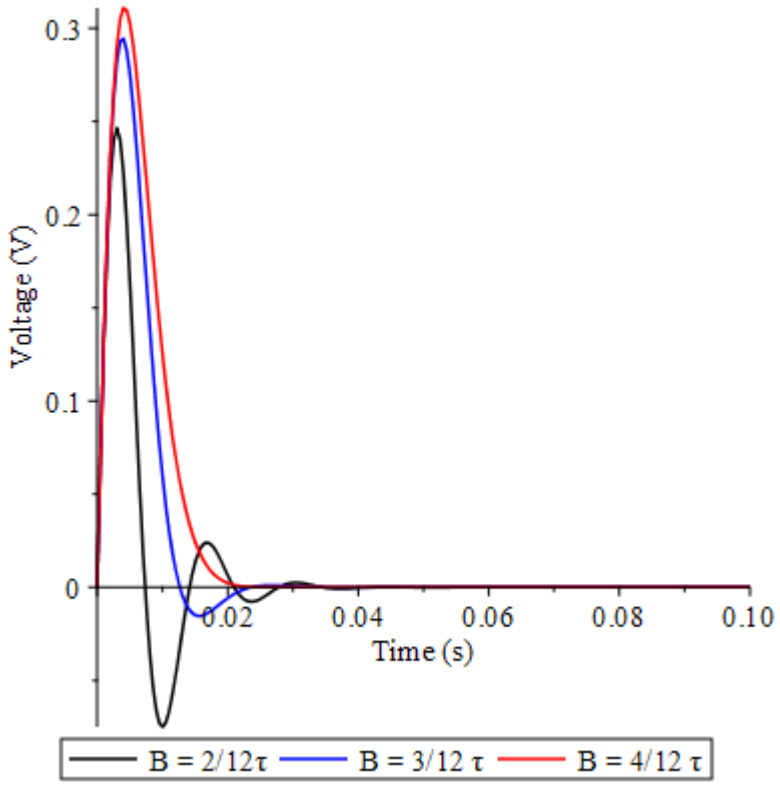


*Figure 63. Response in voltage of the secondary control to a current perturbation step sweeping the real part of the pair of complex conjugate poles with a pair of complex conjugate poles dominant only over the zero*

As before, the best responses to an input step gives the biggest peak when a current perturbation is applied. The best response is the one with $B = \frac{4}{12\,\tau}$ because it gives the fastest response and the current perturbation peak is acceptable because the primary control is already design to make the system work in-between its limits.

#### 3.5.2.2.2. Dynamic response ensuring dominance over the other pole

In this subsection, $B$ and $E$ are selected to fulfil the dominance of the pair of complex conjugate poles over the other pole. Supposing this dominance the behaviour of the second order can be expressed as ( 96 ).

$$\big(s + (B + E\,i)\big)\big(s + (B - E\,i)\big) = s^2 + 2\,wn\,\chi\,s + wn^2 \qquad (96)$$

Where $\chi$ can be expressed in function of the peak, $SP$. Equation ( 53 ) shows the relation between $\chi$ and $SP$. With equations ( 53 ) and ( 96 ), $E$ can be expressed as ( 97 ).

$$E = \frac{-\pi\,B}{\ln(SP)} \qquad (97)$$

Knowing the relation between $B$, $E$ and $SP$, the zero of the system can be shown in a 3D plot to see its value according to $B$ and $SP$. Figure 64 shows this graph where $B$ is swept from 0 to the maximum $B$ to ensure dominance over the other pole, and $SP$ is swept from 0 to a maximum peak of 0.5.

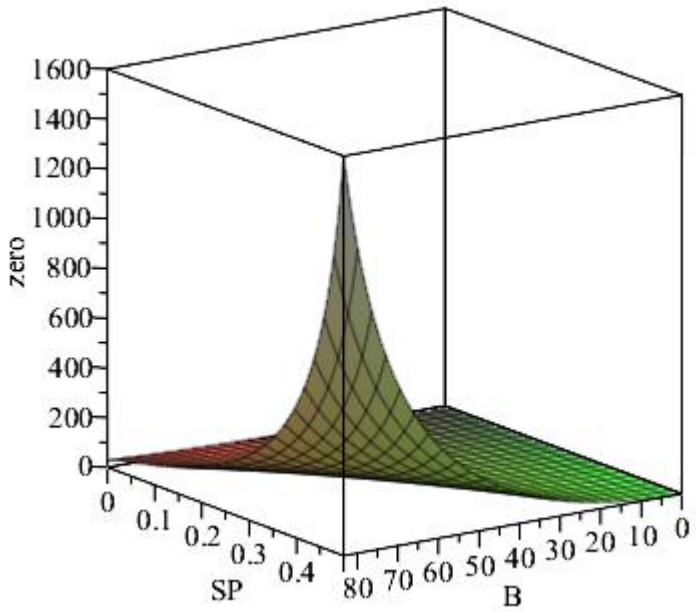


*Figure 64. Zero of the system with the secondary control in function of the peak and the real part of the pair of complex conjugate poles*

It can be seen that, a negative zero cannot be accomplished with these values of $B$ and $SP$. On the one hand, in order to search for a negative zero, if $B$ is increased, the dominance over the other pole is lost, and if $SP$ is increased, the response of the system is not optimum. Therefore, it is concluded that a desirable behaviour of the system trying to make the pair of complex conjugate poles dominant over only the other pole cannot be accomplish.

### 3.5.2.3. Zero cancelation

It is desired to make a zero cancelation in order to simplify the zero of the system with one real pole. This way, there is no effect of the zero in the dynamic response of the system and, moreover, the system will be one degree less which make easy the calculations. Therefore, $A$ is wanted to be equal than $z$, and select $B$ and $E$ according to a suitable dynamic response.

In ( 80 ) the zero of the system is expressed in function of $A$. Equalling this equation ( 80 ) to $A$, the expression that must follow $A$ can be obtained, ( 98 ).

$$A = \frac{C + \sqrt{-4\,C\,C_1\,\tau - 4\,C\,C_2\,\tau + C^2}}{2\,C\,\tau} \qquad (98)$$

Figure 65 plots the relation obtained in ( 98 ).

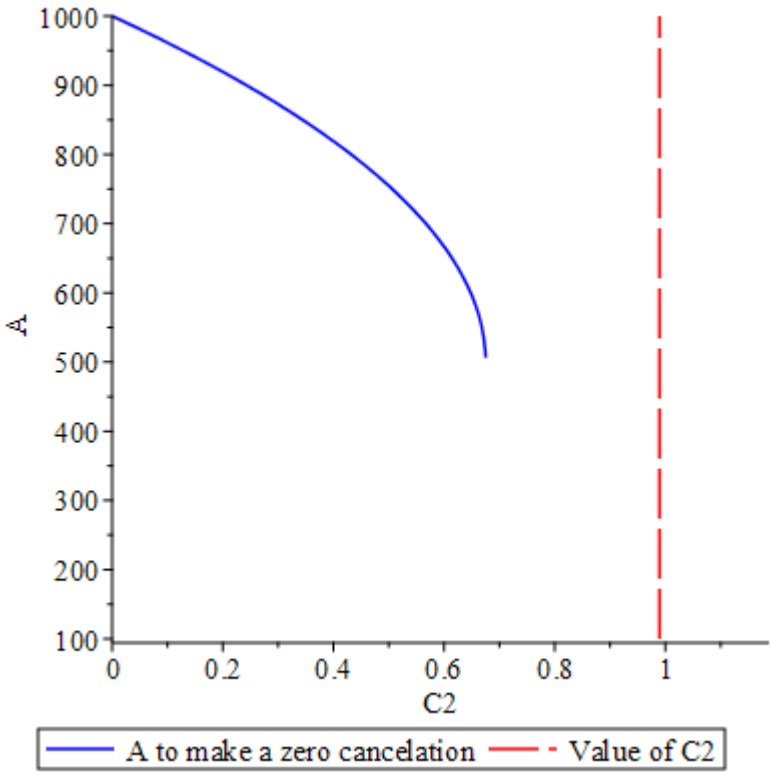


*Figure 65. The real pole in function of C2 to have a zero cancelation*

As it can be seen in Figure 65, the actual value of $C_2$ (which was selected in section 3.4.3.1 and is shown by the red line in the figure) does not have a valid value of $A$ to make the zero cancelation (the blue line ends in the middle of the figure because the equation ( 98 ) starts to have a complex results at this point). Therefore, assuming that $C$ and $\tau$ are fixed by the system, if $C_1$ and $C_2$ are not changed, the zero cancelation cannot be done.

### 3.5.2.4. Final secondary control

To select the final secondary control, a comparison between the two best options is done. These two options are the one making the real pole dominant and the one making the pair of complex conjugate poles dominant only over the zero. The plots in Figure 66 and Figure 67 show the step-response and perturbation-response of these two options.

Therefore, the following two graph shows the behaviour of these two options to an input step and a current perturbation step, Figure 66 and Figure 67, respectively.

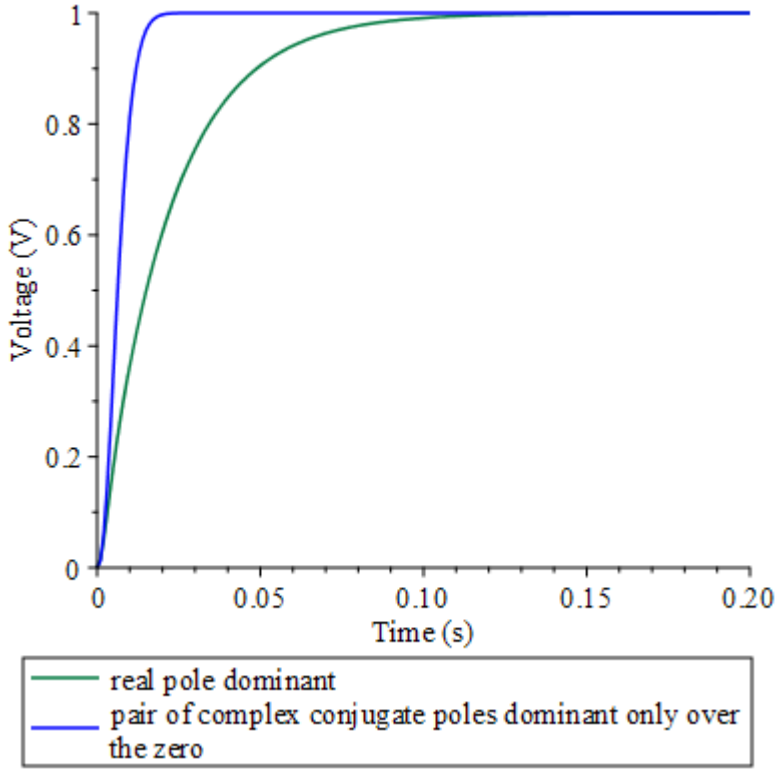


*Figure 66. Comparison of the behaviour to an input step of the two secondary control options*

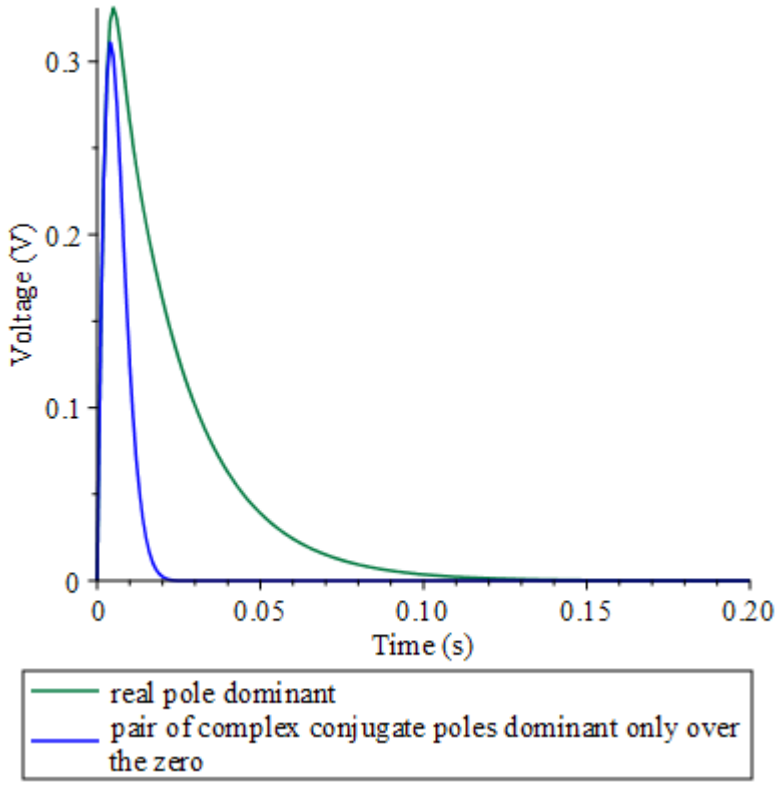


*Figure 67. Comparison of the behaviour to a current perturbation step of the two secondary control options*

Therefore, the best option is the one given by the pair of complex conjugate poles dominant only over the zero because, it gives the fastest response and has the lower peak. With this final decision, the constants of controller are calculated according to 3.5.2.2.1. The results are expressed in ( 99 ) and ( 100 ).

$$k_p = 0{,}043 \quad (99)$$

$$k_i = 145{,}73 \quad (100)$$

### 3.5.3. Extension to more converters

In order to generalize the way to tune the controller of the secondary control, some assumptions have to be made. The first one is to consider that all the converter behave as a first order delay and the tuning is made considering a sum of virtual resistances, $CN$ (expression ( 59 )) as it is explained in 3.4.4. The final transfer function considering N converters is ( 101 ).

$$\frac{V(s)}{V_{REF}(s)} = \frac{\left(k_p\, s + k_i\right) CN}{C\,\tau\, s^3 + C\, s^2 + \left(k_p + 1\right) CN\, s + k_i\, CN} \quad (101)$$

The system will be stable if $CN$ is positive and ( 73 ) is fulfilled. Then, it must be taken into account when tuning the controller to ensure stability. As the characteristic equation is a third order one and it is tried to make pole domination, three different possibilities are analysed: one real pole dominant, pair of complex conjugate poles dominant or zero cancellation.

Writing the characteristic equation in terms of s and equalling it to the equation of poles, expression ( 102 ) is obtained.

$$C\,\tau\, s^3 + C\, s^2 + \left(k_p + 1\right) CN\, s + k_i\, CN = (s + A)(s + (B + Ei))(s + (B - Ei)) \quad (102)$$

Reordering the equation and computing the equation of poles, expression ( 103 ) can be deduced.

$$s^3 + \frac{1}{\tau}\, s^2 + \frac{\left(k_p + 1\right) CN}{C\,\tau}\, s + \frac{k_i\, CN}{C\,\tau} = s^3 + (A + 2\,B)\, s^2 + (2\,A\,B + B^2 + E^2)\, s + A\,(B^2 + E^2) \quad (103)$$

Now it is considered that the capacitor, $C$ and the time constant of the converter, $\tau$ are given by the system and the sum of slopes $CN$ are calculated previously in the primary control.

#### 3.5.3.1. One real pole dominant

As it is wanted to make the real pole dominant, all the terms must be expressed in terms of it. Therefore, equalling all the terms in ( 103 ), the expressions ( 104 ), ( 105 ) and ( 106 ) are obtained for the real part of the complex conjugate poles, and for the proportional and the integrator part of the controller, respectively.

$$B = \frac{1}{2\,\tau} - \frac{A}{2} \quad (104)$$

$$k_p = -\frac{3\,A^2\,C\,\tau^2 - 4\,C\,E^2\,\tau^2 - 2\,A\,C\,\tau + 4\,CN\,\tau - C}{4\,\tau\,CN} \quad (105)$$

$$k_i = \frac{C\,A\,(A^2\,\tau^2 + 4\,E^2\,\tau^2 - 2\,A\,\tau + 1)}{4\,\tau\,CN} \quad (106)$$

The constants of the controller can be calculated according to two parameters: the real pole and the imaginary part of the complex conjugate pole. In order to ensure the dominance over the pole and the zero (making the real pole at least ten time lower), $A$ and $E$ must fulfil expressions ( 107 ) and ( 108 ).

$$A < \frac{1}{21\,\tau} \quad (107)$$

$$E > \frac{\sqrt{\left(C\,(31\,A^2\,C\,\tau^2 - 22\,A\,C\,\tau + 40\,CN\,\tau - 9\,C)\right)}}{6\,C\,\tau} \quad (108)$$

Finally, selecting a value of $A$ (taking into account the limit ( 107 )), the time constant of the controller is set to $\frac{1}{A}$ and then, $E$ can be selected to ensure zero dominance, ( 108 ).

#### 3.5.3.2. Pair of complex conjugate poles dominant

In this section, the pair of complex conjugate poles, all the terms must be expressed in terms of it. Therefore, equalling all the terms in ( 103 ), the expressions ( 109 ), ( 110 ) and ( 111 ) are obtained for the real part of the complex conjugate poles, and for the proportional and the integrator part of the controller, respectively.

$$A = -\frac{2\,B\,\tau - 1}{\tau} \quad (109)$$

$$k_p = -\frac{3\,B^2\,C\,\tau - C\,E^2\,\tau - 2\,B\,C + CN}{CN} \quad (110)$$

$$k_i = -\frac{C\,(2\,B^3\tau + 2\,B\,E^2\,\tau - B^2 - E^2)}{CN} \quad (111)$$

In order to ensure dominance (making the real part of the pair of complex conjugated poles ten times lower than the zero and the real pole), $B$ and $E$ must follow expressions ( 112 ) and ( 113 ).

$$B < \frac{1}{12\,\tau} \quad (112)$$

$$E > \frac{\sqrt{\left(C\,(12\,B\,\tau - 1)\,B\,(28\,B^2\,C\,\tau - 19\,B\,C + 10\,CN)\right)}}{C\,(12\,B\,\tau - 1)} \quad (113)$$

This time $B$ and $E$ does not give so much information about how the system will behave. Therefore, a change of variable can be done in order to select instead the damping factor

and the natural frequency which do give valuable information. To do so, the second order pole equation is expressed as a classical second order equation, ( 114 ).

$$\big(s+(B+Ei)\big)\big(s+(B-Ei)\big)=s^2+2\,\chi\,w_n\,s+w_n^2 \qquad (114)$$

With ( 114 ), $B$ and $E$ can be written in terms of the damping factor and the natural frequency, expressions ( 115 ) and ( 116 ).

$$B=\chi\,w_n \qquad (115)$$

$$E=\sqrt{w_n^2-(\chi\,w_n)^2} \qquad (116)$$

Finally, the wanted system can be defined by the damping factor and the natural frequency, then the values of the complex pole can be calculated with ( 115 ) and ( 116 ), and they must fulfil ( 112 ) and ( 113 ) to ensure dominance, and consequently to ensure the expected behaviour.

#### 3.5.3.3. Zero cancelation

Starting as 3.5.3.1, $B$ is expressed in terms of $A$ and $\tau$, ( 104 ); and $k_p$ and $k_i$ in terms of $A$, $C$, $E$, $CN$ and $\tau$, ( 105 ) and ( 106 ). When trying to make zero cancelation, the real pole must be equal than the zero of the system, then $A$ can be calculated to fulfil this condition, and it must follow expression ( 114 ). It must be said that if the result of expression ( 114 ) is complex, the zero cancelation cannot be accomplished.

$$A=\frac{C\pm\sqrt{-4\,C\,CN\,\tau+C^2}}{2\,C\,\tau} \qquad (117)$$

Consequently, $B$ is also defined by ( 104 ) and the only free variable to fix the behaviour of the system is $E$. As section 3.5.3.2, the system behaviour can be defined by the damping factor and the natural frequency (expressions ( 115 ) and ( 116 )), but this time, selecting one of them will determine the other as $B$ is defined and it will also determine $E$.

### 3.6. Tertiary control

As it is explained before, the tertiary control is normally made by a proportional-integrator controller for each converter to make a horizontal offset to all of the converters, except one, to control the power flow, and the one not controlled is over determined. Therefore, taking into account the previous simplifications: the deletion of saturations to simplify the calculus avoiding a non-linearity and the approximations of the converters to a first order delay, the diagram block is represented in Figure 68.

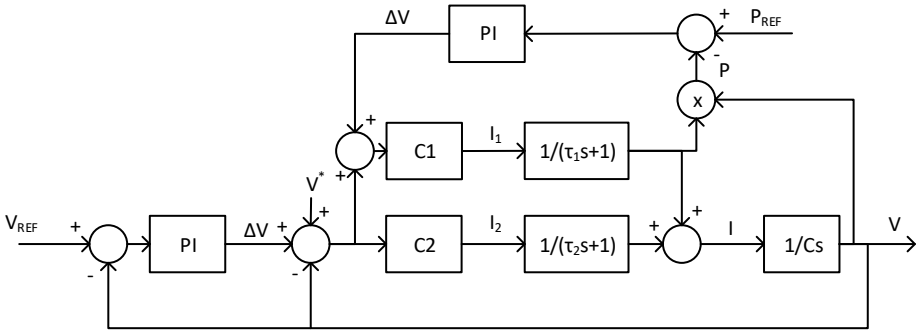


*Figure 68. Block diagram of the system with tertiary control*

As the tertiary control is parallel to the secondary one and, in this case, only acts in one converter, the secondary control as well as the primary control of the slack converter can be considered as perturbations. Therefore, the simplified diagram to tune the controller of the tertiary control is shown in Figure 69.

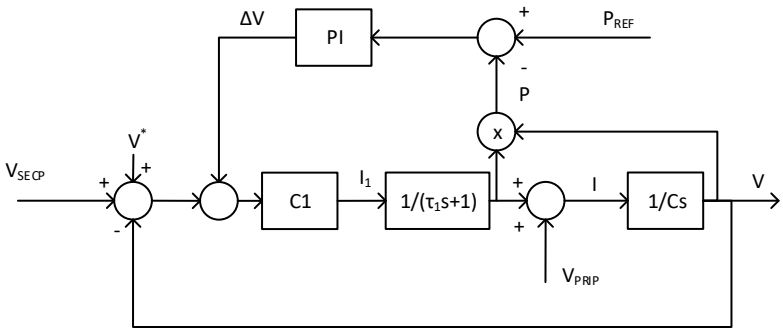


*Figure 69. Block diagram of the system with tertiary control considering perturbations*

Where $V_{SECP}$ and $V_{PRIP}$ are the perturbations of the secondary control and the slack converter primary control, respectively.

The final simplification to tune the converter is to remove the product between the current and the voltage and to treat the behaviour of the capacitor as a perturbation. As the voltage is assumed to be stabilized by the secondary control, this product can be simplified as a constant gain. Reordering the system with these assumptions, the resulting diagram is represented in Figure 70.

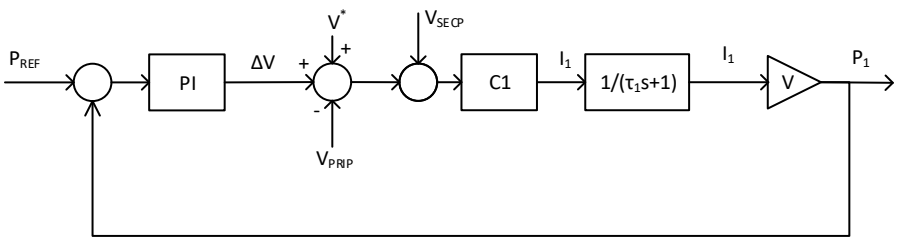


*Figure 70. Block diagram of the tertiary control considering perturbations and removing the product considering the bus voltage constant*

Where $V_{SECP}$ and $V_{PRIP}$ are the perturbations of the secondary control with the perturbation of the capacitor and the slack converter primary control, respectively. Therefore, the transfer function is expressed in ( 118 ).

$$\frac{P(s)}{P_{REF}(s)} = \frac{\left(k_p\, s + k_i\right) C_1\, V}{s^2\, \tau + \left(C_1\, V\, k_p + C_1 + 1\right) s + C_1\, V\, k_i} \qquad (118)$$

### 3.6.1. Stability analysis

In order to have a stable system, all the poles of the characteristic equation must have a negative real part. Taking it into account, the poles of the system can be expressed as ( 119 ).

$$p_{1,2} = \frac{-\left(C_1\, V\, k_p + C_1 + 1\right) \pm \sqrt{\left(C_1\, V\, k_p + C_1 + 1\right)^2 - 4\, \tau\, C_1\, V\, k_i}}{2\, \tau} \qquad (119)$$

There are different scenarios according to the possible solutions of the square root. If the result of the square root is 0, the poles are double and they only have a real part, ( 120 ).

$$\left(C_1\, V\, k_p + C_1 + 1\right)^2 - 4\, \tau\, C_1\, V\, k_i = 0$$

$$p_{1,2} = -\frac{\left(C_1\, V\, k_p + C_1 + 1\right)}{2\, \tau}\ (\text{double}) \qquad (120)$$

As it is wanted to avoid zeros in the right half plane, the $k_p$ must be positive and, consequently the system will have a negative real part considering 0 as a result of the square root. The other possibility is to have a complex result of the square root and then, the poles will be expressed in ( 121 ).

$$\left(C_1\, V\, k_p + C_1 + 1\right)^2 - 4\, \tau\, C_1\, V\, k_i < 0$$

$$p_{1,2} = \frac{-\left(C_1\, V\, k_p + C_1 + 1\right) \pm \sqrt{\left(C_1\, V\, k_p + C_1 + 1\right)^2 - 4\, \tau\, C_1\, V\, k_i}}{2\, \tau} \rightarrow \qquad (121)$$

$$\rightarrow Re\left(p_{1,2}\right) = -\frac{\left(C_1\, V\, k_p + C_1 + 1\right)}{2\, \tau}$$

As before, considering $k_p$ positive, the system will be stable because the poles will have negative real part. The last option is to have a real solution of the square root and the results are expressed in ( 122 ) and ( 123 ).

$$\left(C_1\, V\, k_p + C_1 + 1\right)^2 - 4\, \tau\, C_1\, V\, k_i > 0$$

$$p_1 = \frac{-\left(C_1\, V\, k_p + C_1 + 1\right) + \sqrt{\left(C_1\, V\, k_p + C_1 + 1\right)^2 - 4\, \tau\, C_1\, V\, k_i}}{2\, \tau} \qquad (122)$$

$$p_2 = \frac{-\left(C_1\, V\, k_p + C_1 + 1\right) - \sqrt{\left(C_1\, V\, k_p + C_1 + 1\right)^2 - 4\, \tau\, C_1\, V\, k_i}}{2\, \tau} \qquad (123)$$

The worst-case scenario in this case is the first pole expressed in ( 122 ). If it is wanted to have a negative real pole the condition that $k_p$ and $k_i$ must fulfil to have a stable system is the one expressed in ( 124 ).

$$The\ system\ is\ stable\ if \begin{cases} k_p \geq 0 \\ k_i < \dfrac{\left(k_p\ V\ C_1 + C_1 + 1\right)^2}{4\ C_1\ V\ \tau} \end{cases} \quad (124)$$

### 3.6.2. Controller tuning

Once the conditions for stability are found, the controller must be tuned according them. The time response of this tertiary controller is wanted to be much slower than the secondary control, this way it can be assumed that the primary and secondary controls are fast enough to consider them perturbations in the tuning assumptions, and consequently, the tertiary control will be slow enough not to interfere with the behaviour of the secondary control.

In order to avoid the peaks and make the tertiary control slow, the controller is tuned imposing two real poles, one dominant over the other and fixing a slow time constant. Therefore, the characteristic equation can be equalled to the equation written as the equation of poles, ( 125 ).

$$s^2\ \tau + \left(C_1\ V\ k_p + C_1 + 1\right) s + C_1\ V\ k_i = (s + A)(s + B) \quad (125)$$

Computing and equalling the expression of ( 125 ), the expression obtained is ( 126 ).

$$s^2 + \frac{\left(C_1\ V\ k_p + C_1 + 1\right)}{\tau}\ s + \frac{C_1\ V\ k_i}{\tau} = s^2 + (A + B)\ s + AB \quad (126)$$

With ( 126 ), equalling the term of s and the constant term, the $k_p$ and $k_i$ can be expressed as a function of the poles, ( 127 ) and ( 128 ).

$$k_p = \frac{A\ \tau + B\ \tau - C_1 - 1}{C_1 V} \quad (127)$$

$$k_i = \frac{A\ B\ \tau}{C_1\ V} \quad (128)$$

Expressing one pole in relation with the other as $B = k_{BA}\ A$, the controller can be calculated by selecting properly the pole $A$ and the relation between both poles $k_{BA}$. The pole is selected to fix the behaviour of the system and the relation is selected to ensure dominance and to avoid zeros in the right half plane. Therefore, the relation of poles must follow expressions ( 129 ) and ( 130 ).

$$k_{BA} > 10 \quad (129)$$

$$k_{BA} < -\frac{A\ \tau - C_1 - 1}{A\ \tau} \quad (130)$$

As it is said before, $A$ is selected to ensure no interference between secondary and tertiary control, so the time constant for this control is set to 0,2 seconds, and the relation between

poles is selected to the maximum not to have a zero in the right half plane. Therefore, the final values for $k_p$ and $k_i$ are expressed in ( 131 ) and ( 132 ).

$$k_p = 0 \quad (131)$$

$$k_i = 0{,}01 \quad (132)$$

With these values, the expected behaviour to a step input is shown in Figure 71.

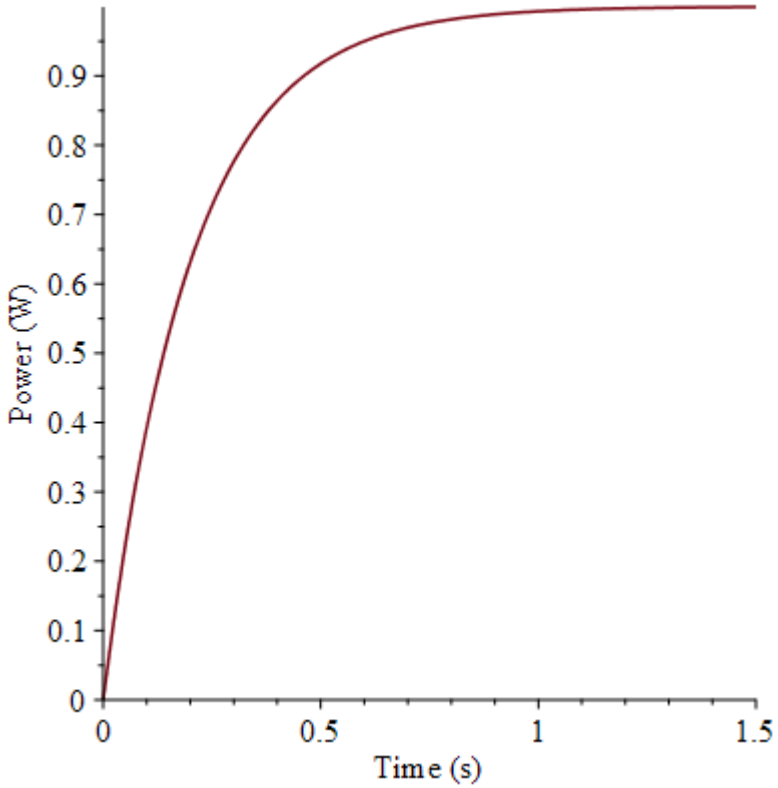


*Figure 71. Behaviour of the system with the tertiary control to a power step input*

### 3.6.3. Extension to more converters

This control is exclusive for each converter and its action will change the power sharing between converters but the bus voltage will not be affected because of the secondary control. Therefore, this control must be designed for each one of the microgrid converters except the slack module and it must be, at least, ten time slower than the secondary converter in order to avoid interferences between both controls as they act in parallel. As the characteristic equation of every simplified system with this control is a second order one, it can be tuned imposing two real poles and one dominant, or assuming classic second order behaviour and tune it according to the damping factor and the natural frequency. Imposing one real pole dominant is already done in section 3.6.2, so in contrast, in this section, the approach will be centered in a classical second order behaviour. Starting from the transfer function ( 118 ), its characteristic equation can be written as classical second order equation, ( 133 ).

$$s^2 + \frac{\left(C_1\, V\, k_p + C_1 + 1\right)}{\tau}\, s + \frac{C_1\, V\, k_i}{\tau} = s^2 + 2\,\chi\, w_n\, s + w_n^2 \quad (133)$$

From this expression ( 133 ), the values of $k_p$ and $k_i$ can be expressed as a function of the desired damping factor and the system natural frequency, ( 134 ) and ( 135 ).

$$k_p = \frac{2\ \chi\ \tau\ w_n - 1}{C_1\ V} \qquad (134)$$

$$k_i = \frac{C\ \tau\ w_n^2 - C_1}{C\ C_1\ V} \qquad (135)$$

Finally, as it is desired the real part of the pole much lower (a minimum of ten times) than the zero, in order to avoid an unpredicted behaviour of the system caused by the action of the zero, the natural frequency must fulfil the following expression, ( 136 ).

$$w_n > \frac{5\ C\ \chi + \sqrt{(-20\ C\ C_1\ \chi^2\ \tau + 25\ C^2\ \chi^2 + C\ C_1\ \tau)}}{C\ \tau\ (20\ \chi^2 - 1)} \qquad (136)$$

### 3.7. Proposed final control - Unified hierarchical DC control

For the development of this master thesis, a new controller that will be mentioned from now on as *unified hierarchical DC control*, is proposed. This control is a combination of the classical secondary and tertiary control all together in a single controller. This proposition can be done under the assumption of having $V^*$ equal to $V_{REF}$. Therefore, the diagram of the unified hierarchical DC control is shown in Figure 72.

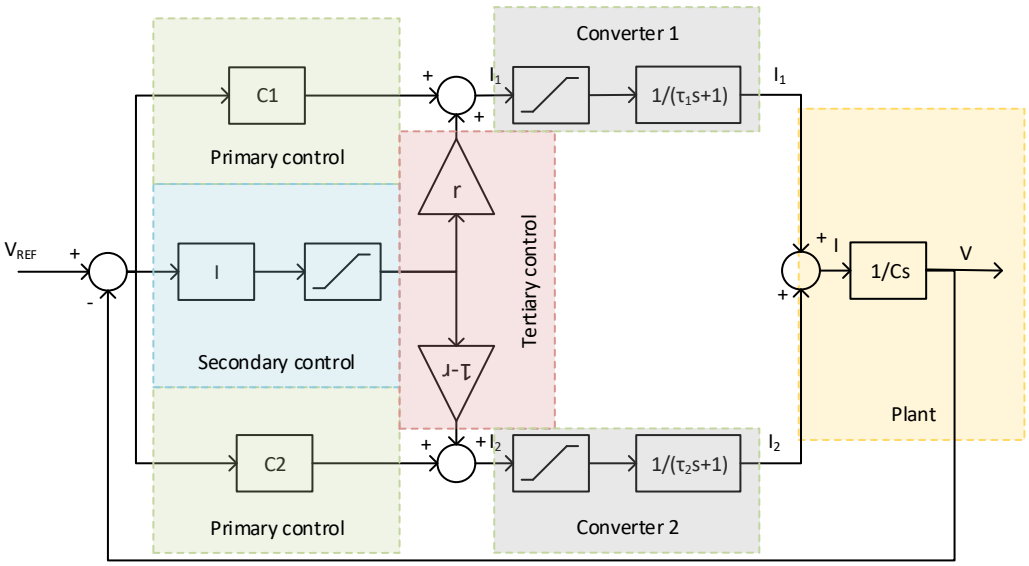


*Figure 72. Proposed final control diagram*

It has the same functions as the classical three-level Droop DC reducing the number of controllers to only one. The main idea of this unified hierarchical DC control is to distribute the action of the secondary control in both converters. This way, while correcting the bus voltage, the power sharing is also accomplished. As the voltage error tends to 0, the converters reference tends to be the output of the secondary multiply by a distribution factor which will determine at the end the power sharing between the converters.

It must be said also that, in this particular case, all the control levels of this proposed control are executed at the commutation frequency accomplishing this way faster and better time responses than the classical controls where the secondary and tertiary are usually executed by external controllers.

The concept of the primary control remains the same. There is a virtual resistance that relates the bus voltage with a given current but, in this case the reference is no longer $V^*$ but $V_{REF}$. Now, the secondary control does not give a horizontal offset to the primary control but a vertical one as it is added at the end. Moreover, this controller has only an integrator because the proportional part is already included in the inverse of the virtual resistance, therefore, the primary control. Finally, the tertiary control is applied by controlling the distribution of the secondary control.

As it is done before, in order to tune the controller, the saturations will be removed to avoid non-linearity and simplify the calculus. With this assumption, the block diagram is simplified as shown in Figure 73.

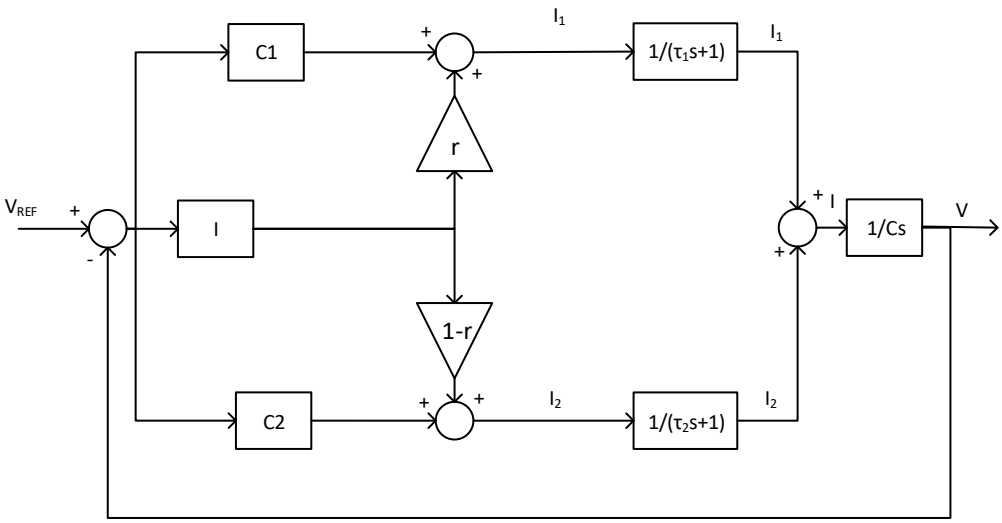


*Figure 73. Proposed simplified tertiary control diagram*

Therefore, the transfer function of this block diagram is expressed in ( 137 ).

$$\frac{V(s)}{V^*(s)} = \frac{(C_1\,\tau_2 + C_2\,\tau_1)\,s^2 + (C_1 + r\,k_i\,\tau_2 + C_2 + (r-1)\,k_i\,\tau_1)\,s + k_i}{s^4\,C\,\tau_1\,\tau_2 + C\,(\tau_1+\tau_2)\,s^3 + (C_1\,\tau_2 + C_2\,\tau_1 + C)\,s^2 + X\,s + k_i} \qquad (137)$$

Where $X = (C_1 + r\,k_i\,\tau_2 + C_2 + (r-1)\,k_i\,\tau_1)$.

Taking the same assumption as the previous sections (both converters current time constants have the same value), the distribution constant $r$ is simplified and the resulting transfer function obtained is ( 138 ).

$$\frac{V(s)}{V^*(s)} = \frac{(C_1 + C_2)\,s + k_i}{C\,\tau\,s^3 + s^2\,C + (C_1 + C_2)\,s + k_i} \qquad (138)$$

As the characteristic equation is a third order one, the stability analysis is made applying the Routh–Hurwitz theorem and the tuning of the controller is done as before trying to imposing dominance of poles.

### 3.7.1. Stability analysis

To evaluate the stability of the system, as the characteristic equation is a third order one, the Routh–Hurwitz theorem has been applied. Expression ( 139 ) shows the result of this theorem.

$$\begin{matrix} s^3 & C\,\tau & C_1 + C_2 \\ s^2 & C & k_i \\ s & -\tau\, k_i + C_1 + C_2 & 0 \\ 1 & k_i & 0 \end{matrix} \qquad (139)$$

In order to ensure stability, the theorem affirms that must be no sign change in the first column, resulting in the following expression ( 140 ).

$$The\ system\ is\ stable\ if \begin{cases} C\,\tau > 0 \\ C > 0 \\ -\tau\, k_i + C_1 + C_2 > 0 \\ k_i > 0 \end{cases} \qquad (140)$$

Taking the theorem into account, knowing that $C$, $\tau$, $C_1$ and $C_2$ are positive and imposing that $k_i$ must be positive to avoid zeros in the right half-plane, the conditions that $k_i$ must follow to accomplish the system stability can be deduced, ( 141 ).

$$The\ system\ is\ stable\ if \begin{cases} k_i < \dfrac{C_1 + C_2}{\tau} \\ k_i > 0 \end{cases} \qquad (141)$$

Therefore, it can be concluded that the system will be always stable if $k_i$ is greater than 0 a lower than $\frac{C_1+C_2}{\tau} = 2638.04$.

### 3.7.2. Controller tuning

Taking the stability condition into account, the $k_i$ parameter will be selected according to the system behaviour. Starting from ( 138 ) and following the steps as the previous sections, the characteristic equation can be expressed as a function of the poles, ( 142 ).

$$C\,\tau\,s^3 + s^2\,C + (C_1 + C_2)\,s + k_i = (s + A)(s + (B + E\,i))(s + (B - E\,i)) \qquad (142)$$

Simplifying ( 142 ) and collecting the terms of s, the resulting expression is ( 143 ).

$$s^3 + \frac{s^2}{\tau} + \frac{(C_1 + C_2)\,s}{C\,\tau} + \frac{k_i}{C\,\tau} = s^3 + (A + 2\,B)\,s^2 + (2\,A\,B + B^2 + E^2)s + A\,(B^2 + E^2) \qquad (143)$$

From now, the calculations must be done according to the assumption of having one real pole dominant, having a pair of complex conjugate poles dominant or simplifying the expression with a zero cancelation.

#### 3.7.2.1. One dominant real pole

Following the previous reasoning, as it is wanted to make one pole dominant, all the parameters should be calculated according to this pole. Therefore, the terms of $s^2$ remains the same as before and, consequently the relation between $A$ and $B$. This relation can be expressed as ( 144 ).

$$B = \frac{1}{2\,\tau} - \frac{A}{2} \quad (144)$$

In order to ensure stability, all the poles should be negative which means that $B$ must be positive. According to this, a maximum value for $A$ can be found to ensure stability, ( 145 ).

$$A < \frac{1}{\tau} \quad (145)$$

The zero of the system can be expressed in terms of $C_1$, $C_2$ and $k_i$, ( 146 ).

$$z = -\frac{k_i}{C_1 + C_2} \quad (146)$$

In this assumption, the real pole should dominate over the other poles and over the zero of the system which means that $A$ must be much lower than the other poles and the zero, expressions ( 147 ) and ( 148 ), respectively.

$$A \ll B \quad (147)$$

$$A \ll z \quad (148)$$

With ( 144 ) and ( 147 ) and supposing that dominance is accomplish only if $A$ is lower than ten times $B$, the ( 149 ) condition should be fulfilled by $A$.

$$A < \frac{1}{21\,\tau} \quad (149)$$

Therefore, if the dominance over the pole can be made, the system will be stable because the limits of dominance are in-between the limits of stability. Imposing the same dominance over the zero (being $A$ ten times lower than $z$), the expression ( 150 ) is obtained which relates $A$ and $k_i$ keeping the dominance.

$$k_i > 10\,A\,(C_1 + C_2) \quad (150)$$

Taking into account the constant term and the $s$ term of the characteristic equation, another relation between $A$ and $k_i$ can be obtained, ( 151 ).

$$k_i = A^3\,C\,\tau - A^2\,C + A\,C_1 + A\,C_2 \quad (151)$$

Plotting equations ( 150 )-( 151 ) and the limits of stability and dominance over the other pole (( 145 ) and ( 149 ), respectively) to have a visual representacion of the relation between $A$ and $k_i$, Figure 74 is obtained.

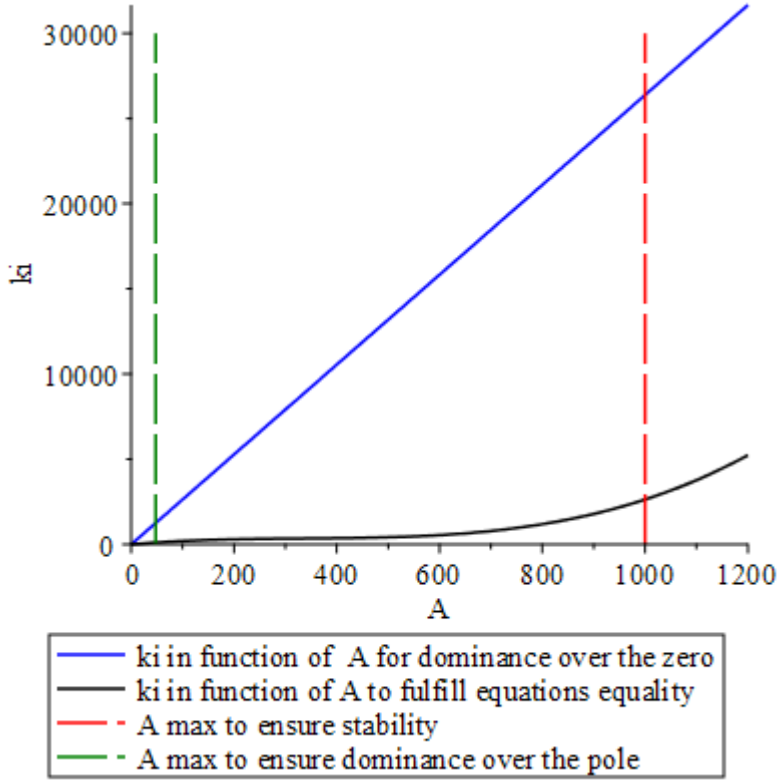


*Figure 74. Relation between $A$ and $k_i$ to ensure dominance over the zero and to fulfil the equations*

Observing Figure 74, it can be said that there is no $A$ which ensures dominance over the other poles and the zero in-between the limits of stability because there is no cross point between the function which relates $A$ and $k_i$ to dominate over the zero and the function which relates these two parameters to fulfil the initial equation ( 143 ). As it is not possible to ensure overall dominance, a swept of $A$ is done to see the behaviour of the system to select the value of $k_i$. Figure 75 and Figure 76 show the behaviour of the system to a step input and a current step perturbation sweeping the real pole.

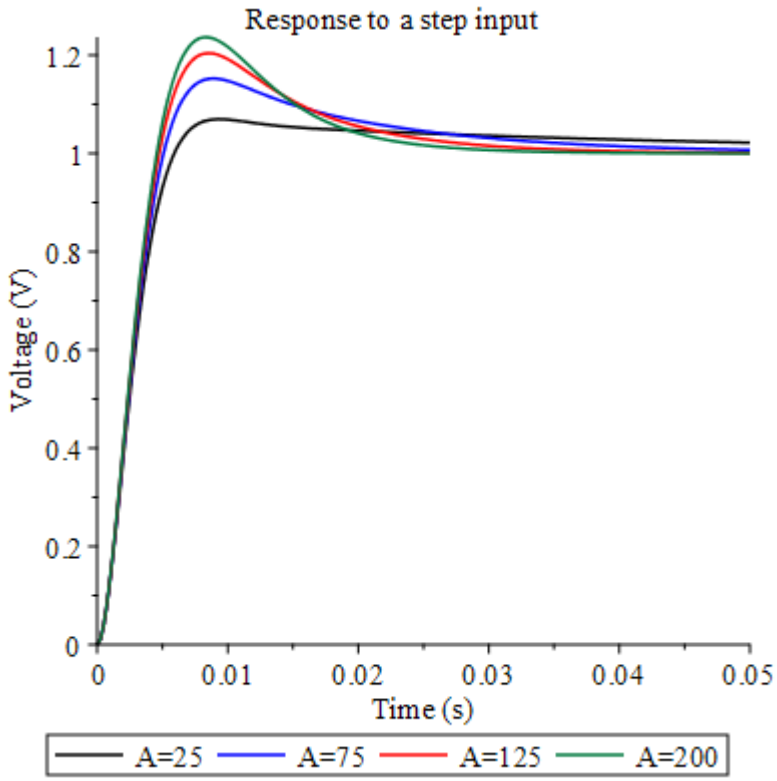


*Figure 75. Response to a step input of the final control trying to make the real pole dominant and sweeping it*

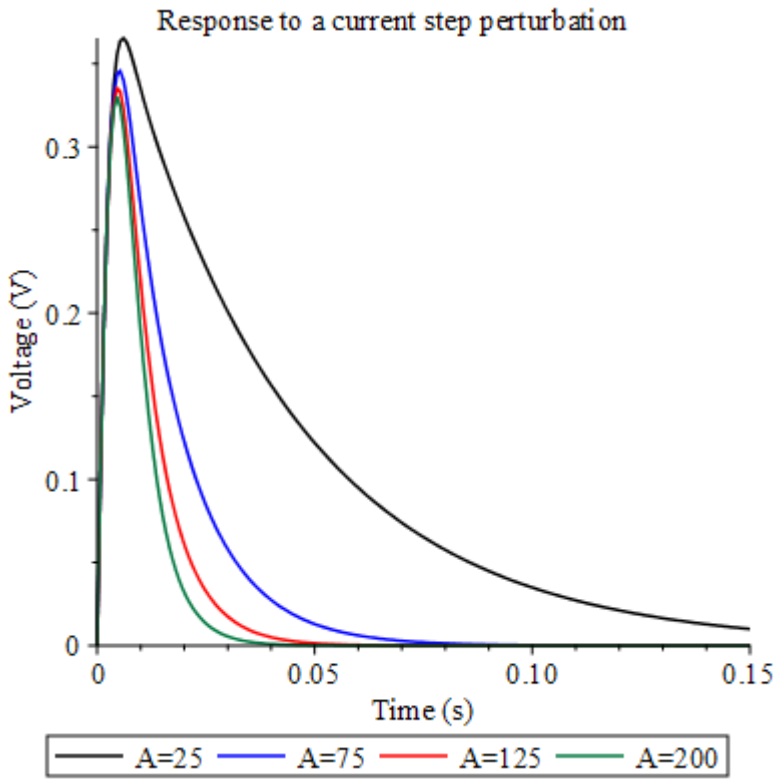


*Figure 76. Response to a current step perturbation of the final control trying to make the real pole dominant and sweeping it*

### 3.7.2.2. Pair of dominant complex conjugate poles

This time, in order to make the pair of complex conjugate poles dominant, all parameters should be expressed as a function of them. For this reason, from equation ( 143 ) it can be obtained the relation of the real part of the pair of complex conjugate poles and the real pole equalling the terms of $s^2$, ( 152 ).

$$B = -\frac{2\,B\,\tau - 1}{\tau} \quad (152)$$

As it is wanted to have all real parts of the poles negative to ensure stability, the maximum value for $B$ can be calculated, ( 153 ).

$$B < \frac{1}{2\,\tau} \quad (153)$$

The zero of the system can be expressed as before, ( 154 ).

$$z = -\frac{k_i}{C_1 + C_2} \quad (154)$$

In order to make the pair of complex conjugate poles dominant, the real part of them should be much lower than the other pole and the zero, ( 155 ) and ( 156 ).

$$B \ll A \quad (155)$$

$$B \ll z \quad (156)$$

Assuming that dominance is only accomplished if $B$ is at least ten times lower than the other pole and the zero, expressions ( 157 ) and ( 158 ) can be obtained.

$$B < \frac{1}{12\,\tau} \quad (157)$$

$$k_i > 10\,B\,(C_1 + C_2) \quad (158)$$

As before, equalling the constant term and the $s^2$ of the equation ( 143 ), the relation between $k_i$ and $B$ can be obtained in order to fulfil the equations, ( 159 ).

$$k_i = -\frac{(2\,B\,\tau - 1)\,(4\,B^2\,C\,\tau - 2\,B\,C + C_1 + C_2)}{\tau} \quad (159)$$

Equalling ( 158 ) and ( 159 ), the values of $k_i$ and $B$ can be obtained to ensure the overall dominance of the pair of complex conjugate poles. These values are expressed in ( 160 ) and ( 161 ).

$$B = 61{,}75 \quad (160)$$

$$k_i = 1629{,}07 \quad (161)$$

The problem with these values are the system response, the peak obtained is greater than 50%, Figure 77 and Figure 78 show the response to a step input and to a current step perturbation. Therefore, this response is not acceptable.

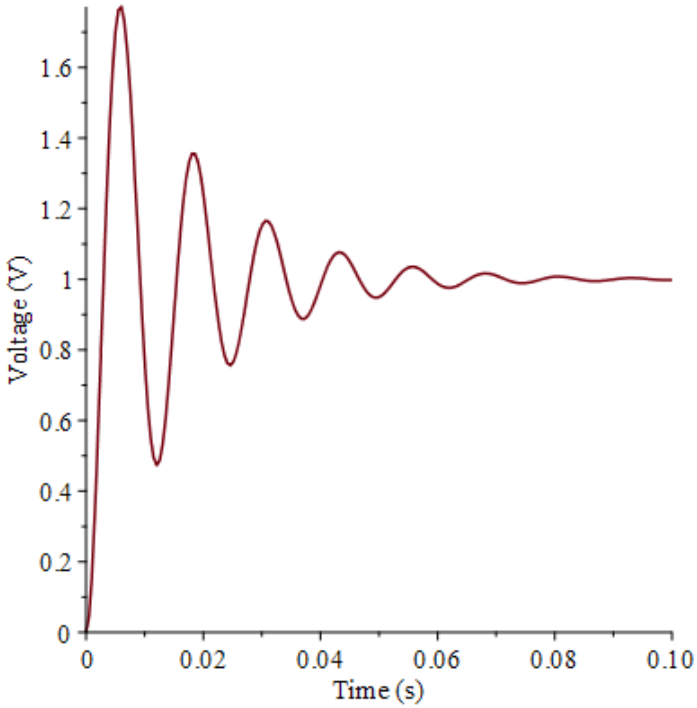


*Figure 77. Response to a step input of the final control trying to making the pair of complex conjugate poles dominant*

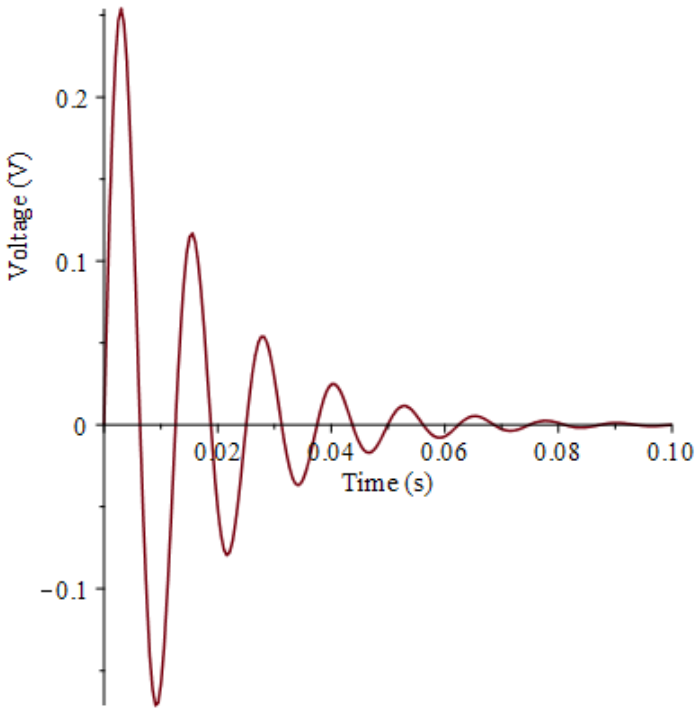


*Figure 78. Response to a current step perturbation of the final control trying to making the pair of complex conjugate poles dominant*

### 3.7.2.3. Zero cancelation

The last option to tune the controller is trying to simplify the zero with the real pole. Therefore, the real pole is wanted to be equal to the zero of the system. With this assumption, the function which relates the pole and the zero can be expressed as ( 162 ).

$$A = \frac{k_i}{C_1 + C_2} \quad (162)$$

With ( 162 ) and ( 143 ), there are four equations and four unknowns variables. The results of this system of equations is expressed in ( 163 ), ( 164 ), ( 165 ) and ( 166 ).

$$A = 1000 \quad (163)$$

$$B = 0 \quad (164)$$

$$E = 605{,}3 \quad (165)$$

$$k_i = 2638{,}05 \quad (166)$$

These result is also unacceptable, because the poles of the system will be purely imaginary and consequently, the system will be critically damped.

### 3.7.2.4. Final controller

As the only acceptable behaviours are accomplished in 3.7.2.1, a closer look is done to the Figure 75 and Figure 76. It can be said that the best behaviour to a input step is accomplish by $A = 25$ but it has the slower response and the greater peak before a current step perturbation. The behaviour obtained by the following value $A = 75$ is better in terms of peak and stabilization time to a current step perturbation but it has a greater peak to an input step. Therefore, a closer sweep is done between these two values.

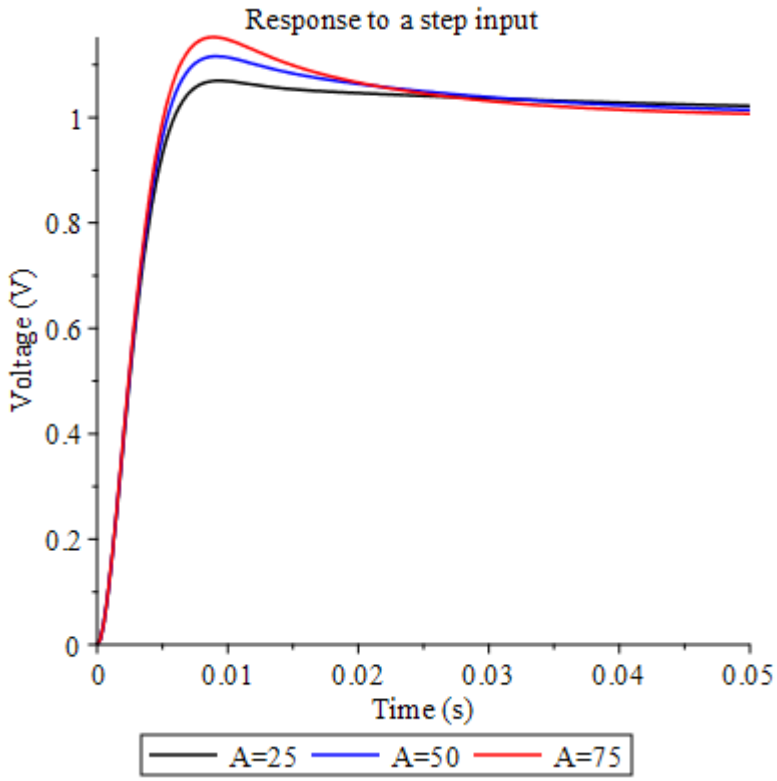


*Figure 79. Response to a step input of the final control trying to make a more accurate sweep of the real pole*

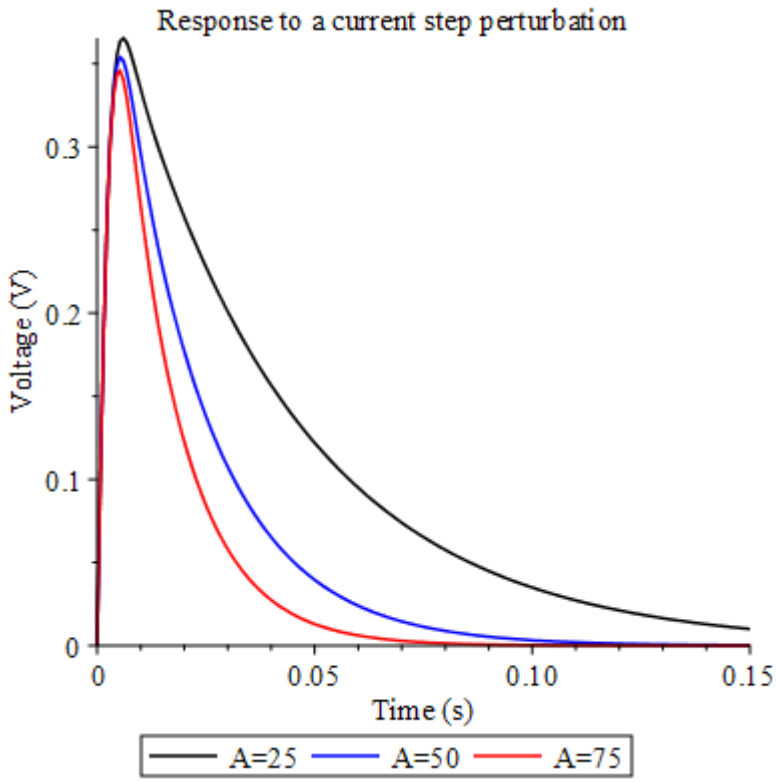


*Figure 80. Response to a current step perturbation of the final control trying to make a more accurate sweep of the real pole*

Finally, the selected behaviour is the one obtained with $A = 50$ because it has a relative acceptable peak of 10% and a considerable fastest response to a current step perturbation than $A = 25$. With this final value of the real pole, $k_i$ is calculated as ( 167 ).

$$k_i = 114{,}8 \qquad (167)$$

# 4. Results

In this section, the results of the previous calculations and design are presented. The results are divided into simplified simulations and experimental tests. In most of the cases, both results are presented together in order to have a fast interpretation of the differences between the simulation and the reality, but in some special cases, only simulations are made. The results are divided into different sections, the first two sections explain how the simulations and the experimental test were made, the third one shows the result of the behaviour of a single converter to a current input step, the fourth section present the results of the primary and secondary control only with one converter, and the last section shows the results of all the controllers with the two DAB converters.

## 4.1. Simulation setup

*All simulations are made using MATLAB Simulink and the system, as explained in section 3 is simplified using current sources acting as the two converters and the load, and the bus capacitor,*

Figure 40. Therefore, this schematic is implemented in Simulink with the Simscape Power System toolbox. Figure 81 shows the implementation of the simplified system in Simulink.

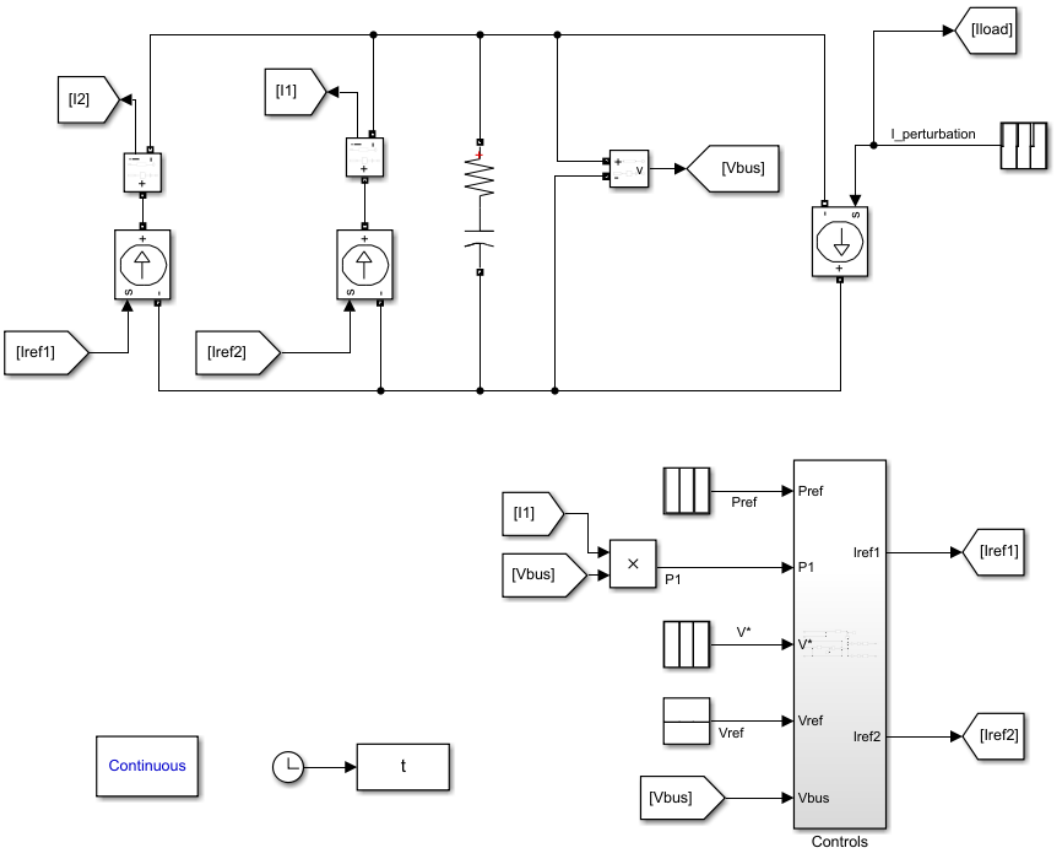


*Figure 81. Simulink model to simulate the microgrid*

As it can be seen, there are two controlled current sources which reference is given by the box called controls, the bus capacitor, and another current source which acts as a load. Inside the Controls box, the three control levels are implemented: the primary, the secondary and the tertiary. In order to simulate every control, there are two options for this Controls box, the one corresponding to the classical Droop control calculated in sections

3.4, 3.5 and 3.6, and the one corresponding to the proposed unified final control calculated in section 3.7. Figure 82 shows the Simulink blocks diagram of the Controls subsystem of the classical Droop control and Figure 83 shows the Simulink blocks diagram of the Controls subsystem of the proposed final control.

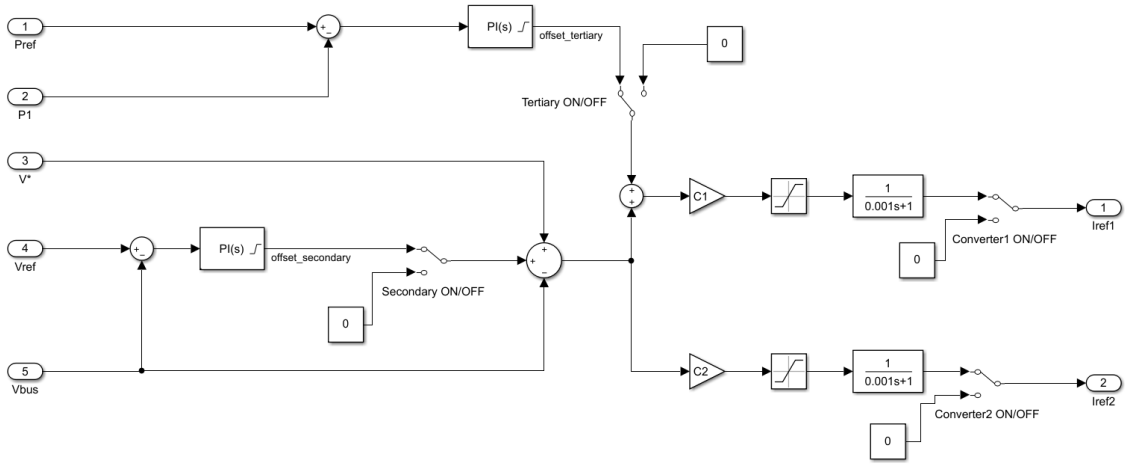


*Figure 82. Simulink model to simulate the classical controls of the microgrid*

There are several switches to enable or disable the secondary and the tertiary control, and even two switches to enable or disable the converters to be able to simulate the behaviour of only one converter. After the primary control, the saturation is added and the first order delay which simulates the behaviour of each converter.

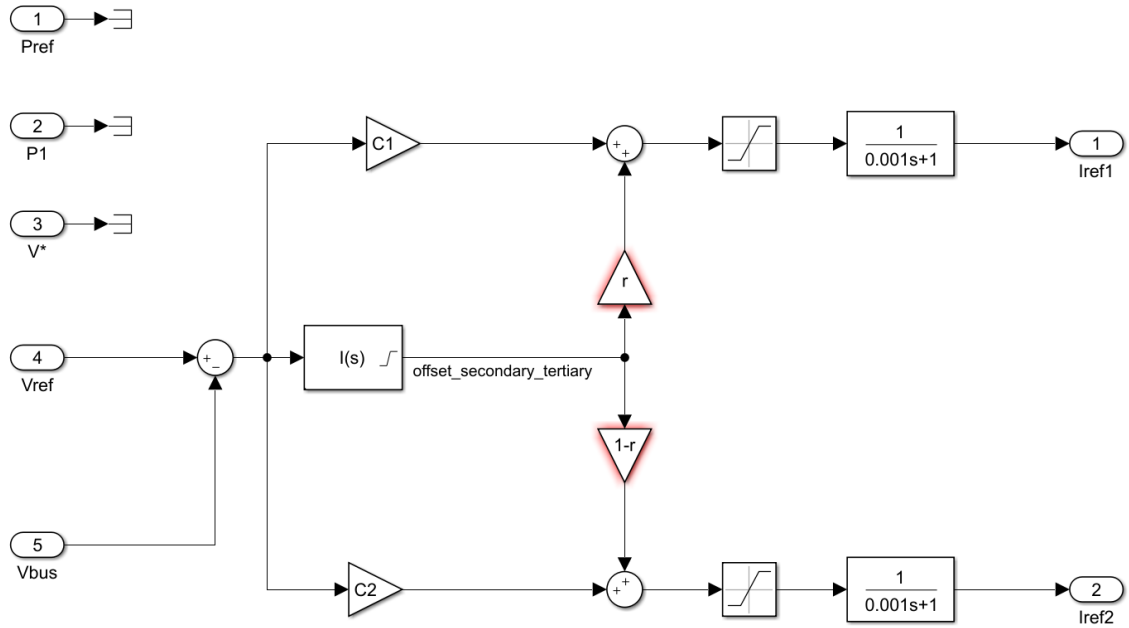


*Figure 83. Simulink model to simulate the proposed controls of the microgrid*

In the unified proposed control case, there are no switches to enable or disable anything because, the secondary and tertiary works together, and if it is disable, the resulting system is only the primary which is already simulated with the previous controls.

It must be said that all simulations are made in continuous time and the PI/I controllers have saturation limits and a clamping anti-windup.

## 4.2. Experimental setup

The experimental test had been done thanks to the hardware of the European H2020 project, RESOLVD, developed in CITCEA-UPC. This hardware consists in two Dual Active Bridge converters, the two batteries, some bank resistors to act as a load, all the additional hardware needed to interconnect and protect everything, an oscilloscope (Yokogawa DLM2024) with its proves to capture all the results and a laptop to program and debug in real-time the microcontroller. Figure 84 shows a photo of the experimental setup.

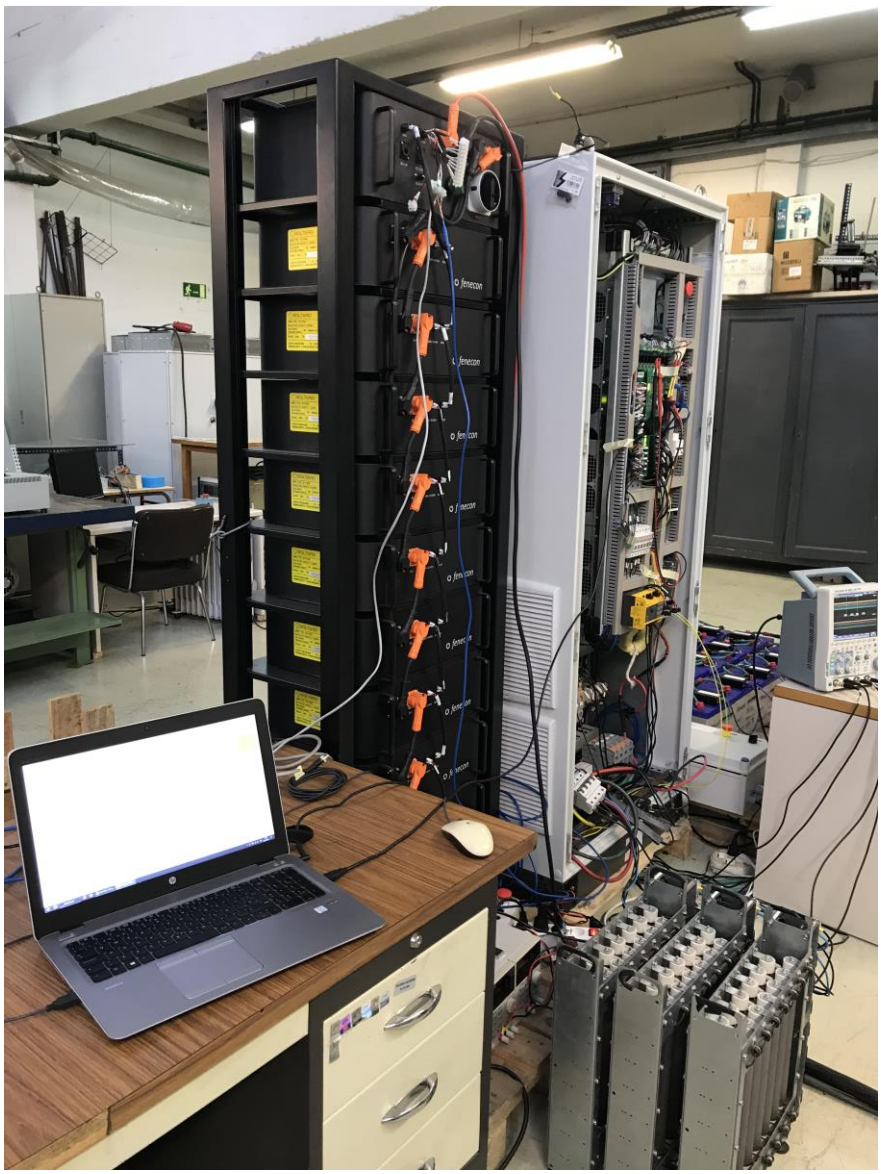

*Figure 84. Experimental setup*

In the image can be seen the setup explained before. The laptop can be seen clearly, the lithium battery is the tall black cabinet, the following cabinet has the converters and the control board, under this cabinet there are the resistances controlled with a relay which act has a load and at the end the oscilloscope and under it, the lead batteries. Figure 85 shows a closer view of the cabinet which contains the converters, the interconnections and the control board. Figure 86 shows a closer view to the lead battery.

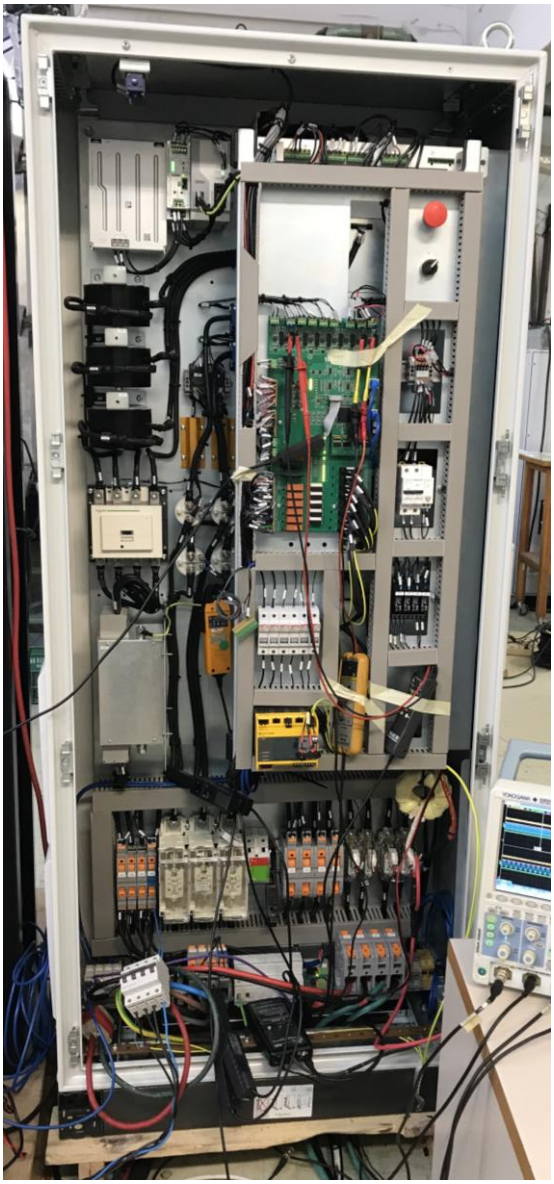

*Figure 85. Closer view to the cabinet of the power electronics and the control board*

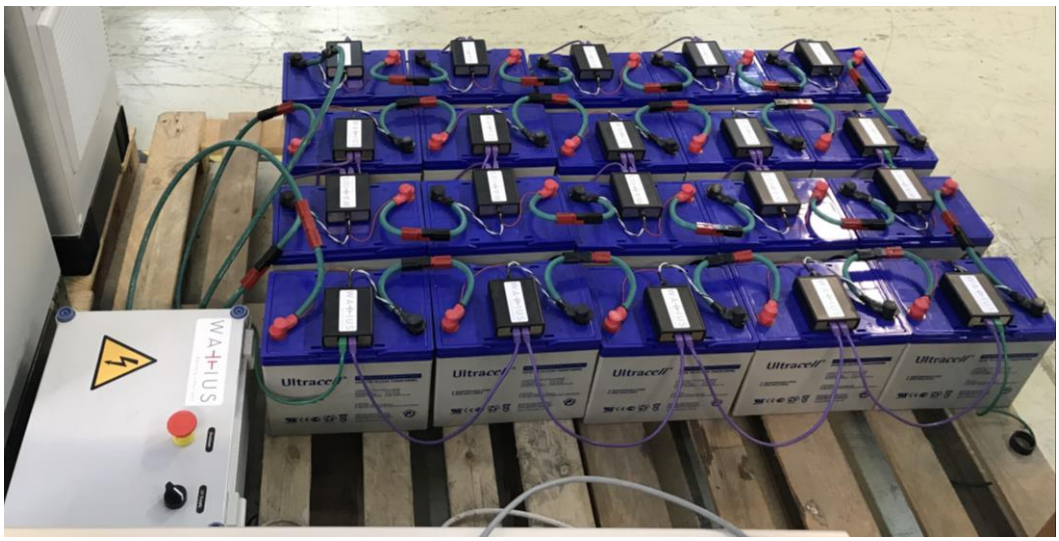


*Figure 86. Closer view to the lead battery*

The control board (Figure 87) is based in a TMS320F28378D microcontroller from the Texas Instrument Delfino family. As it is said before, this microcontroller has two DSP cores and two control law accelerators (CLA) that runs at a 200 Mhz clock frequency. It has also 4 different 16-bit ADC with 12 inputs each which are used to make all the measurements, the bus voltage, the battery voltages, the temperatures and the currents. The PWMs to control all the switches are generated by 16 out of its 24 PWMs modules. There are also two used PWMs to control the fans of the converters, one PWM for each converter. The peripheral for all kinds of digital communication are available, but in this project the only communications used were SSI, SCI (for the Modbus) and CAN. Finally, there are enough digital inputs/outputs to control all the relays for disconnect or connect one battery to the converter; to make the precharge of the input filter, to be able two know if there is something wrong in the shutdown chain such as, the door is not well closed or the shutdown button is pressed; to know if the drivers of the switches had any fault; and to be able to generate the enable signal for the SCI transceiver and the reset signal for the switches drivers.

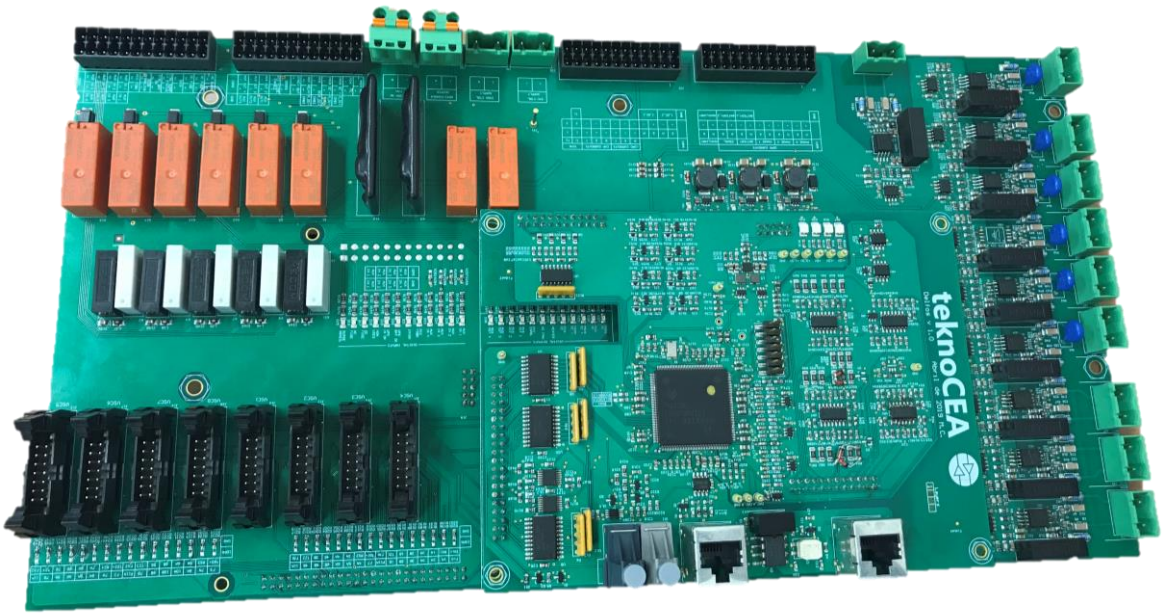


*Figure 87. Closer view to the control board*

All of these explained features of the microcontroller were programmed taking into account the hardware. The implemented program for the microcontroller is divided in two, one part for each core. The first core is the main one and it is the one responsible to decide which peripheral, GPIO or memory section is controlled by which core and it starts the program of the second core. Therefore, firstly the first core starts with the distribution of peripheral, GPIOs and memory section and then both cores make the configuration of their peripheral, CLA, interrupts, memory and GPIOs and with the variable's initializations. Then, both main loops are executed based on the simplified state machine schematized in Figure 88.

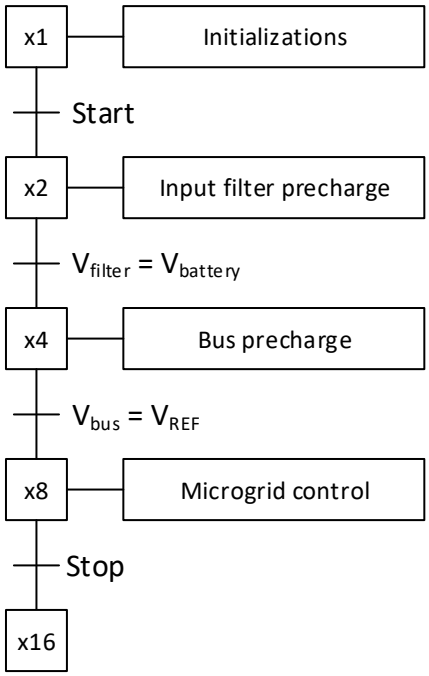


*Figure 88. Microcontroller state machine*

It must be said that the controls run in the CLAs parallel to the cores, but the cores, or, specifically the state-machines are the ones to enable or disable the control loops depending on the state of the converters. The CLAs are also in charge of evaluating all the alarms which are the following ones:

- Overcurrent: it is an alarm that triggers when the battery current or the output current is greater than the imposed limits.
- Overvoltage: it triggers when a battery or bus voltage is greater than the maximum one.
- Undervoltage: it triggers when the minimum bus voltage to ensure the correct behavior of the converter using the implemented technique is not reached.
- Over phase: it triggers when the calculated phase between PWMs is greater or lower than 180º.
- Shutdown button: it triggers when the shutdown button is pressed.
- Communication error: it triggers when there is no communication between the battery and the converter during more than 1 second or when more than 5 messages are not correct.
- Drivers error: it triggers when it is received an error from the drivers by the digital inputs ports. This error could be a supply error or an over current through the switch.
- Battery error: it triggers when the battery reports an internal error through the communications.
- Precharge error: it triggers when the precharge stage is not fulfilled in the maximum time allowed.

All the PI controllers were designed in continuous time but, they are executed in discrete time in the CLA. In order to implement them keeping the same performance, the controllers were transformed into discrete time using the bilineal approximation and executed at 40 kHz.

All the experimental results are captured by an oscilloscope in csv format to plot them afterwards together with the simulations.

### 4.3. Time constant estimation

This result is the only one that does not follow the simulation and experimental setups. The simulation is made as it is explained in the section 3.4 with a first order delay and the CL filter. The experimental result is made connecting the converter to the battery and the other end to a voltage source of 770 V in order to be able to make a real current step without all the controls. Figure 89 shows the result of the simulation and the experimental test.

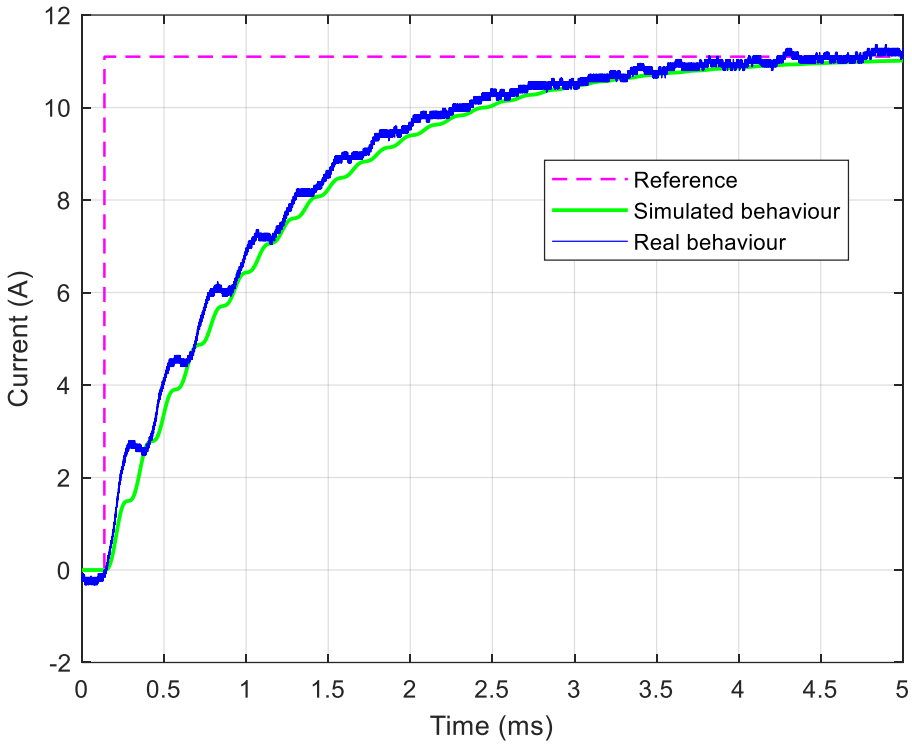


*Figure 89. Results of the simulation and the experimental test of the behaviour of the converter to a current input step*

As it can be seen, the simplification of the converter into a first order system is verified because there is no significant difference between the simulated behaviour and the real one obtained in experimental testing.

### 4.4. One converter setup

In this subsection, the results of simulating and testing the setup with only a single converter are presented. This step has been done for two reasons. The first one was to validate easily the setup, because only one program had to be made and only one converter had to work, validating that the simulations corresponded to the real behaviour and the second reason was to implement all the controls step by step, first in one converter, and then in both. It must be said that the converter used in all the results of this section is the one which is connected to the lead battery.

### 4.4.1. Primary control

As it is said before, one objective of simulating and testing only one converter was to validate the simulations. For that reason, the primary control is tested with different values of virtual resistance to accomplish different behaviour in the simulations and the experimental test and check that the simulation and the results of the test match.

#### 4.4.1.1. First order behaviour

In order to accomplish an overall first order behaviour with only one converter the virtual resistance used was 1,48 Ω although it is not the final virtual resistance. With this virtual resistance value, there are carried out a battery of simulations and experimental tests. The first one was to apply a positive current perturbation, Figure 90. The second one was applying a negative current perturbation by removing the load resistors, Figure 91. The third one and the fourth one were a change of the voltage setpoint, Figure 92 and Figure 93, respectively. The last one was a big change of the reference setpoint to force the saturation of the converter, Figure 94.

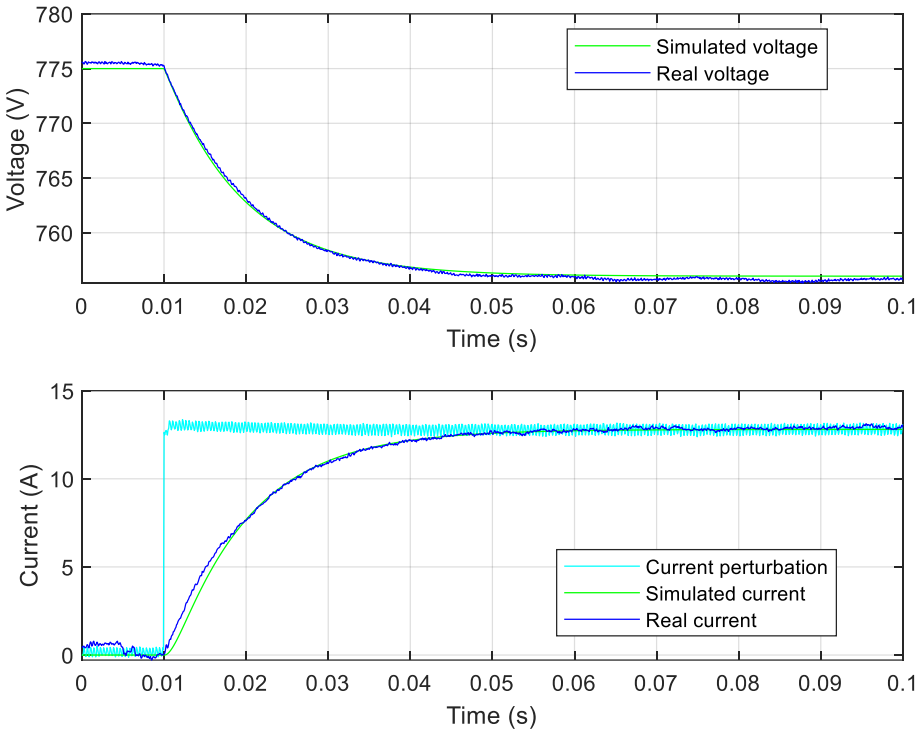


*Figure 90. Results of the simulation and the experimental test of the primary control with only one converter forcing a first order behaviour to a positive current perturbation*

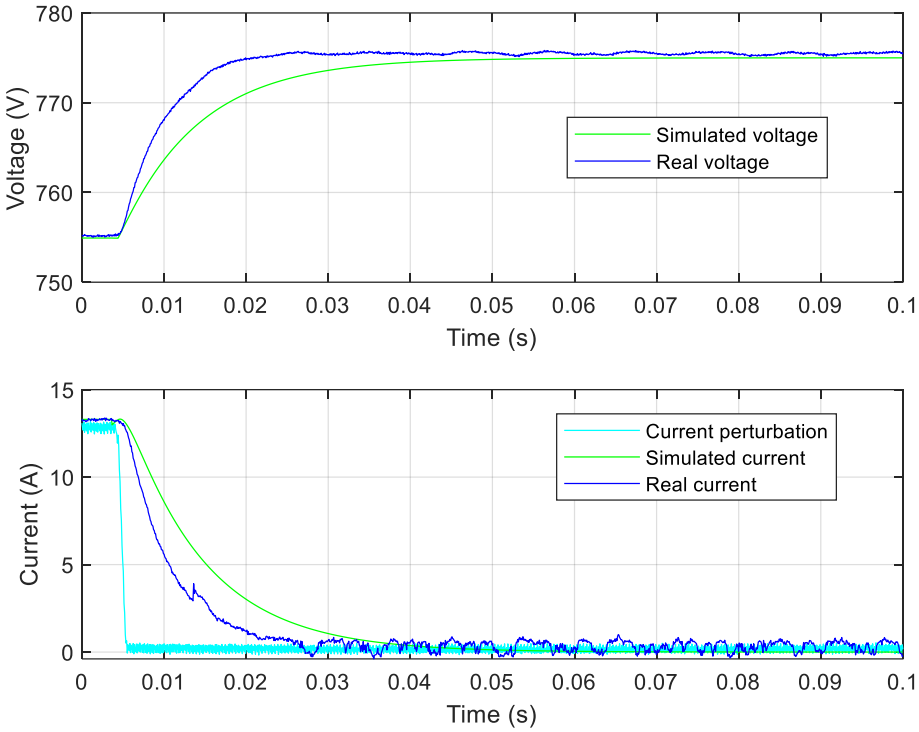


*Figure 91. Results of the simulation and the experimental test of the primary control with only one converter forcing a first order behaviour to a positive negative perturbation*

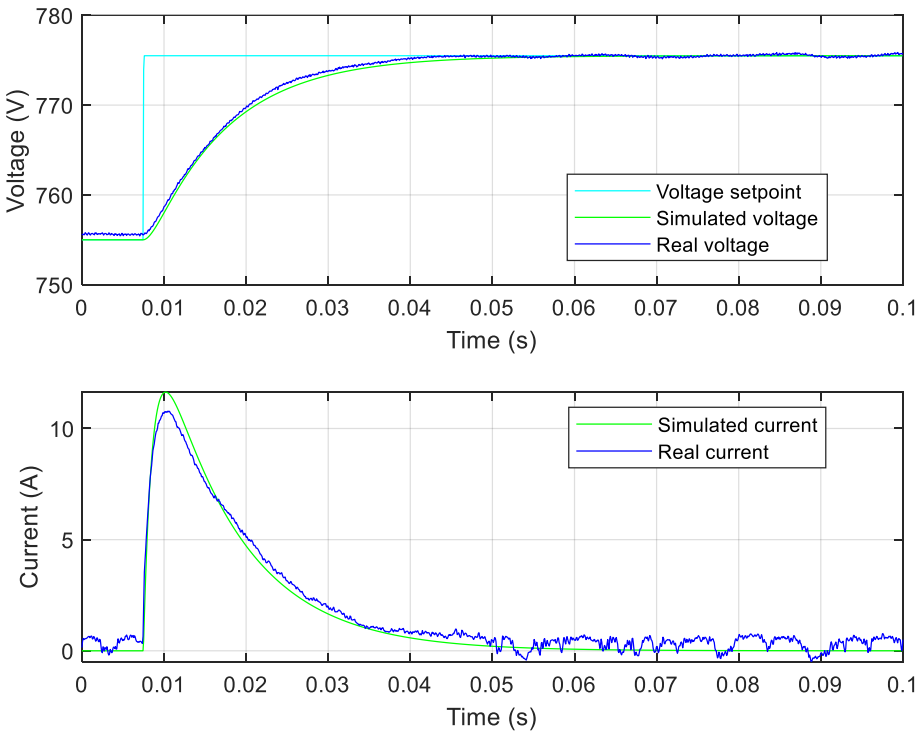


*Figure 92. Results of the simulation and the experimental test of the primary control with only one converter forcing a first order behaviour to a positive reference change*

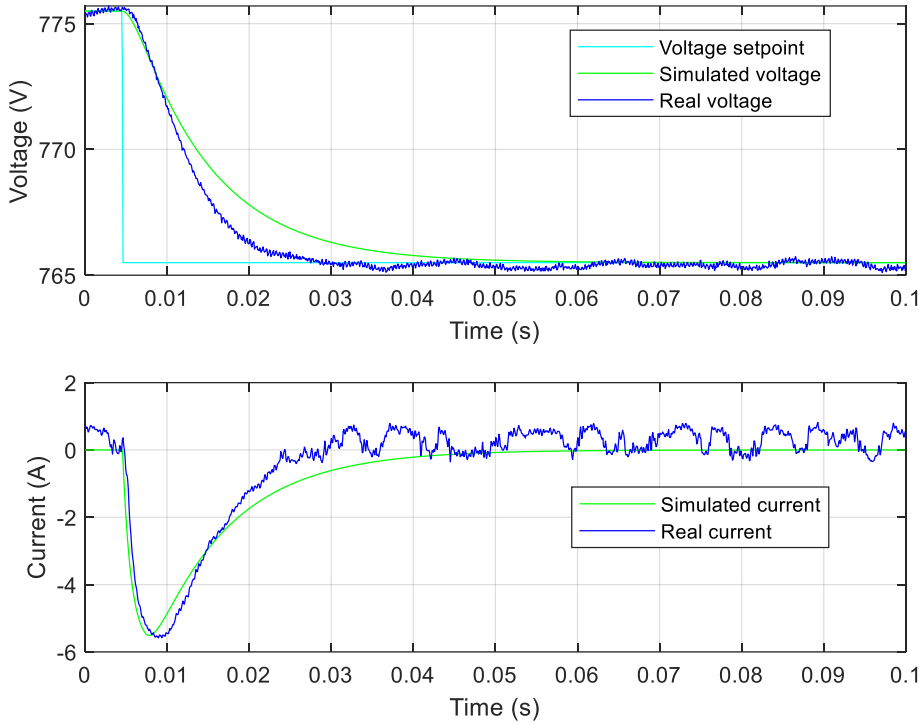


*Figure 93. Results of the simulation and the experimental test of the primary control with only one converter forcing a first order behaviour to a negative reference change*

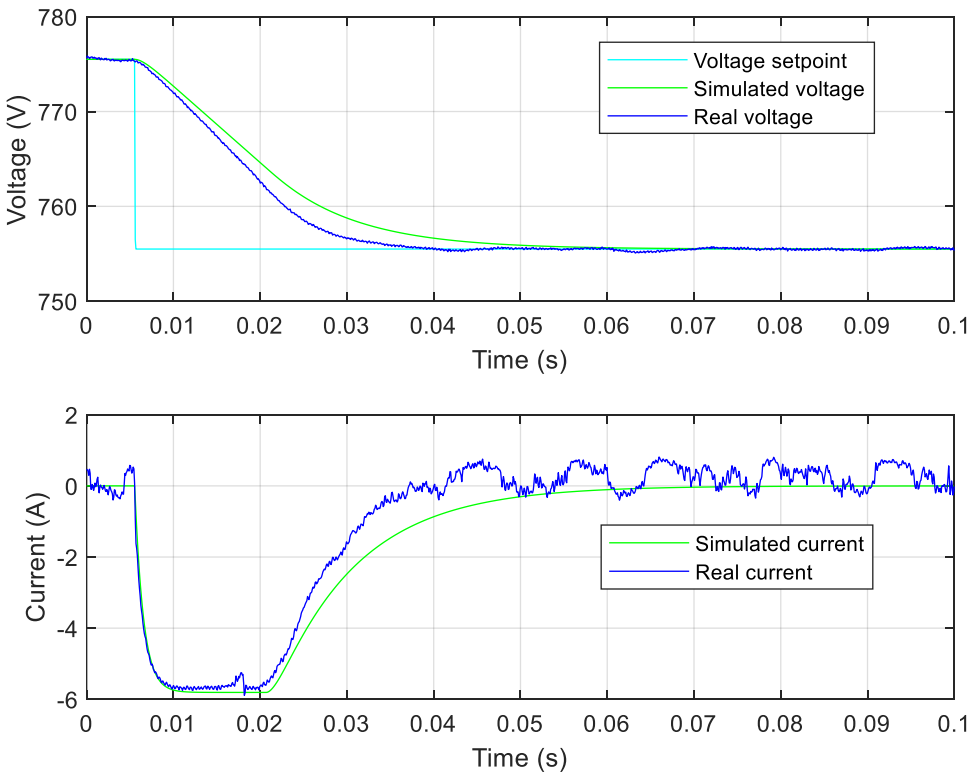


*Figure 94. Results of the simulation and the experimental test of the primary control with only one converter forcing a first order behaviour to a big negative reference change*

As it can be seen in Figure 90, Figure 91, Figure 92, Figure 93 and Figure 94 the simulations match the results obtained with the experimental tests with no significant differences. Therefore, it can be said that all the made simplifications to do the simulations are acceptable and that the simulations are good enough to verify the behaviour of the microgrid in a more complex setup with 2 or more converters.

In Figure 90, Figure 92, the simulations match almost perfectly the experimental results but in Figure 91, Figure 93 and Figure 94 there are little differences. These differences are not significant and moreover, in these cases the real behaviour was better than the simulated one because it was faster without any peak. The causes for these differences are the difference on the load: in the simulation is a current source while in reality is a resistor and the assumption of having an ideal system when simulating but it is not and actually, it has losses and parasitic components. In this concrete case, the inequalities appear when the voltage bus drops and it may be cause by the load which is a resistor in reality and an ideal current source in simulations and by the parasitic resistances of the capacitor and the balanced resistor which allow the bus voltage decrease faster.

It also must be said that, in steady-state conditions, the real behaviour had oscillations due to the noise captured on the measurements.

#### 4.4.1.2. Underdamped second order behaviour

In this subsection, the primary control is simulated and test selecting a virtual resistance of 0,11 Ω (although it is not the final virtual resistance) which ensures an underdamped second order behaviour of the system. These simulations and experimental tests have been done to make sure that the simulations correspond with reality and to see the effect off the saturations when the behaviour has oscillations. The first result shown in Figure 95 is a change of the reference and the second test in Figure 96 is the response of the system to a current perturbation while the saturation of the converter is forced by software to be the load current, this way the behaviour of the converters before a maximum power perturbation can be validated.

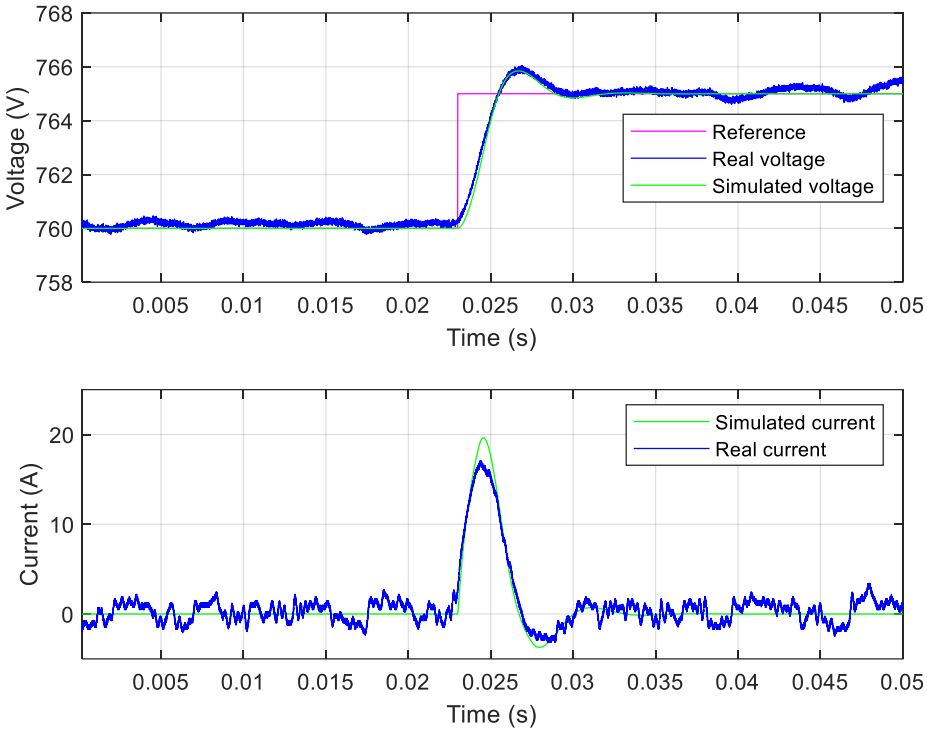


*Figure 95. Results of the simulation and the experimental test of the primary control with only one converter forcing a second order behaviour to a positive reference change*

As it can be seen in Figure 95, the simulation matches the experimental results with slightly differences, the experimental results show the same time response with a lower current peak.

In the second test case, as the system has a peak, the effect of the saturation must be analysed. As the system cannot give the give the peak and the converter behaves as a first order delay, the bus voltage will stabilize in an unexpected value when a current perturbation is applied. Therefore, the simulation and experimental test were to force the saturation of the current to the applied current perturbation, Figure 96. This way, the effect of the saturation is reproduced as the converter was working in maximum power. Moreover, in order to compare the behaviour with and without saturation, the system is also simulated without it.

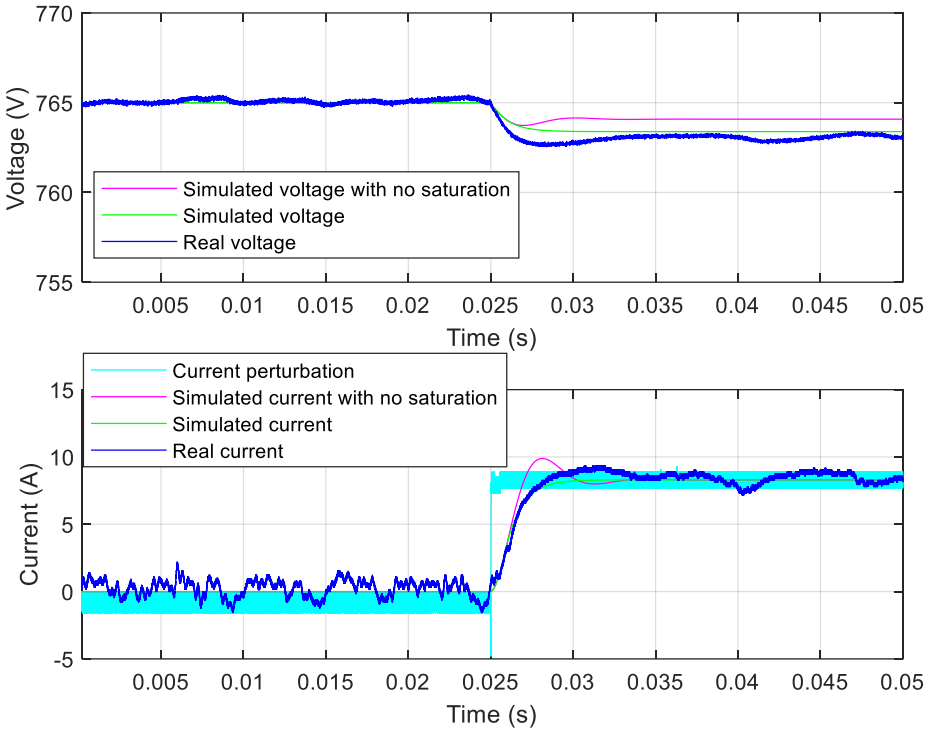


*Figure 96. Results of the simulation and the experimental test of the primary control with only one converter forcing a second order behaviour and the saturation to a positive current perturbation*

In Figure 96 the behaviour of the system forcing the saturation to the current perturbation is shown. It can be seen that the real test current matches perfectly the simulated one but with some oscillations in steady-state due to the noise measurement. Moreover, it can be seen that there are some non-significant differences in the dynamic response of the bus voltage, but the simulated one and the real one stabilizes at the same value of 763 V while it should have stabilized in 764 V as it is shown in the simulation without saturation. This voltage difference in steady-state is due to the saturation effect because as the converter cannot give the expected current peak, the voltage peak cannot be corrected producing this way a deviation from the expected bus voltage.

#### 4.4.1.3. Final behaviour

As the simulations have been proven to be well done, the final desired behaviour has to be simulated and tested. In section 3.4.3.1, the final virtual resistances are selected, and, as it is used the second converter (the one connected to the lead battery), the virtual resistance tuned was 1 Ω.

The simulations and experimental test made were the following ones. The first one was to apply a positive current perturbation, Figure 97. The second one was applying a negative current perturbation by removing the load resistors, Figure 98. The third and the fourth ones were a change of the voltage setpoint, Figure 99 and Figure 100.

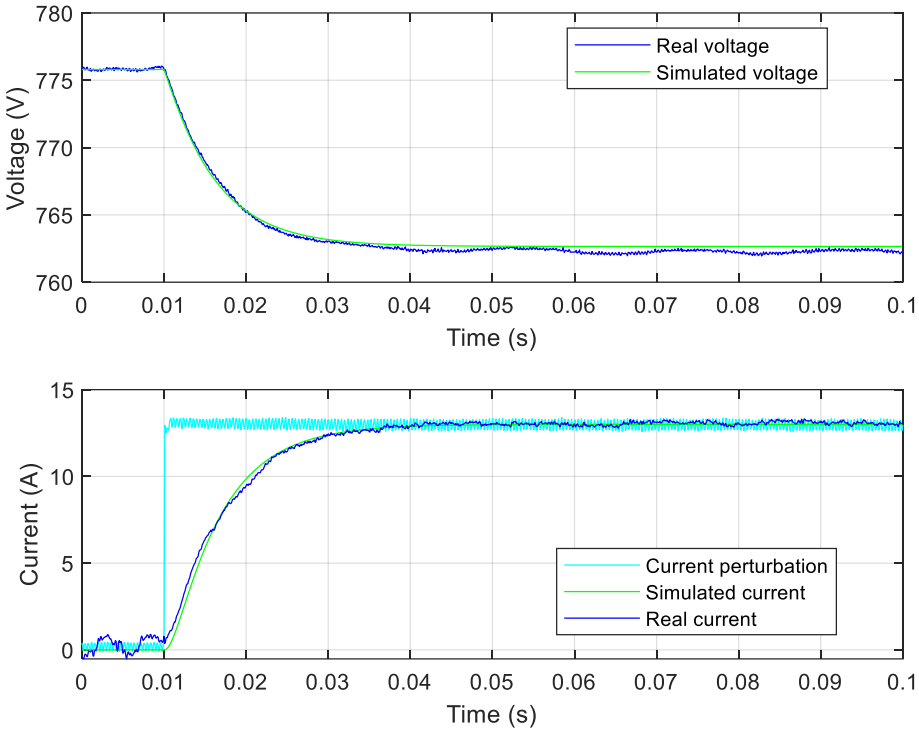


*Figure 97. Results of the simulation and the experimental test of the primary control with only one converter to a positive current perturbation*

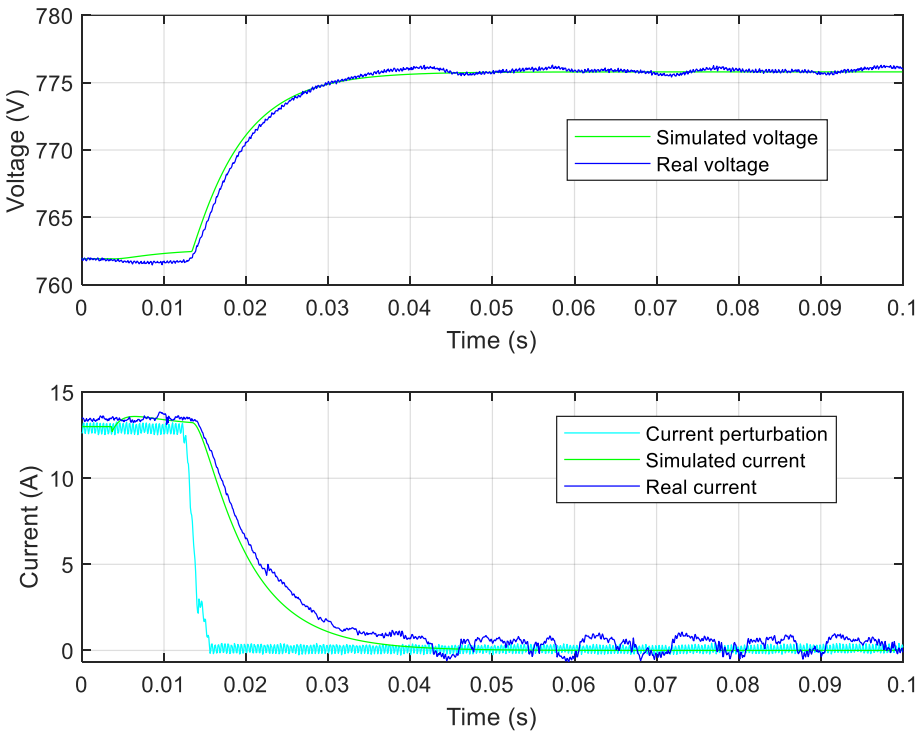


*Figure 98. Results of the simulation and the experimental test of the primary control with only one converter to a negative current perturbation*

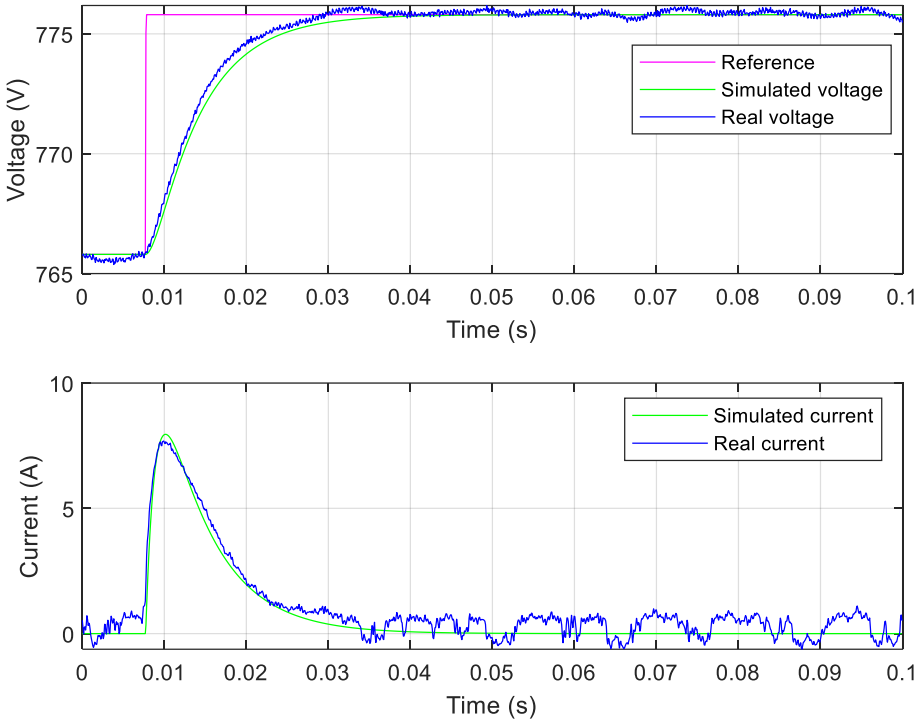


*Figure 99. Results of the simulation and the experimental test of the primary control with only one converter to a positive reference change*

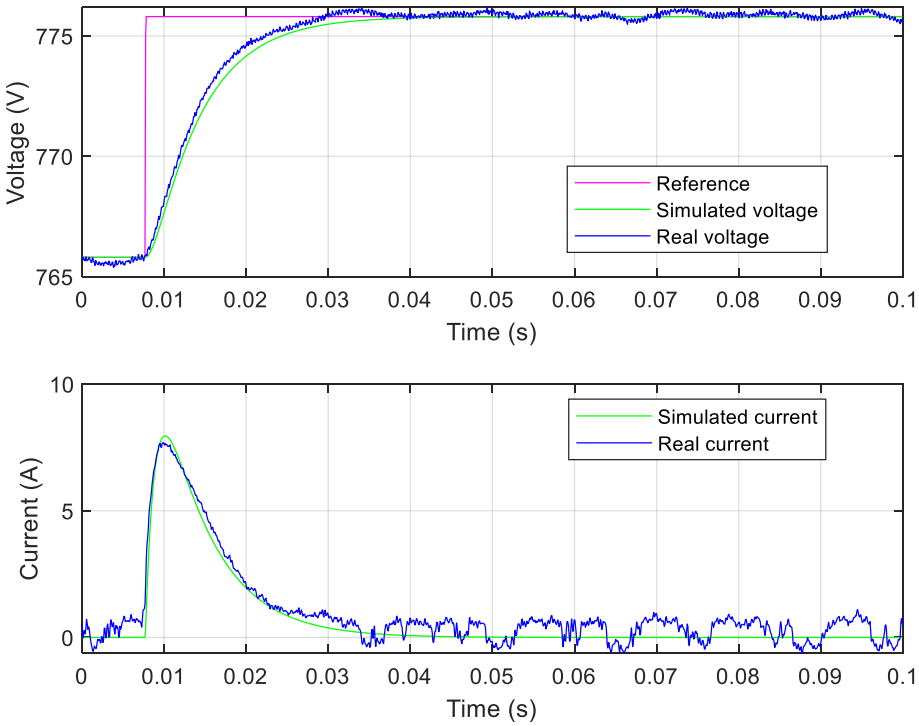


*Figure 100. Results of the simulation and the experimental test of the primary control with only one converter to a negative reference change*

As expected, the simulation matches the real results with little differences in steady-state state due to the explained oscillations generated by the measurement acquisition noise and some dynamic slightly mismatches response because of the simplifications applied to the simulated system. Therefore, it can be concluded that the primary control with only one converter behaves as expected.

### 4.4.2. Secondary control

In order to implement the controls step by step, the secondary control was tested in only one converter with the constants selected in section 3.5.2.4 ($k_p$ = 0,043 and $k_i$ = 145,73). The simulations and experimental test made were a positive current perturbation (Figure 101), a positive setpoint change (Figure 102) and a negative setpoint change (Figure 103).

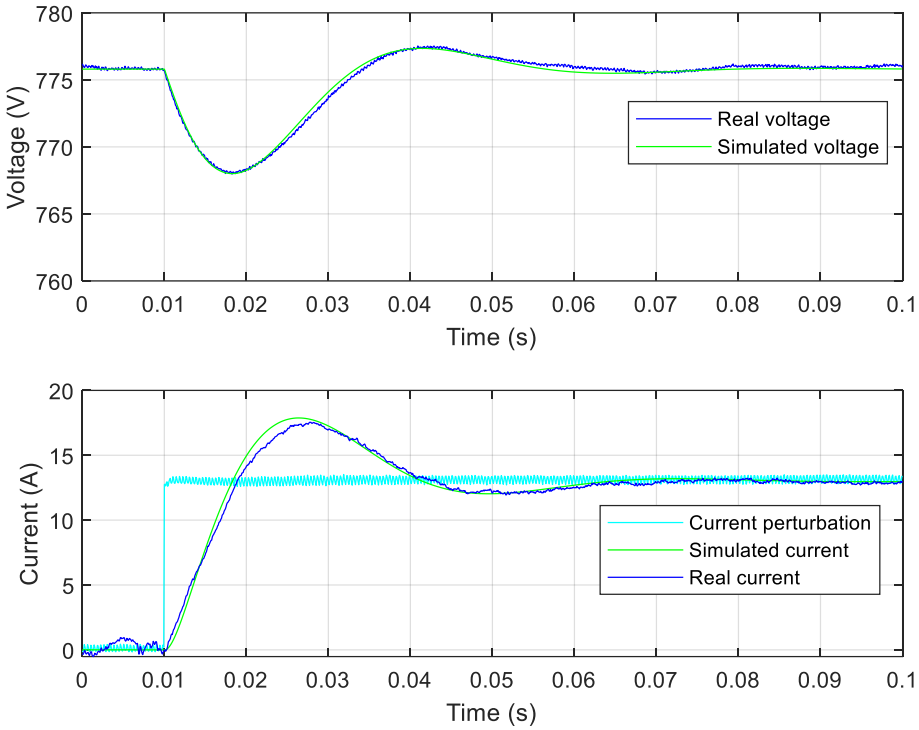


*Figure 101. Results of the simulation and the experimental test of the secondary control with only one converter to a positive current perturbation*

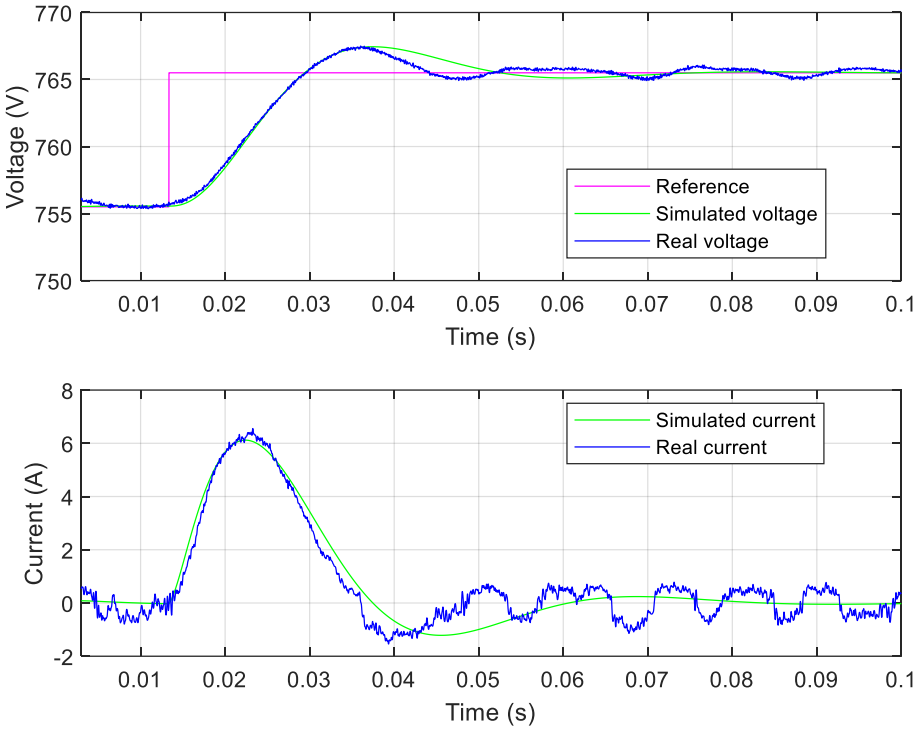


*Figure 102. Results of the simulation and the experimental test of the secondary control with only one converter to a positive reference change*

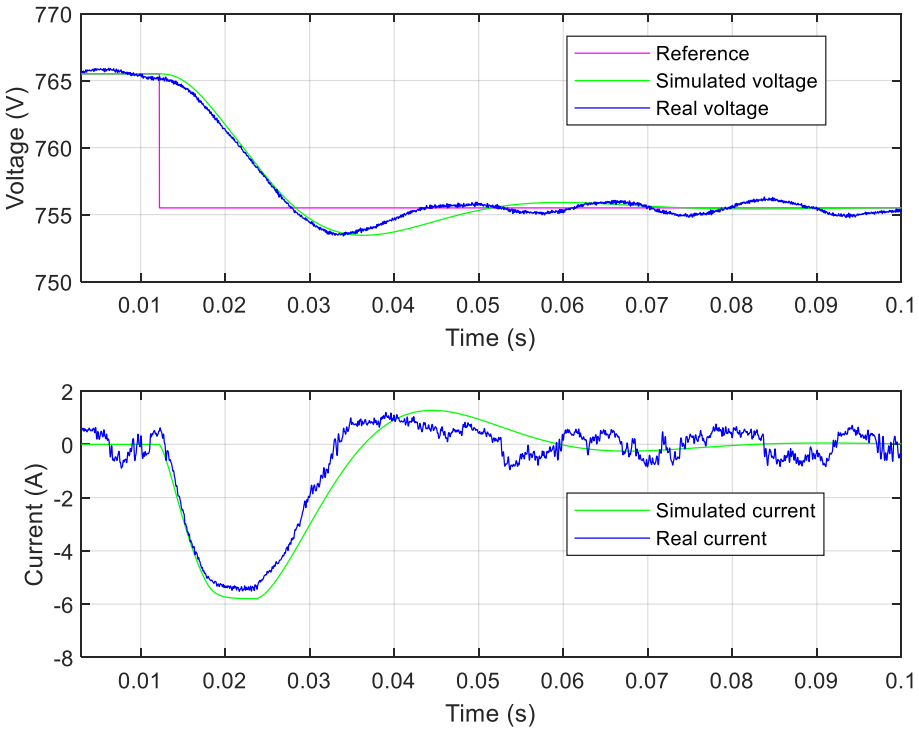


*Figure 103. Results of the simulation and the experimental test of the secondary control with only one converter to a negative reference change*

In Figure 101, the simulation matches perfectly the experimental results but in Figure 102 and in Figure 103 there are slightly differences in the dynamic response of the system being the experimental results a little bit faster than the simulated behaviour. Although these little differences, it can be said that the system works as expected. Therefore, it is expected to have a proper behaviour representation of the system when implementing this secondary control to both converters.

#### 4.4.2.1. Saturation effect

In order to simulate the saturation effect of the PI controller, its limits had been set to ±7 V. The expected behaviour of the secondary control with this saturation was to be able only to correct 7 V. Therefore, the simulation and the experimental test consisted in applying a current perturbation which would produce a voltage drop of 12,65 V which is bigger than this 7 V value, Figure 104. This situation resembles the maximum power one when the secondary controller cannot give more offset and, therefore, cannot increase the current because the system is already at maximum power.

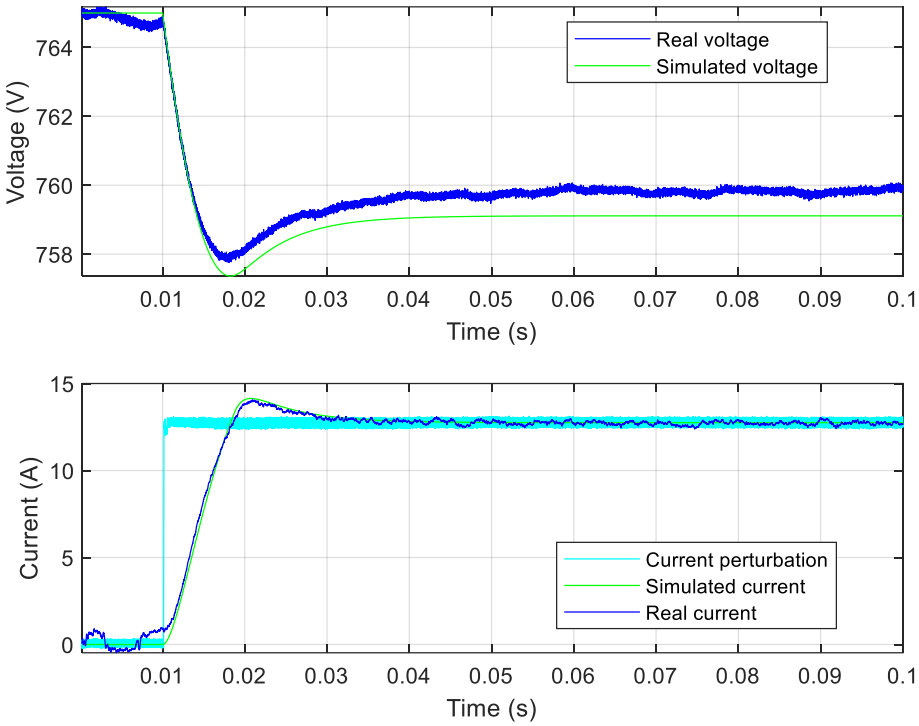


*Figure 104. Results of the simulation and the experimental test of the secondary control with only one converter forcing a lower saturation to a positive current perturbation*

The simulations and the results show that the simulation current and the experimental current matches perfectly but the voltage have some differences because the simulated one has a bigger peak and it stabilizes at a lower voltage than the real one. It must be said that although the PI controller saturates, the integral part will not accumulate error because an antiwindup is implemented.

The conclusion of these simulations and experimental test of the secondary control is that it works correctly with only one converter, even better than expected in some situations. Therefore, all the calculations made in the previous sections are valid because the expected behaviour matches the real one.

## 4.5. Two converters setup

Once the primary and secondary controls are simulated, implemented and tested in one converter, the same procedure must be done this time with both converters. For this reason, the different control levels are implemented and tested progressively. This section is divided in the following subsections: in the first one the results of the implementation of the primary control presented in section 3.4 are shown; in the second one the results of the implementation of the secondary control of section 3.5 are presented; then the results of the implementation of the classic tertiary control calculated in section 3.6 are shown in the third subsection; and finally, in the last one, the results of the implementation of the proposed control in section 3.7 are presented.

### 4.5.1. Primary control

The primary control implemented is the one selected in 3.4.3.1 with virtual resistances of 0,6 Ω for the first converter and 1,0 Ω for the second converter. With these values the expected behaviour of the system was a second order one with a low peak of 2%. In order to test the system, the simulations and experimental test were made.

The first test was to apply to the capacitor a current perturbation with the resistor bank, Figure 105. The second one was to remove this load simulating a negative current perturbation, Figure 106. The third one was a positive change in the setpoint, Figure 107. Finally, the last one was a negative change in the setpoint, Figure 108.

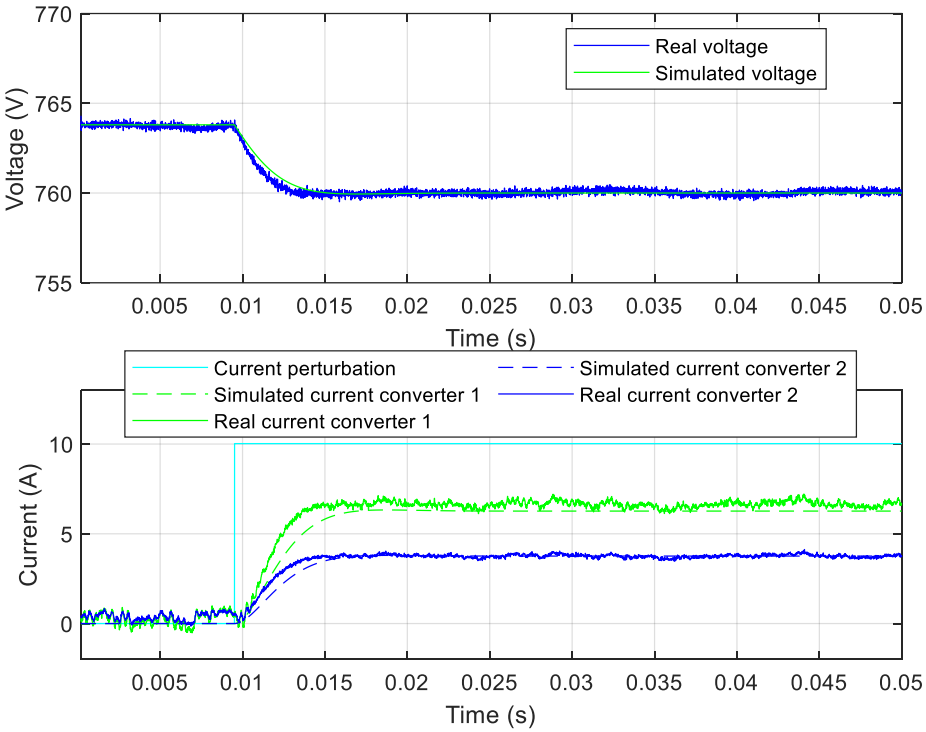


*Figure 105. Results of the simulation and the experimental test of the primary control with two converters to a positive current perturbation*

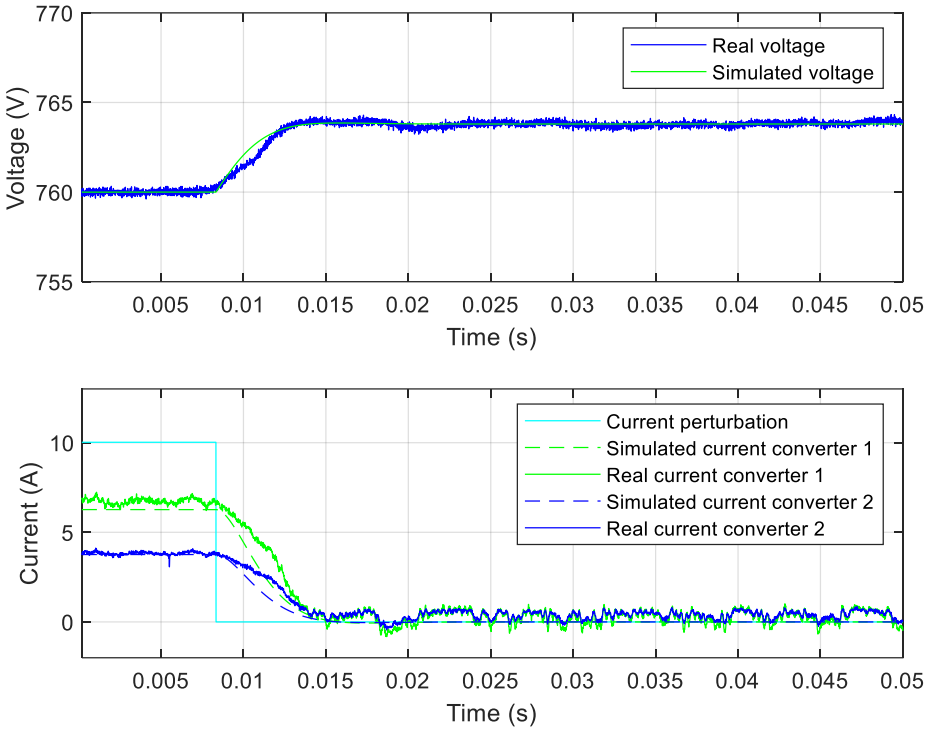


*Figure 106. Results of the simulation and the experimental test of the primary control with two converters to a negative current perturbation*

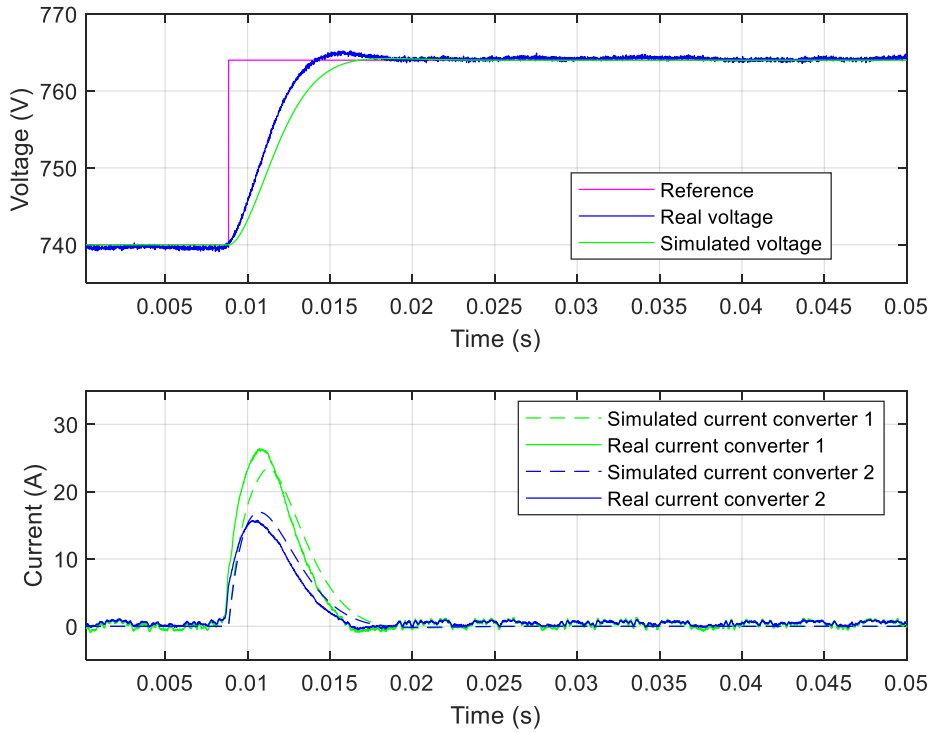


*Figure 107. Results of the simulation and the experimental test of the primary control with two converters to a positive reference change*

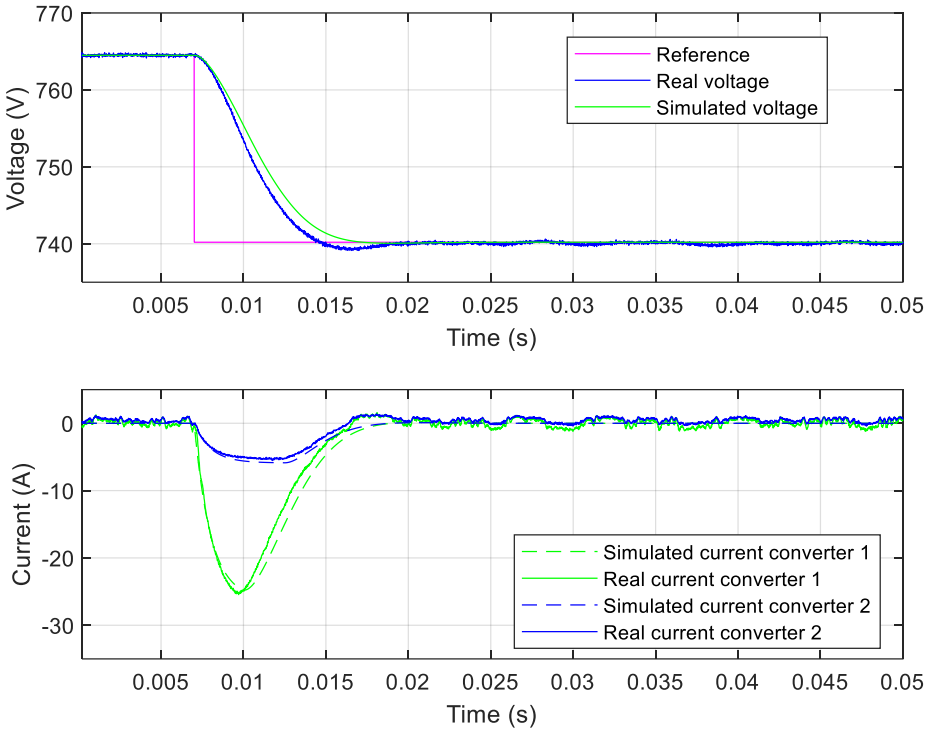


*Figure 108. Results of the simulation and the experimental test of the primary control with two converters to a negative reference change*

The experimental test shows that the system has a similar but not identical behaviour than the expected one. The real behaviour has a faster response with a slightly greater peak, around 4 % instead of the expected 2 %. This 2 % deviation is acceptable because the system has a very low peak and a fast response as expected. Therefore, the simplifications and calculations of the primary control for the two converters are valid and the implementation of the primary control is finished.

### 4.5.2. Secondary control

The secondary control with two converters was implemented once the primary was tested. The constants used to simulate and to carry out the experimental tests were the ones calculated and selected in section 3.5.2.4 being $k_p = 0{,}043$ and $k_i = 145{,}73$. The simulations and experimental test consisted in the application of a current perturbation to the capacitor (Figure 109) and a positive and a negative change in the setpoint (Figure 110 and Figure 111, respectively). Finally, there is another subsection with a simulation and an experimental test forcing the saturation of the controller.

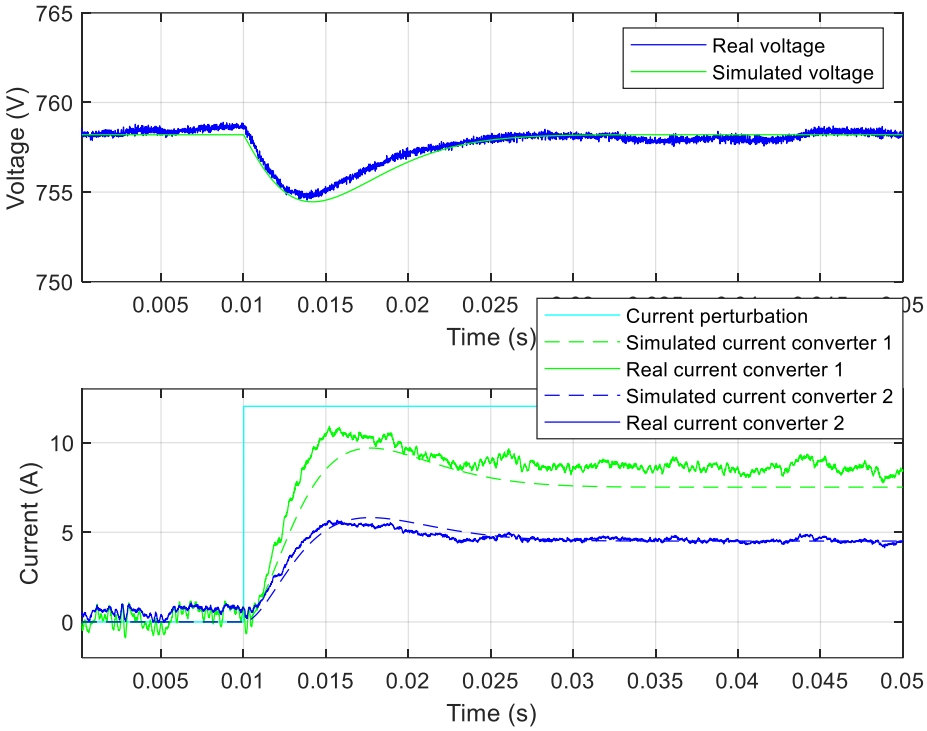


*Figure 109. Results of the simulation and the experimental test of the secondary control with two converters to a positive current perturbation*

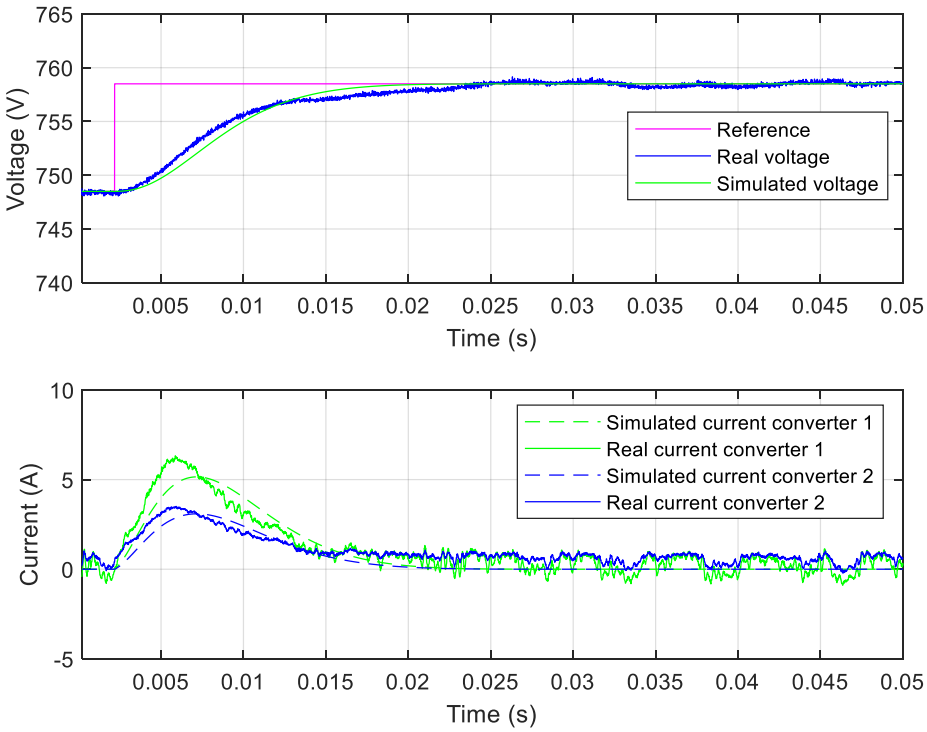


*Figure 110. Results of the simulation and the experimental test of the secondary control with two converters to a positive reference change*

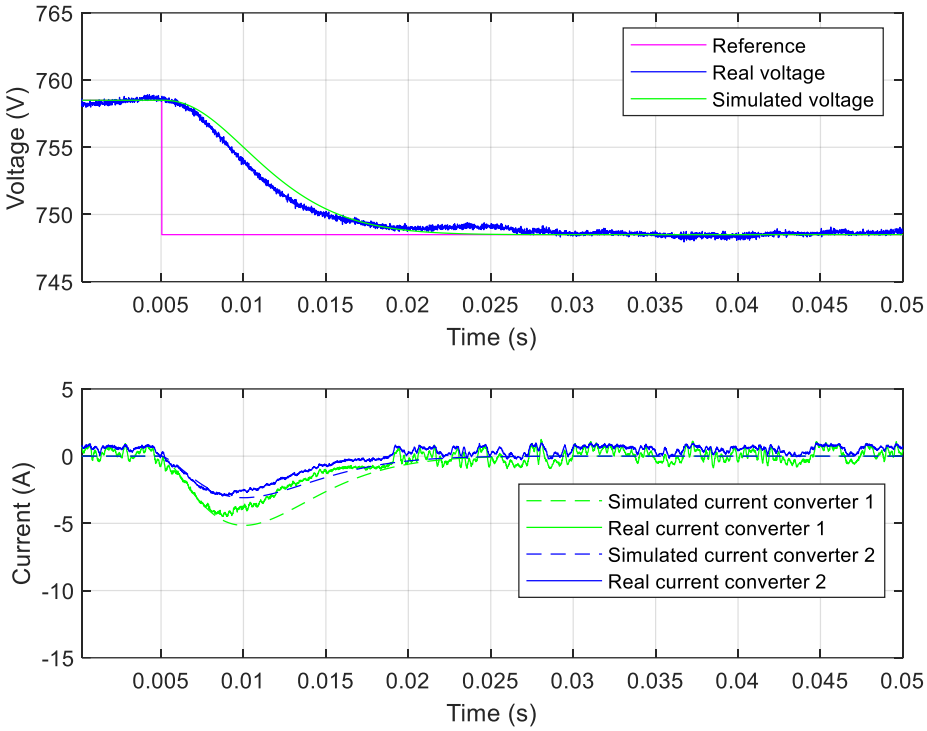


*Figure 111. Results of the simulation and the experimental test of the secondary control with two converters to a negative reference change*

As it can be seen in the results figures, the implemented secondary control behaves as expected because the real behaviour obtained with the experimental test matches the simulated one. As before, the most significant differences appear in the steady-state conditions because of the measurement noise.

Although these small differences, it can be concluded that all the simplifications to tune the controller are correct and, consequently, the system behaves as expected. Therefore, the constants of the controller are valid and they will be kept for the simulation and implementation of the tertiary control.

#### 4.5.2.1. Saturation effect

In addition to the previous results, the effect of the saturations is check by doing another simulation and experimental test where the limits of the controller were set to ±2 V. Therefore, the secondary control will be able to correct only this voltage excursion. The simulation and experimental test consisted in applying a current perturbation which would produce a 4,5 V droop and check the behaviour of the secondary control, Figure 112.

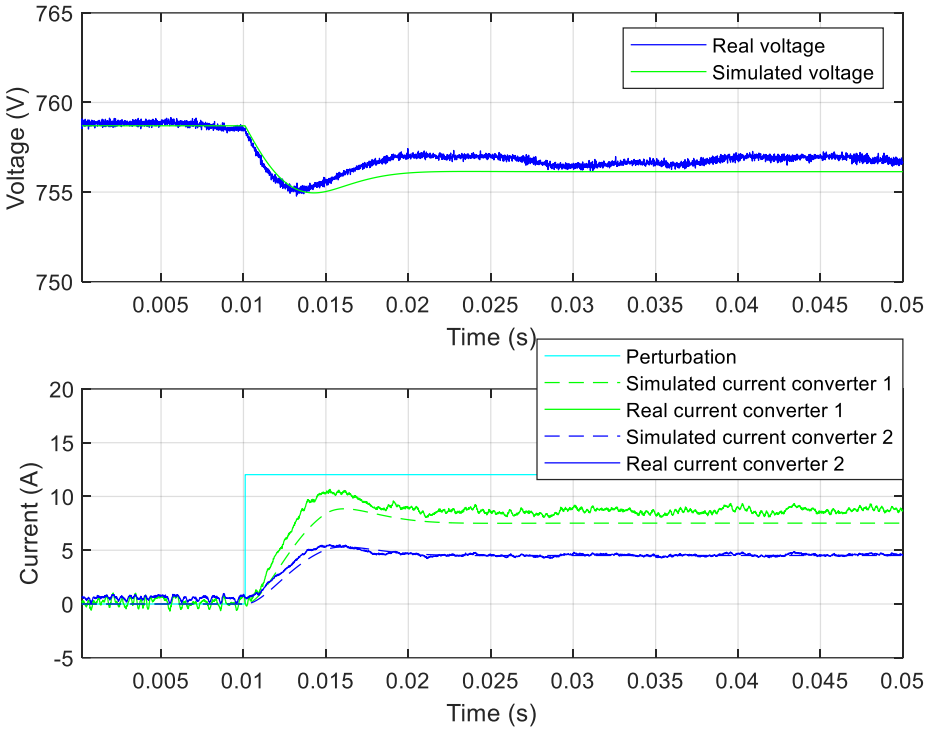


*Figure 112. Results of the simulation and the experimental test of the secondary control with two converters forcing a lower saturation to a positive current perturbation*

As expected, the real voltage cannot stabilize at the desired value but it stabilizes at a little bit higher value than the simulated one. This simulation and experimental test resemble the behaviour of the system when a maximum current perturbation is applied and the secondary control is not able to correct the voltage deviation. This situation is not critical because the primary control was already calculated to work in-between the bus voltage limits. Moreover, as it is explained before, although the PI controller saturate, it will not accumulate error because an antiwindup method is implemented.

### 4.5.3. Tertiary control

The last level of the classical control is the tertiary control to fix the power sharing in steady-state conditions. As the primary and the secondary were already tested and validated, the tertiary was implemented as explained in section 3.6 with the constants selected in section 3.6.2, being $k_p = 0$ and $k_i = 0{,}01$. The simulations and experimental test are very similar to the previous ones. The first simulation is the application of a current perturbation to the capacitor and fixing a power reference of 10 kW, Figure 113. The second simulation is the same situation but the power reference is 12 kW, Figure 114. The third simulation is a power reference change, from 8kW to 12 kW, Figure 115. The fourth one, the current perturbation is applied when there is a current interchange between the two converters because the reference was 2 kW, Figure 116. Finally, the last one is a voltage reference change while the reference of the power was 2 kW, Figure 117.

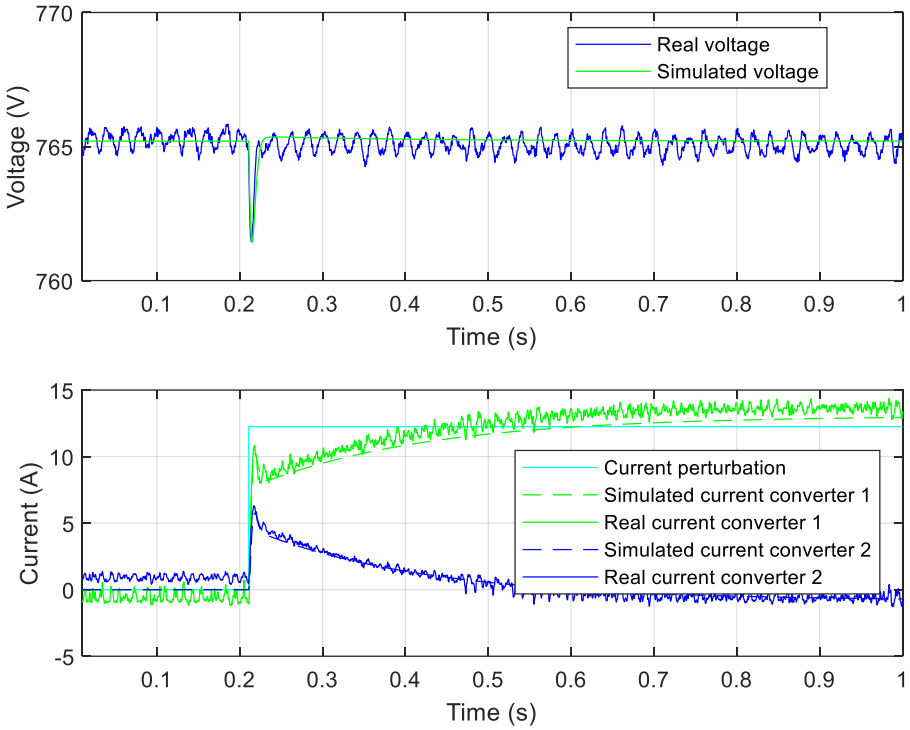


*Figure 113. Results of the simulation and the experimental test of the tertiary control to a positive current perturbation fixing the power reference to 10 kW*

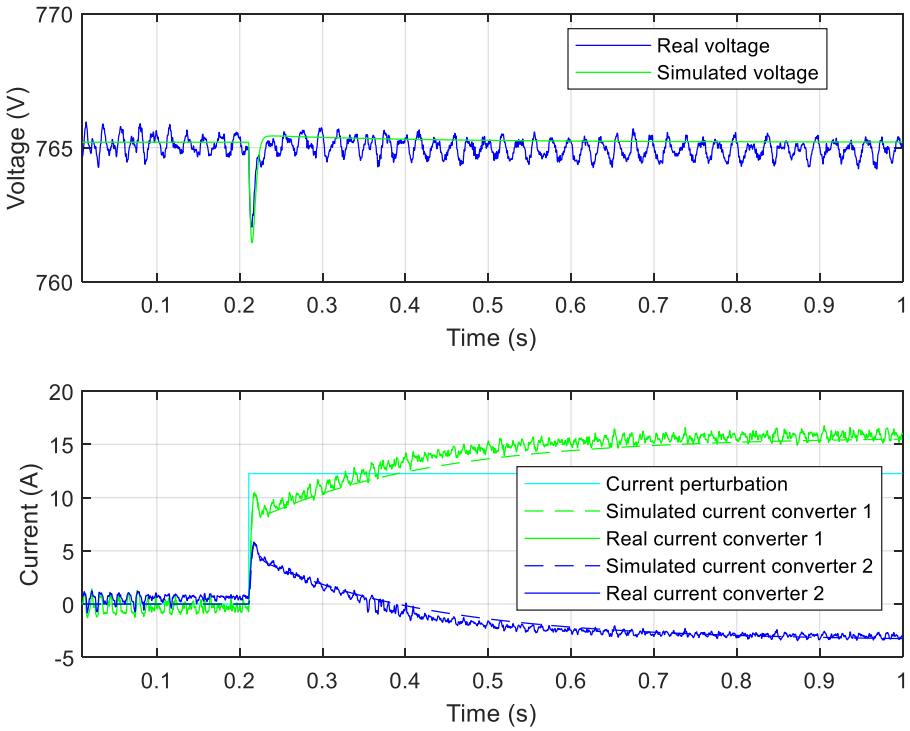


*Figure 114. Results of the simulation and the experimental test of the tertiary control to a positive current perturbation fixing the power reference to 12 kW*

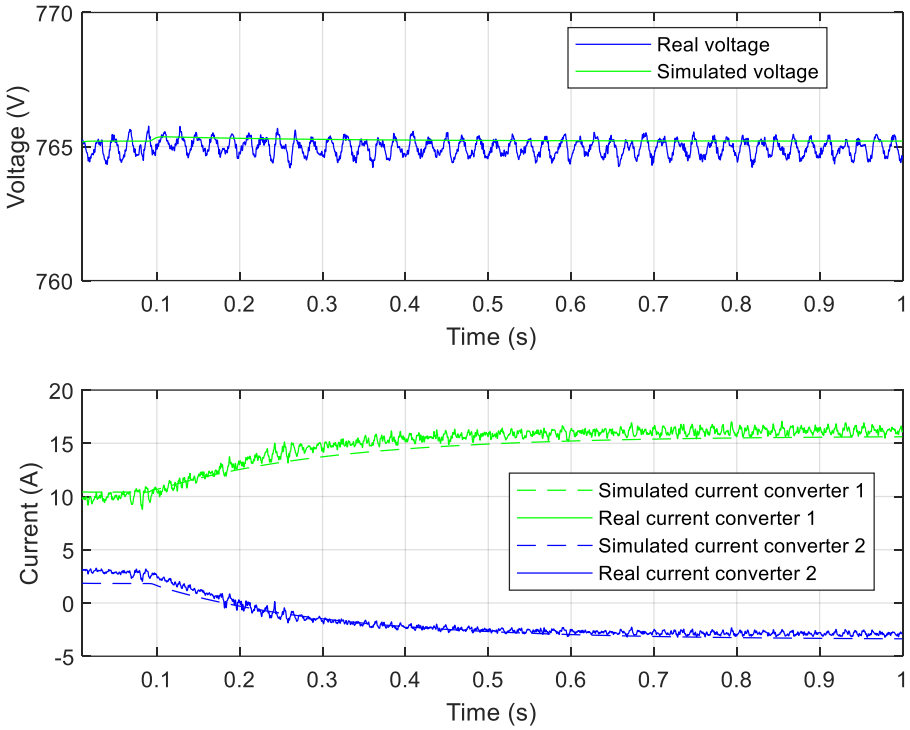


*Figure 115. Results of the simulation and the experimental test of the tertiary control to a power reference change, from 8 kW to 12 kW*

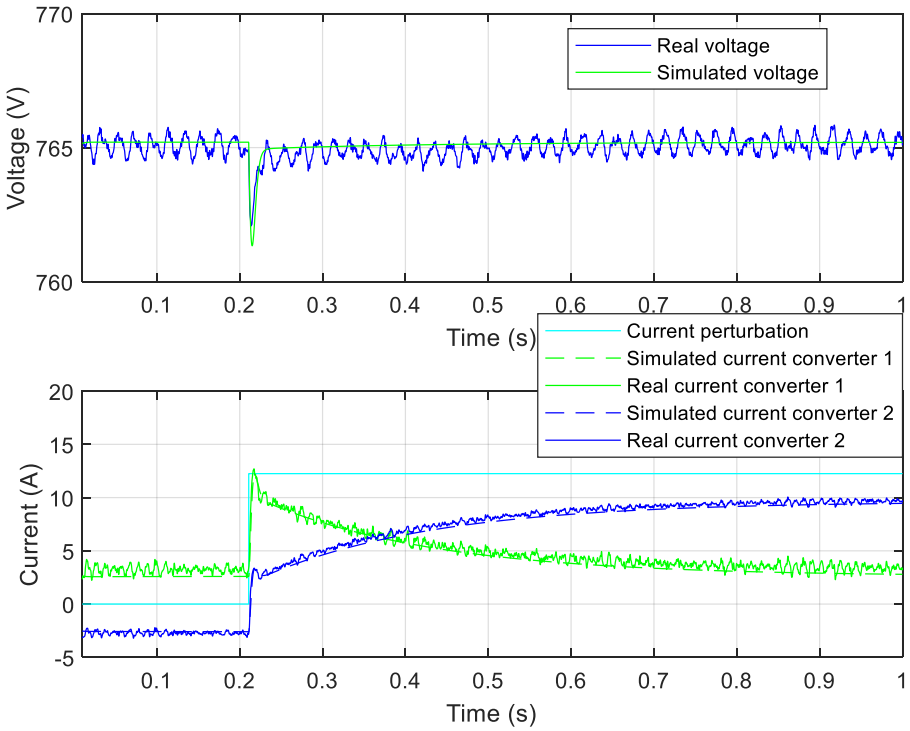


*Figure 116. Results of the simulation and the experimental test of the tertiary control to a positive current perturbation fixing the power reference to 2 kW*

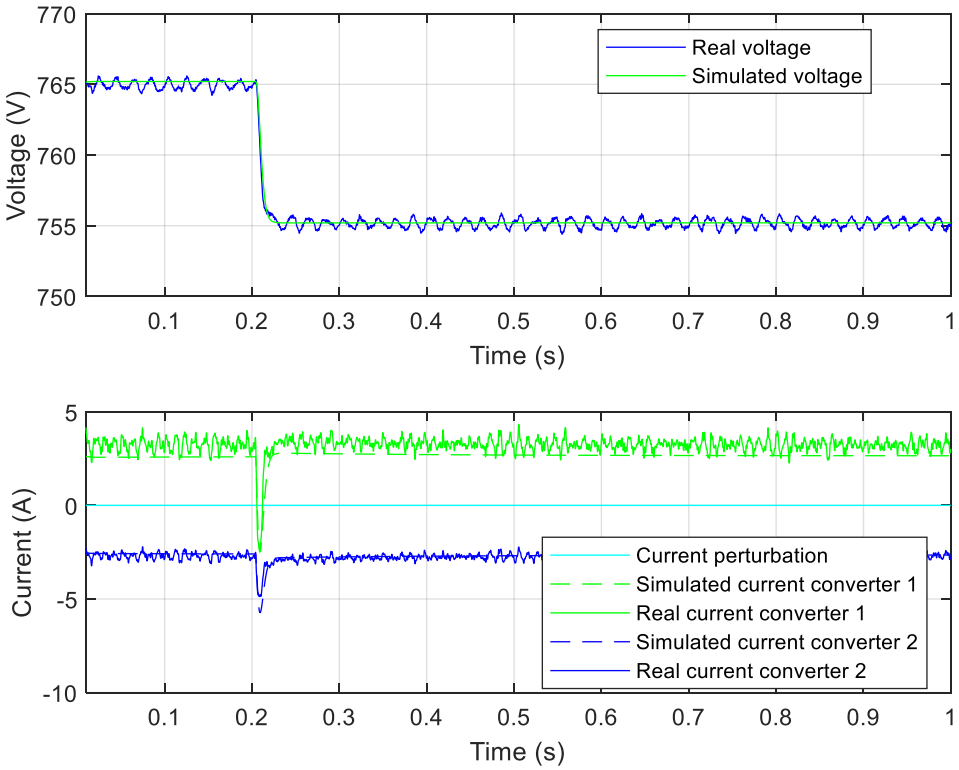


*Figure 117. Results of the simulation and the experimental test of the tertiary control to a positive current perturbation fixing the power reference to 2 kW*

The final real behaviour matches perfectly the expected simulated behaviour. The behaviour matches better than the secondary control one because, as the control of the Dual Active Bridge is an open loop calculation and may be mismatches between the calculations and reality, there is no close loop which ensure that the converter follows its reference. By adding this tertiary control, the power loop of one converter is closed and consequently, the converter is force to follow the current reference given by the controls. The power of the other converter is over determinate by the power of the load and the power of the other controlled converter.

As a conclusion of this Droop DC control with three levels, it can be said that it works as expected, and therefore, all the simplifications, assumptions, calculations and simulations are validated.

### 4.5.4. Unified hierarchical DC control

As it was explained, the final proposed control is a combination between the secondary control and the tertiary and it has been called as *unified hierarchical DC control*. Therefore, in order to implement it step by step, first the primary control must be tested which already is and then implement and test the controller which acts as a secondary plus tertiary control thanks to the distribution constant. The two first simulations and experimental test were the application of a current perturbation to the capacitor (Figure 118) and a negative change of the setpoint (Figure 119) with a distribution constant of 0,5 which means that in steady-state the power is distributed equally between the converters (50% each one).

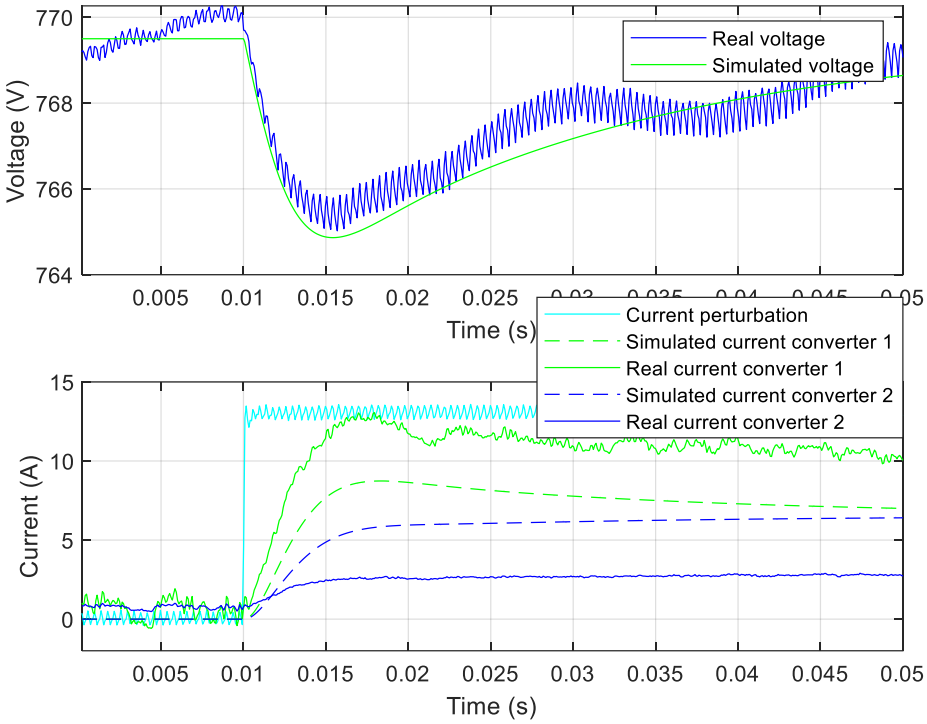


*Figure 118. Results of the simulation and the experimental test of the final control with two converters to a positive current perturbation*

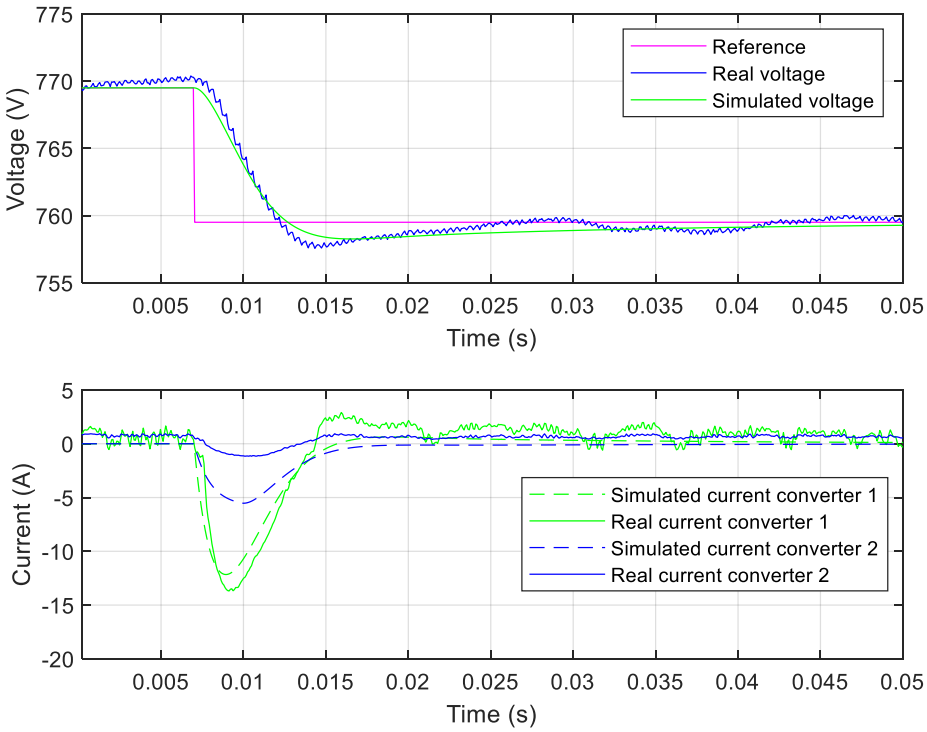


*Figure 119. Results of the simulation and the experimental test of the final control with two converters to a negative reference change*

As it can be seen the real behaviour of the bus voltage matches the simulated one, but the currents of the converters do not. This differences in the current are caused by the inherent open loop control of the Dual Active Bridge converters. It is given a current setpoint to the converter, and the control calculates the needed phase of the PWMs to accomplish this setpoint but it does not have any negative feedback to ensure that the setpoint is followed correctly. Therefore, the bus voltage dynamics is not affected because the overall behaviour of the sum of current remains constant although the distribution is not the expected one. It can be seen that the first converter gives around 3 A more than the expected and, consequently, the second converter gives around 3 A less.

The following experimental test consisted in changing the distribution constant from 0,5 to 0,7 which means that the first converter should give the 50 % or the power at the beginning and the 70 % of the power at the end, Figure 120.

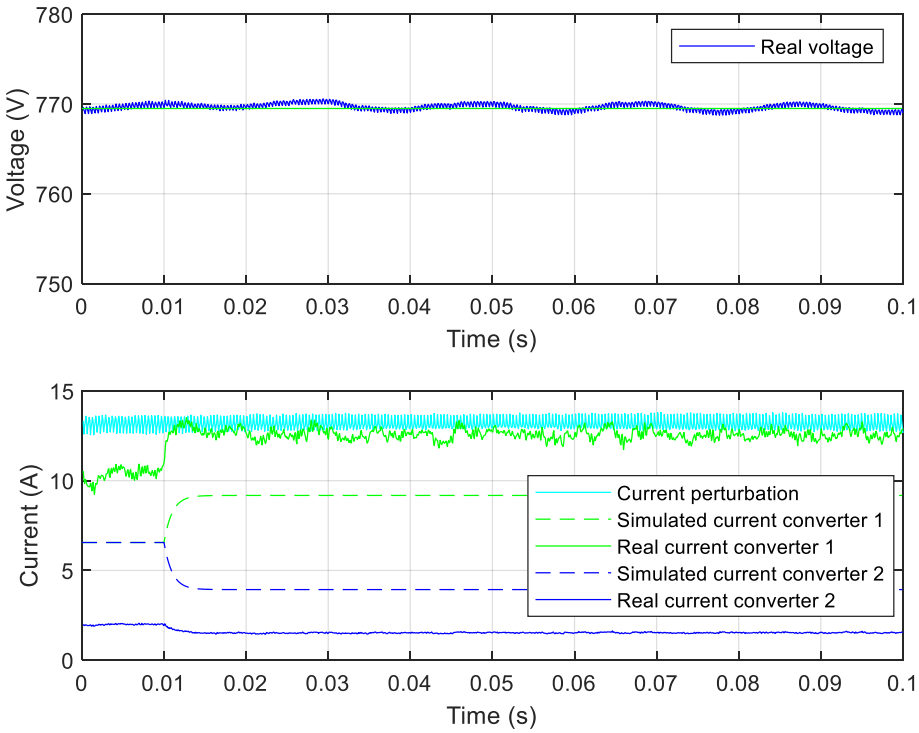


*Figure 120. Results of the simulation and the experimental test of the final control with two converters to a distribution constant change*

The changing of the distribution constant does not affect the bus voltage as it can be seen in the results shown in Figure 120. Although the converters do not follow their setpoint accurately, it can be seen that the increment of the distribution constant produces an increment of the power of the first converter and a reduction of power in the second converter. The expected distribution was a 70/30 but the obtained one was 88/12 because of the explained open loop control of the converters.

In conclusion, this final control does not work exactly as expected due to the current open loop control of the converters, but it shows a correct qualitative behaviour and there are possible solutions to solve the problem. Moreover, if this control is applied to a microgrid with converters whose controls have a negative feedback, this problem will not appear and the control will work correctly.

#### 4.5.4.1. Corrected final control

In order to correct this mismatch between the setpoint of the converters and the real output, it is added a PI controller whose output is added to the setpoint of one converter, Figure 121. Its objective is to make sure that one converter follows the setpoint and, consequently, the other converter will give the expected power because it will be determinate by the load current and the given power of the other converter. This controller was implemented by an Integrator controller whose constant was 0,01.

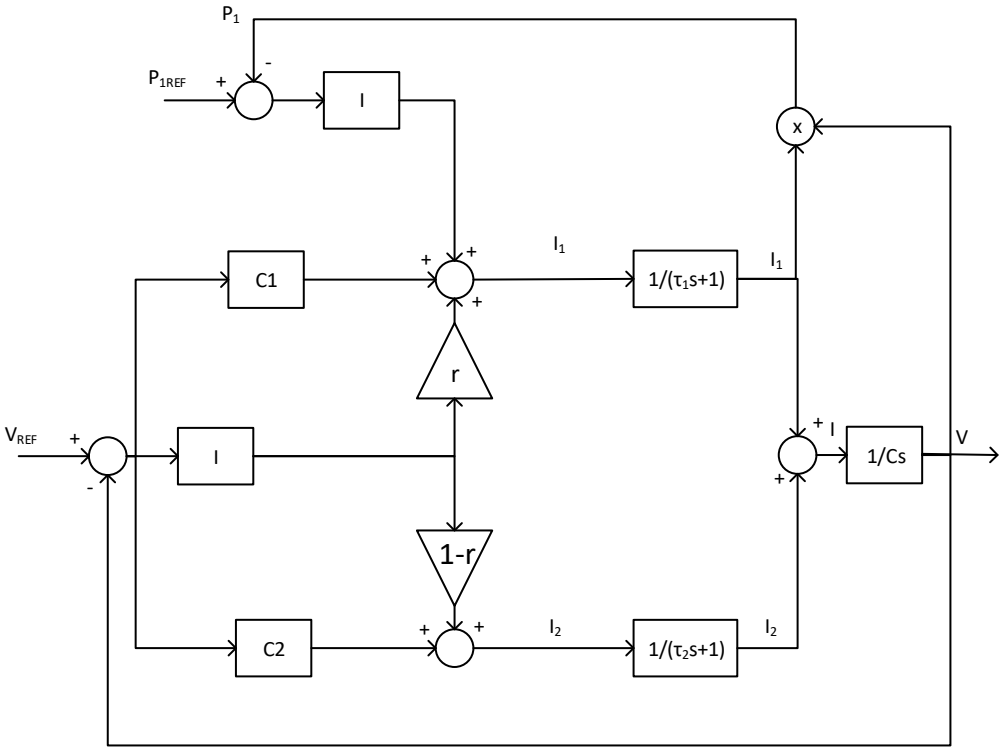


*Figure 121. Corrected final control diagram*

Firstly, it can be thought that this scheme is similar to the classical secondary and tertiary control scheme but it is a little bit different because of the distribution constant. The advantage of this implementation instead of the classical secondary and tertiary control is that the distribution constant already fix some distribution and the power loop only has to correct the power output of the convert instead of be in charge of all the power distribution. It must be said that the saturation limits of the Integral controller where set to ±5 A because it was considered that the current deviation from the reference will not be bigger than this.

In this case, simulations were not made because the deviation from the reference of both converters are not linear and moreover, it was not modeled. Once this controller was implemented to correct this mismatch, the experimental tests were the application of a current perturbation to the capacitor with different values of distribution constant and power reference (Figure 122, Figure 123, Figure 124, Figure 125 and Figure 126) and the change of distribution constant (Figure 127).

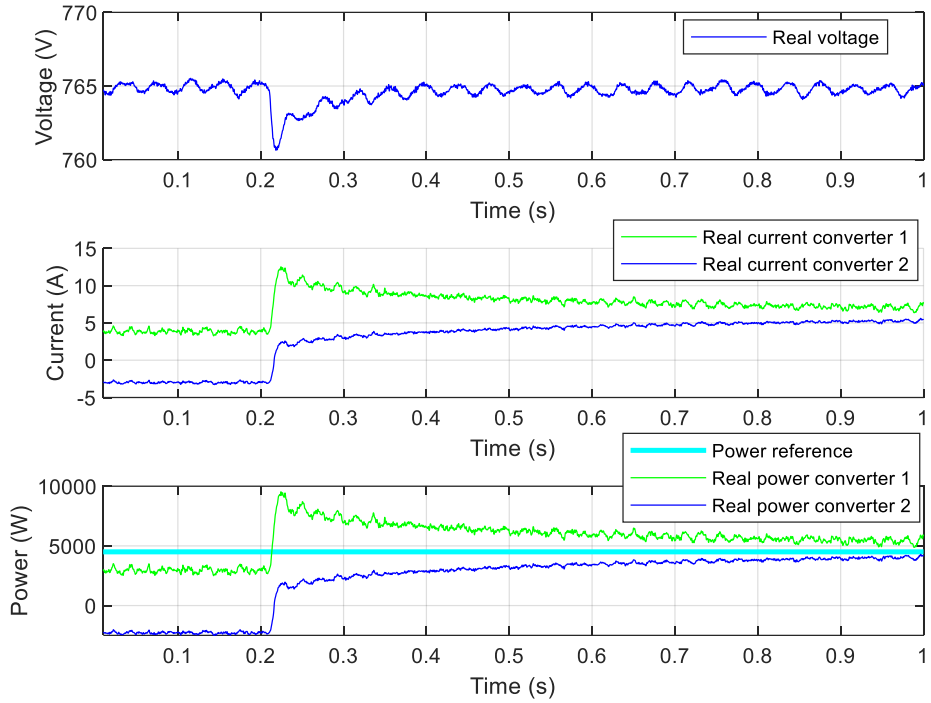


*Figure 122. Results of the experimental test of the corrected final control with two converters to a current perturbation being the distribution constant at 0.5 and the power reference 4500 W*

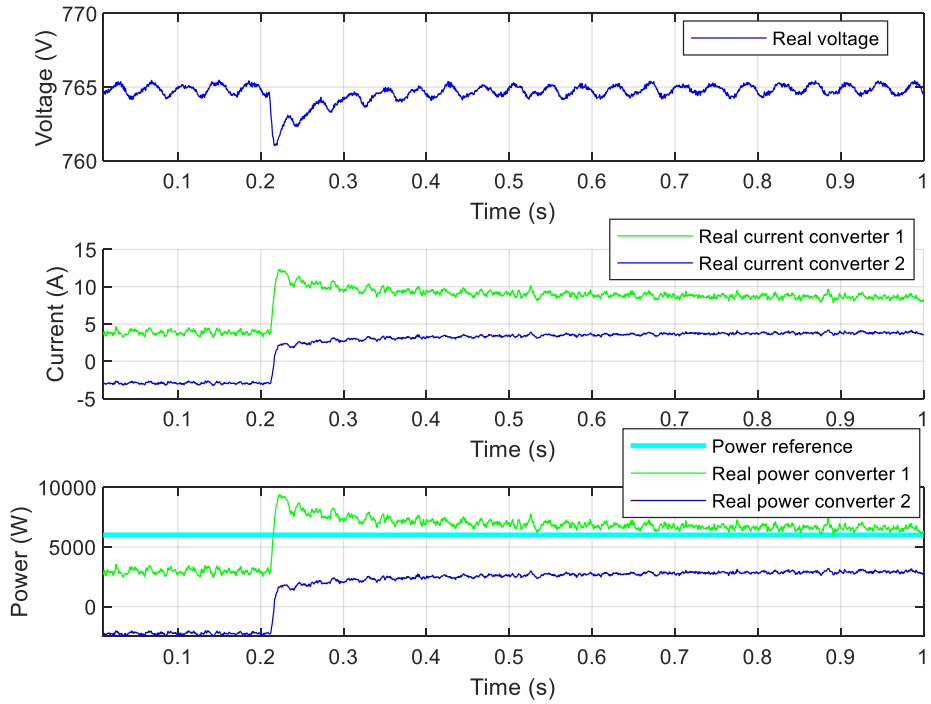


*Figure 123. Results of the experimental test of the corrected final control with two converters to a current perturbation being the distribution constant at 0.5 and the power reference 6000 W*

As it can be seen in Figure 122 and Figure 123, when there is no current perturbation, the power of the converters are given by this additional loop to correct the power. Initially, the controller is saturated but the implemented antiwindup make it not to accumulate error. In these two experimental test, the power given by the first converter is modified to see the capabilities of these power loop. Although, the distribution constant was set to 0,5, the power loop can be used to match this distribution or to have a controllable deviation.

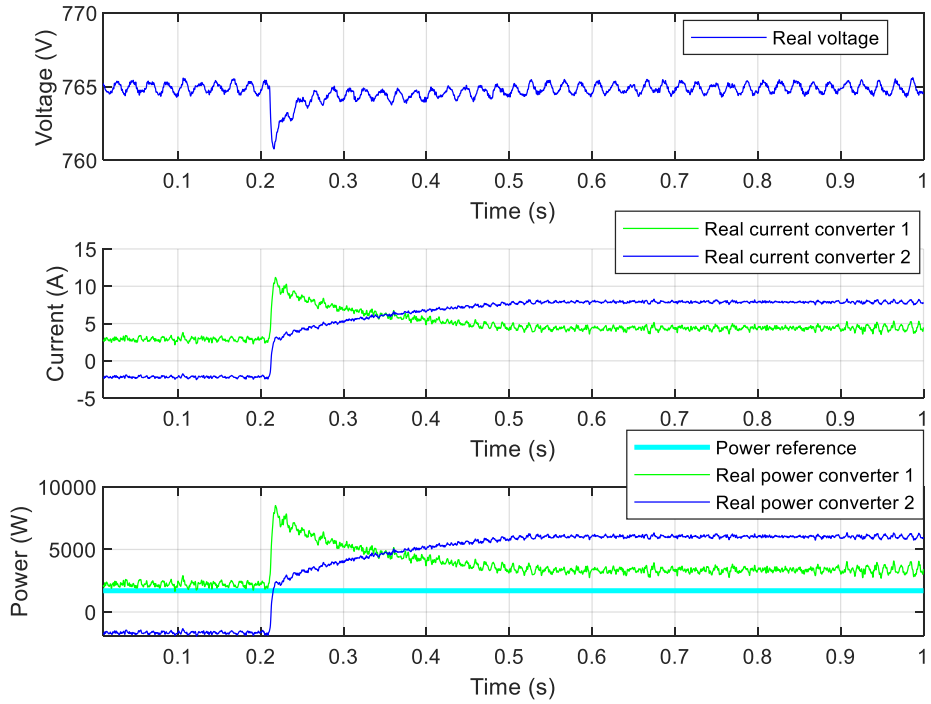


*Figure 124. Results of the experimental test of the corrected final control with two converters to a current perturbation being the distribution constant at 0.5 and the power reference 1700 W*

In Figure 124, another situation is presented where the controller of the power loop saturates. As before, initially the power given by the converters is set by the power loop. But, then, when the current perturbation is applied, the power reference cannot be accomplished because the distribution constant is set to 0,5 (which means, in this particular case, that each converter should give 4500 W approximately) and the controller saturates because it can only correct ±5 A. The saturation occurs because the distribution constant, the power reference and the load power are not coherent. This situation resembles a non-feasible references of upper controls which will set the power reference and the distribution constant.

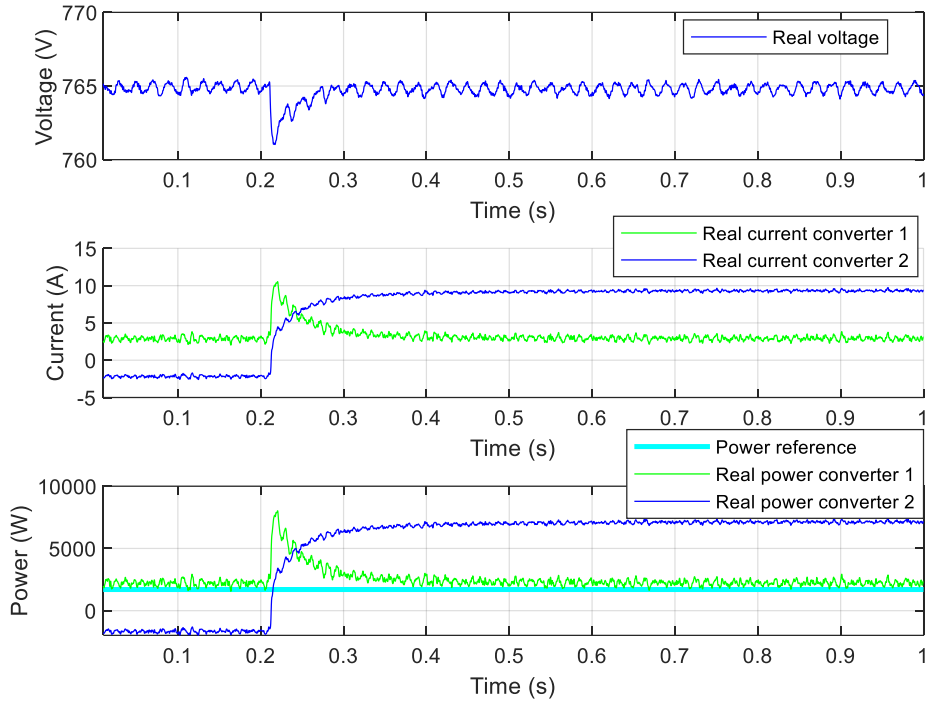


*Figure 125. Results of the experimental test of the corrected final control with two converters to a current perturbation being the distribution constant at 0.2 and the power reference 1700 W*

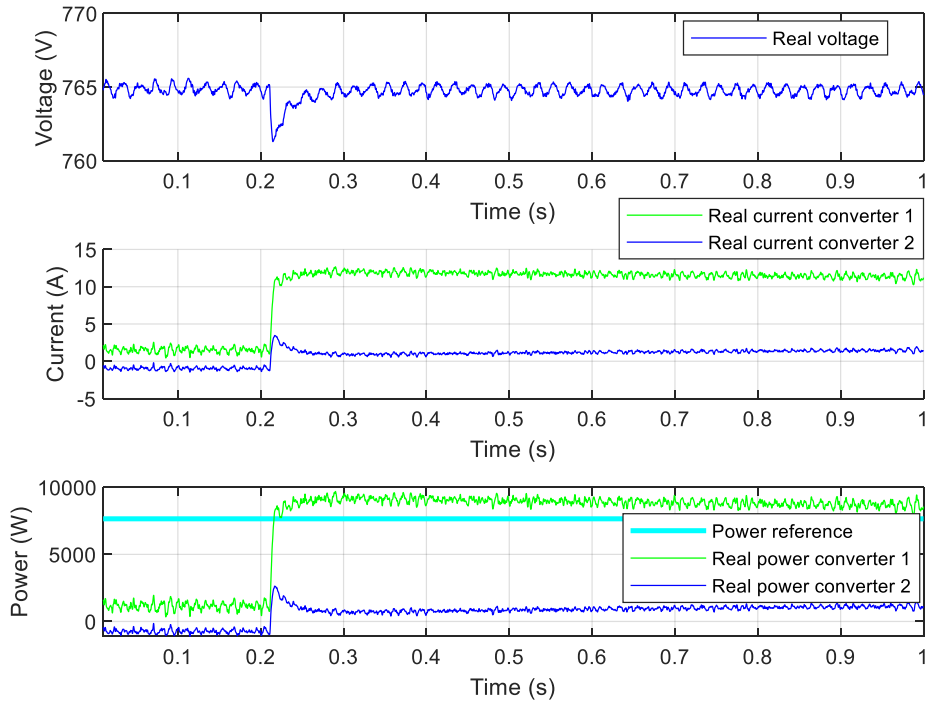


*Figure 126. Results of the experimental test of the corrected final control with two converters to a current perturbation being the distribution constant at 0.9 and the power reference 7650 W*

In contrast with Figure 124, Figure 125 and Figure 126 show the behaviour of the system with coherent references of power and distribution constant. Initially, the power is set by the power loop. Afterwards, when the current perturbation is applied, the final control sets the dynamic behaviour of the system. Finally, the power loop corrects the power of the first converter to match the reference, and consequently, the power of the second converter is determined by the power of the first converter and the power of the load.

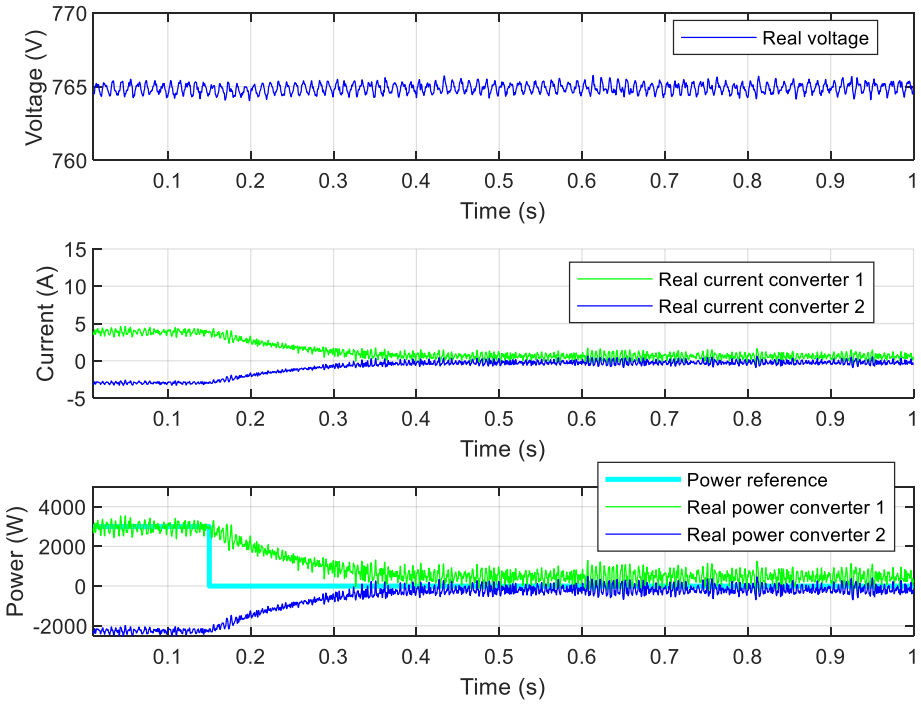


*Figure 127. Results of the experimental test of the corrected final control with two converters to power reference change from 3000 W to 0 being the distribution constant at 0.5*

Finally, Figure 127 shows the behavior of the system to a power reference change. As it can be seen, the stabilization time is much greater than the one of the simple final control. Therefore, this added power loop does not interfere with the final control and it only works to correct mismatches between the power reference and the power output.

In conclusion, the proposed final control works correctly if this correct power loop is added. Therefore, some of the advantages added by the proposed control are lost due to the open loop control of the Dual Active Bridge converter. The final performance is very similar to the classical one at the end, because the corrected final control and the classical droop control with three level have parallel loops where one of them has to be much slower not to interfere with the other.

# 5. Budget

The budget for this master thesis is made taking into account some assumptions. The first one is that all the hardware to implement the thesis is given for the elaboration of the RESOLVD project, and, therefore, its cost is not computed. The second one is that the used devices to make the experimental tests and the needed software to develop the thesis will have an amortization time of 5 years. The last one is that the thesis has last 6 months. All the prices presented takes into account the amortization following ( 168 ).

$$Price_{thesis} = \frac{Price_{total}}{5\ years}\frac{1\ year}{12\ months}\ 6\ months \qquad (168)$$

The budget can be divided in different parts. The first part is the one corresponding to all the software used to do the thesis, Table 7. Then, the second part is the cost of all the needed additional devices to do the experimental tests, Table 8. Finally, the last part of the budget corresponds to the working hours, Table 9.

*Table 7. Software budget*

| | |
|---|---|
| Laptop | 100 € |
| MATLAB | 2.600 € |
| Maple | 1.000 € |
| **TOTAL** | **3.700 €** |

*Table 8. Experimental tests budget*

| | |
|---|---|
| Oscilloscope | 1.200 € |
| Isolated voltage proves | 50 € |
| Current proves | 20 € |
| Multimeter | 30 € |
| **TOTAL** | **1.300 €** |

*Table 9. Working hours' budget*

| | |
|---|---|
| Price | 15 €/h |
| Total hours | 900 h |
| **TOTAL** | **13.500 €** |

Once all the different parts of the budget are presented, a summary table can be done to summarize the cost of every part and to show clearly the total cost of the thesis, Table 10. More than the 70 % of the budget corresponds for the working hours. Then, the following higher cost is the one corresponding to the software costs and, finally, the experimental tests cost is the lower one.

*Table 10. Total budget*

| | |
|---|---|
| Software budget | 3.700 € |
| Experimental tests budget | 1.300 € |
| Working hours budget | 13.500 € |
| **TOTAL** | **18.500 €** |

# 6. Environment Impact

The environment impact of the possible applications of this master thesis is potentially high. Indeed, the real application can have a considerable environment impact because it gives flexibility to the grid. When the predictions of power consumptions are lower than the real ones, this system allows the injection of power thanks to its batteries, avoiding this way the extra energy production of huge plants. Then, the batteries could be recharged when there is an over production of energy due to the renewable's sources or when the price of the energy is lower. It must be said that this project it is a prototype and, therefore, its impact would depend on the futures implementations.

The implementations of batteries and consequently DC microgrids, allow to reduce the emissions by two main reasons. They give more flexibility to the grid avoiding extra energy generation by the huge plants based on fossil energies. They allow to take profit of all the energy produced by renewable sources reducing this way the necessity of energy production based on fossil energies.

Although the use of a battery itself does not generate pollution, the fabrication, the transportation and the recycling of them do. Therefore, it must be need to perform a Life Cycle Analysis, LCA, to take into account the carbon footprint of the whole life of the battery to improve the overall environment impact. This analysis is out of the scope of this project, resulting in a whole other different project. However, in other European H2020 project antecessor of this one, a LCA analysis was performed to validate the potential environmental impact of using batteries for flexibility purposes in peak hours, resulting in a positive impact in countries like Spain, Bulgaria or Germany with energy mixes not fully renewable [40].

On the other side, in order to reduce this carbon footprint, this project is made by second-life batteries, which means that they have been already used and, consequently, their characteristics are a little bit degraded from the initial ones but they expand their life and, therefore, they reduce their carbon footprint. This carbon footprint concept does not only apply to the batteries, but to all components. Moreover, in order to improve the environment impact in electronic components level, the directive RoHS should be followed to reduce the use of pollutant materials.

The applications of DC microgrids are not only applicable at large scale, but also for users who can have a small DC microgrid in their house composed for example, by an electrical vehicle, photovoltaic panels, a battery, the grid inverter and many other loads or renewable sources. The emissions and the energy consumption produced by polluted sources is also reduced in the user application for the same reasons, the flexibility it gives and the profitability of all renewable energy.

Moreover, the development and investigations in DC microgrids also favor the introduction of electric vehicles allowing fast chargers to be connected directly to the DC microgrids. The more electric vehicles are bought, the less combustions ones are used. Therefore, all ease that allow faster introduction of sustainable transport have a considerable environment impact.

# 7. Conclusions and future development

The control of a DC microgrid formed by the parallelization of two DC/DC converters has been designed, calculated, simulated, implemented and tested. The work started with the state of the art and the research from the literature to understand better the microgrids, its controls and the converter. Then, the used hardware was presented and characterized in order to be able to select one suitable control method for the DC microgrid. The chosen control method was the Droop DC composed by three levels: the primary, the secondary and the tertiary controls. The primary control was calculated to work in-between the bus voltage limits and to have the fastest response. The secondary control was designed to stabilize the bus voltage as fast as possible avoiding excessive over peaks. Finally, the tertiary control was calculated to be slow enough not to interfere with the secondary control as they act in parallel. Moreover, a variant of the selected Droop DC control was proposed and called *unified hierarchical DC control*. It combined the secondary and tertiary controls in order to reduce the number of controller to only one, and make the system faster combining the actions of stabilizing the bus voltage and fixing the power sharing of the converters in steady-state.

Once everything was designed, the implementation was made gradually, first with only one converter and afterwards, with the two converters. Finally, the results of the simulations and the experimental test were presented together to compare them and conclude that all the calculations and simulations where valid. On the one hand, the final behaviour with the designed classical three-level Droop DC control shows a bus voltage stabilization time below 20 ms with no over peak and a power sharing stabilization time of 500 ms without interfere with the secondary control. On the other hand, the results of the unified hierarchical DC control are much better accomplishing both voltage bus stabilization and power sharing stabilization in less than 50 ms. Finally, as a consequence of the open loop behaviour of the Dual Active Bridge, a controller to correct the reference deviation of the converter was added worsening this way the behaviour of the proposed control. The final behaviour with the corrected unified hierarchical DC control keeps the bus voltage stabilization time but increases the power sharing stabilization time to 350 ms.

A generalised procedure for all three levels of the classical three-level Droop DC to tune the virtual resistances and the controllers is also presented in this master thesis but, in future works, the controls should be redesigned for more than two converters following these proposed procedures. The designs should be simulated and tested experimentally in order to validate the presented calculus for expanding the controls to more than two converters. Besides the classical controls, the unified hierarchical DC control can be studied for applying it in larger microgrid with more than two converters. A generalised procedure to tune the control can be calculated for N converters as it is done with the classical controls, and then, the simulations and experimental test should be made to validate all the calculations and assumptions. Moreover, a close loop control for the Dual Active Bridge converter which ensures a first order behaviour should be studied to avoid the added correction to the proposed unified hierarchical DC control. Another possible future work is to study the behaviour of the control when one battery is fully charged or discharged.

In conclusion, all the objectives of the thesis have been fulfilled successfully and the result is a working DC microgrid composed by two converters connected in parallel which

interconnect two different types of batteries. Moreover, the design procedures for increasing the number of converters in the DC microgrid has been developed.

# Bibliography

[1] Red eléctrica de España, *"Avance del Informe del sistema eléctrico español 2018".* [Online], Available: https://www.ree.es/sites/default/files/11_PUBLICACIONES/Documentos/InformesSistemaElectrico/2019/Avance_ISE_2018.pdf .

[2] Red eléctrica de España, *"Avance del Informe del sistema eléctrico español 2014"*. [Online], Available: (https://www.ree.es/sites/default/files/downloadable/avance_informe_sistema_electrico_2014b.pdf)

[3] Heredero Peris, D. *"Control contributions to AC microgrid inverters".* Tesi doctoral, UPC, Departament d'Enginyeria Elèctrica, 2017.

[4] Department of Energy Office of Electricity Delivery and Energy Reliability. (2012). Summary Report: 2012 DOE Microgrid Workshop. [Online]. Available: http://energy.gov/sites/prod/files/2012% 20Microgrid%20Workshop%20Report%2009102012.pdf.

[5] R. Bayindir, E. Hossain and S. Vadi, *"The path of the smart grid -the new and improved power grid,"* 2016 International Smart Grid Workshop and Certificate Program (ISGWCP), Istanbul, 2016, pp. 1-8.

[6] E. Hossain, E. Kabalci, R. Bayindir, R. Perez, *"Micro grid testbeds around the world: State of art"*, Energy Conversion and Management, vol. 86, pp. 132-153, October 2014.

[7] S. Parhizi, H. Lotfi, A. Khodaei and S. Bahramirad, *"State of the Art in Research on Microgrids: A Review,"* in IEEE Access, vol. 3, pp. 890-925, 2015.

[8] X. Jin, "*Analysis of microgrid comprehensive benefits and evaluation of its economy,"* 10th International Conference on Advances in Power System Control, Operation & Management (APSCOM 2015), Hong Kong, 2015, pp. 1-4.

[9] T. Dragičević, X. Lu, J. C. Vasquez and J. M. Guerrero, *"DC Microgrids—Part II: A Review of Power Architectures, Applications, and Standardization Issues,"* in IEEE Transactions on Power Electronics, vol. 31, no. 5, pp. 3528-3549, May 2016.

[10] Justo JJ, Mwasilu F, Lee J, Jung JW, *"AC-microgrids versus DC-microgrids with distributed energy resources: a review. Renew Sustain Energy,"* Rev 2013;24:387–405.

[11] S. Peyghami, H. Mokhtari, F. Blaabjerg, *"Hierarchical power sharing control in DC microgrids,"* in: Magdi S. Mahmoud (Ed.), Microgrid, First. Elsevier Science & Technology, 2017, pp. 63–100.

[12] M. Gulin, *"Control of a DC Microgrid,"* University of Zagreb, Zagreb, 2012.

[13] S. Anand, B. G. Fernandes and J. Guerrero, *"Distributed Control to Ensure Proportional Load Sharing and Improve Voltage Regulation in Low-Voltage DC Microgrids,"* in IEEE Transactions on Power Electronics, vol. 28, no. 4, pp. 1900-1913, April 2013.

[14] P. Chaudhari et al., *"Novel control strategy for dynamic load sharing between DC-DC converters for DC microgrid,"* 2015 IEEE International Conference on Signal Processing, Informatics, Communication and Energy Systems (SPICES), Kozhikode, 2015, pp. 1-5.

[15] N. Kondrath, *"Bidirectional DC-DC converter topologies and control strategies for interfacing energy storage systems in microgrids: An overview,"* 2017 IEEE International Conference on Smart Energy Grid Engineering (SEGE), Oshawa, ON, 2017, pp. 341-345.

[16] L. E. Zubieta and P. W. Lehn, *"A high efficiency unidirectional DC/DC converter for integrating distributed resources into DC microgrids,"* 2015 IEEE First International Conference on DC Microgrids (ICDCM), Atlanta, GA, 2015, pp. 280-284.

[17] K. M. Nisar, A. Sivaprasad, S. Kumaravel and P. Ananthakrishnan, *"Implementation of closed loop controller in a dual input DC-DC converter for DC-microgrid application,"* 2016 IEEE Annual India Conference (INDICON), Bangalore, 2016, pp. 1-6.

[18] Prajof P. and V. Agarwal, "*Novel solar PV-fuel cell fed dual-input-dual-output dc-dc converter for dc microgrid applications,"* 2015 IEEE 42nd Photovoltaic Specialist Conference (PVSC), New Orleans, LA, 2015, pp. 1-6.

[19] Dong-Keun Jeong, H. Kim, J. Baek, Ju-Yong Kim and Hee-Je Kim, *"Dual active bridge converter for Energy Storage System in DC microgrid,"* 2016 IEEE Transportation Electrification Conference and Expo, Asia-Pacific (ITEC Asia-Pacific), Busan, 2016, pp. 152-156.

[20] A. Khiareddine, O. Gam and M. F. Mimouni, *"Techno-economic analysis of the lithium-ion and lead-acid battery in Photovoltaic pumping system,"* 2019 19th International Conference on Sciences and Techniques of Automatic Control and Computer Engineering (STA), Sousse, Tunisia, 2019, pp. 417-422.20

[21] B. Zhao, Q. Song, W. Liu and Y. Sun, *"Overview of Dual-Active-Bridge Isolated Bidirectional DC–DC Converter for High-Frequency-Link Power-Conversion System,"* in IEEE Transactions on Power Electronics, vol. 29, no. 8, pp. 4091-4106, Aug. 2014.

[22] Boletín Oficial del Estado (BOE), num. 295, Pág. 130045. [Online]. Available: https://www.boe.es/boe/dias/2011/12/08/pdfs/BOE-A-2011-19242.pdf

[23] Wikipedia, *"Electrical Grid"*, [Online]. Available: https://en.wikipedia.org/wiki/Electrical_grid#/media/File:Electricity_Grid_Schematic_English.svg

[24] European Council, *"A policy framework for climate and energy in the period from 2020 to 2030",* Brussels, 22.1.2014.

[25] European Council, *"Assessment of the draft National Energy and Climate Plan of Spain".* Brussels, 18.6.2019.

[26] European Comission, *"Europe 2020 targets: statistics and indicators for Spain"*, [Online]. Available: https://ec.europa.eu/info/business-economy-euro/economic-and-fiscal-policy-coordination/eu-economic-governance-monitoring-prevention-correction/european-semester/european-semester-your-country/spain/europe-2020-targets-statistics-and-indicators-spain_en

[27] E. G. Shehata, J. Thomas, R. M. Mostafa and M. A. Ghalib, *"An Improved Droop Control for a Low Voltage DC Microgrid Operation,"* 2018 Twentieth International Middle East Power Systems Conference (MEPCON), Cairo, Egypt, 2018, pp. 850-855.

[28] M. R. Jyothish and E. A. Jasmin, *"Load Sharing Control and Circulating Current Minimization of Parallel DC-DC Converters Based on Droop Index,"* 2018 International CET Conference on Control, Communication, and Computing (IC4), Thiruvananthapuram, 2018, pp. 84-88

[29] L. Li, Y. Han, P. Yang, Q. Huang, Z. Zhang and Y. Xu, *"A New Distributed Control Strategy for DC Microgrids with Droop Coefficient Correction and DC Bus Voltage Restoration,"* 2019 IEEE Innovative Smart Grid Technologies - Asia (ISGT Asia), Chengdu, China, 2019, pp. 3908-3913.

[30] I. U. Nutkani, W. Peng, P. C. Loh and F. Blaabjerg, *"Cost-based droop scheme for DC microgrid,"* 2014 IEEE Energy Conversion Congress and Exposition (ECCE), Pittsburgh, PA, 2014, pp. 765-769.

[31] Xiaoliang Yang, Fen Tang, Xuezhi Wu and Xinmin Jin, *"Hierarchical control strategy of grid-connected DC microgrids,"* 2016 IEEE 8th International Power Electronics and Motion Control Conference (IPEMC-ECCE Asia), Hefei, 2016, pp. 3723-3727.

[32] J. M. Guerrero, J. C. Vasquez, J. Matas, L. G. de Vicuna and M. Castilla, *"Hierarchical Control of Droop-Controlled AC and DC Microgrids—A General Approach Toward Standardization,"* in IEEE Transactions on Industrial Electronics, vol. 58, no. 1, pp. 158-172, Jan. 2011.

[33] S. A. Gorji, H. G. Sahebi, M. Ektesabi and A. B. Rad, *"Topologies and Control Schemes of Bidirectional DC–DC Power Converters: An Overview,"* in IEEE Access, vol. 7, pp. 117997-118019, 2019.

[34] D. Yadeo, P. Chaturvedi and S. K. Saketi, *"A New Five Level Dual Active Bridge DC-DC Converter for Solid State Transformer,"* 2018 IEEE International Conference on Power Electronics, Drives and Energy Systems (PEDES), Chennai, India, 2018, pp. 1-5.

[35] G. Barone et al., *"A dual active bridge dc-dc converter for application in a smart user network,"* 2014 Australasian Universities Power Engineering Conference (AUPEC), Perth, WA, 2014, pp. 1-5.

[36] A. Burgio, D. Menniti, M. Motta, A. Pinnarelli, N. Sorrentino and P. Vizza, *"A two-input dual active bridge converter for a smart user network using integrated power modules,"* 2015 IEEE PES Asia-Pacific Power and Energy Engineering Conference (APPEEC), Brisbane, QLD, 2015, pp. 1-6.

[37] A. Safaee, P. Jain and A. Bakhshai, *"Time-domain analysis of a wide-range dual-active-bridge bidirectional series resonant converter,"* IECON 2015 - 41st Annual Conference of the IEEE Industrial Electronics Society, Yokohama, 2015, pp. 004139-004145.

[38] J. Wu, Y. Li, X. Sun and F. Liu, *"A New Dual-Bridge Series Resonant DC–DC Converter With Dual Tank,"* in IEEE Transactions on Power Electronics, vol. 33, no. 5, pp. 3884-3897, May 2018.

[39] Hossain, E., Kabalci, E., Bayindir, R., Perez, R., *"Microgrid testbeds around the world: State of art,"* Energy Conversion and Management, vol. 86, pp. 132–153, 2014.

[40] Munné-Collado, I.; Aprà, F.M.; Olivella-Rosell, P.; Villafáfila-Robles, R. *"The Potential Role of Flexibility During Peak Hours on Greenhouse Gas Emissions: A Life Cycle Assessment of Five Targeted National Electricity Grid Mixes". Energies* 2019, *12*, 4443.

# Glossary

| | |
|---|---|
| DAB | Dual Active Bridge |
| DC | Direct Current |
| AC | Alternating Current |
| H2020 | Horizon 2020 |
| MGCC | Microgrid Central Controller |
| LC | Local Controller |
| DSO | Distribution System Operator |
| TSO | Transmission System Operator |
| PID | Proportional–Integral–Derivative |
| PI | Proportional–Integral |
| CL | Current control Loop |
| VL | Voltage control Loop |
| CCB | Central Control Board |
| PV | Photovoltaic |
| BOE | Boletín Oficial del Estado |
| IGBT | Insulated Gate Bipolar Transistor |
| MOSFET | Metal-Oxide-Semiconductor Field-Effect Transistor |
| Si | Silicon |
| SiC | Silicon Carbide |
| SPS | Single Phase Shift |
| EPS | Extended Phase Shift |
| DPS | Dual Phase Shift |
| TPS | Three Phase Shift |
| PWM | Pulse-Width Modulation |
| ZVS | Zero Voltage Switching |
| ZCS | Zero Current Switching |
| CLA | Control Law Accelerator |
| CAN | Controller Area Network |
| SPI | Serial Peripheral Interface |
| SCI | Serial Communication Interface |
| GPIO | General Purpose Input/Output |
| RoHS | Restriction of Hazardous Substances |